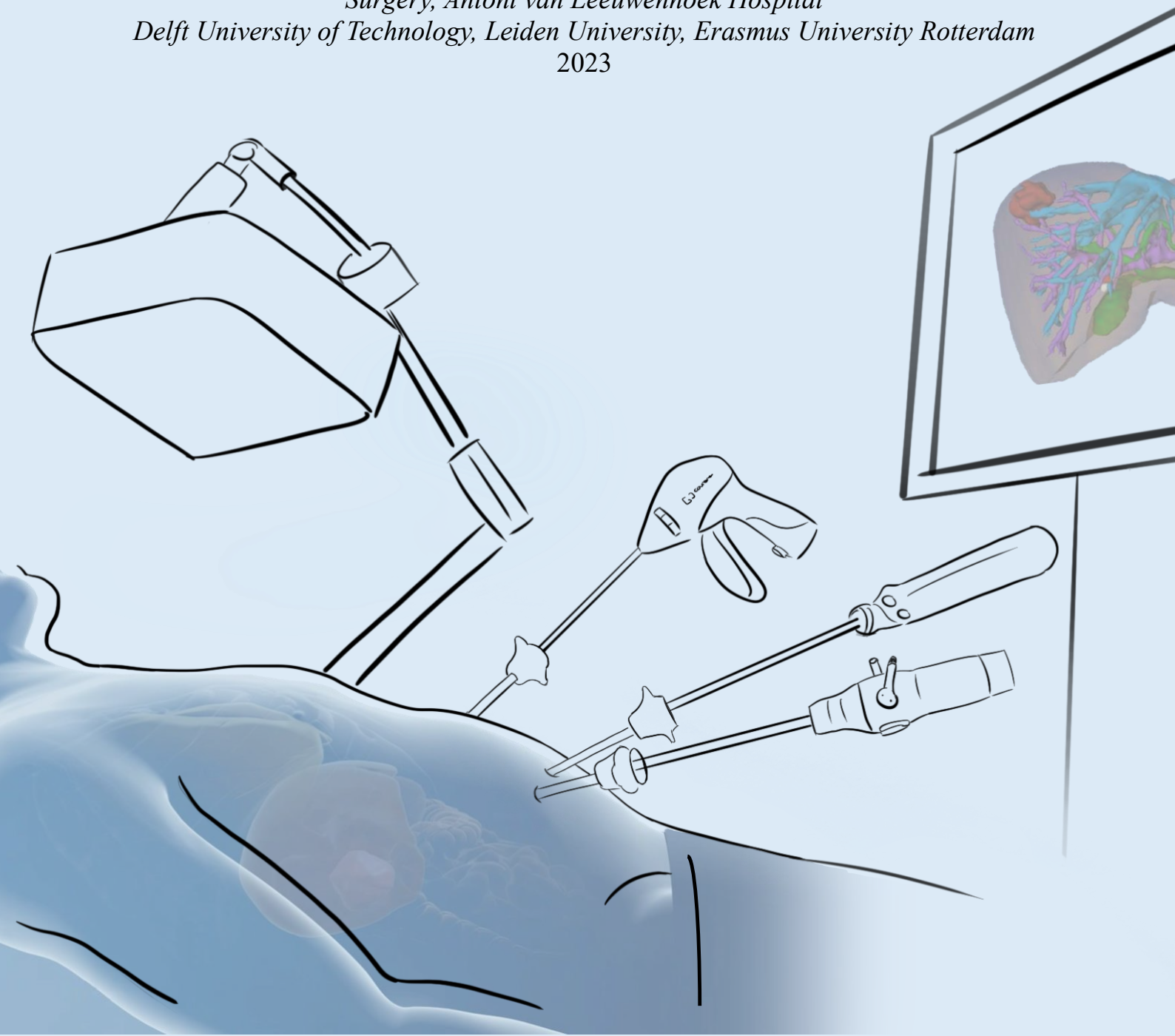


Towards clinical implementation of ultrasound-based navigation for laparoscopic liver resection

Julia Greeven

*Surgery, Antoni van Leeuwenhoek Hospital
Delft University of Technology, Leiden University, Erasmus University Rotterdam
2023*



Master thesis

Towards clinical implementation of ultrasound-based navigation for laparoscopic liver resection

Final Report

Julia Greeven
4483820

Thesis in partial fulfilment of the requirements for the joint degree of Master of Science in
Technical Medicine

Leiden University ; Delft University of Technology ; Erasmus University Rotterdam

MSc Technical Medicine

3mE - Faculty of Mechanical, Maritime and Materials Engineering
Delft University of Technology
Master thesis project (TM30004 ; 35 ECTS)

Supervisors

Prof. Dr. T.J.M. Ruers
Dr. K.W.A Van Dongen
Dr. M. Fusaglia
Msc. K.A. Olthof

Thesis committee members

Prof. Dr. Ir. J. Harlaar (Chair)
Prof. Dr. T.J.M. Ruers
Dr. K.W.A Van Dongen
Msc. K.A. Olthof

Start project: 30-01-2023

Report issued: 22-09-2023

Defense date: 06-10-2023

An electronic version of this thesis is available at <http://repository.tudelft.nl/>.



Summary

Liver cancer ranks seventh in global cancer prevalence and stands as the third leading cause of cancer-related deaths. Surgical resection is considered the gold standard for treatment of liver malignancies and has witnessed a shift toward minimally invasive techniques in recent decades. Surgeons rely on laparoscopic observations, preoperative imaging, and laparoscopic ultrasound for image guidance. However, these methods pose challenges in accurately representing the complex three-dimensional (3D) structure of the liver in a two-dimensional (2D) view. Surgical navigation devices aim to enhance this process by providing additional information for improved lesion localization and vascular structure visualization with respect to tracked surgical instruments. This study's objective was to establish an electromagnetically guided laparoscopic liver resection workflow at Netherlands Cancer Institute – Antoni van Leeuwenhoek (NKI-AvL) to be implemented into clinical practice.

A method was developed for tracking instruments in laparoscopic surgery, with a focus on the laparoscopic sealer/divider. An adapter was developed with an embedded electromagnetic sensor to allow tracking. Calibration employed a dedicated device, followed by a comprehensive validation process encompassing usability, sterilizability, attachment reproducibility, and calibration accuracy. The adapter was produced from a non-ferromagnetic material, ensuring sterilizability and straightforward surgeon attachment, exhibiting positive results in reproducibility and virtual visualization. Nevertheless, the calibration accuracy, at 2.5 mm, could be enhanced, primarily through calibration method adjustments. Additionally, a fast calibration method for the laparoscopic ultrasound (LUS) probe adapter was developed, involving a dedicated calibration tool. Validation assessments to ascertain its reproducibility showed positive results. However, accuracy measurements can be further improved as ultrasound calibration method evaluation showed a root mean squared error (RMSE) of 3.6 mm. This is important as the navigation performance relies on the calibration accuracy of the tracked LUS probe. The workflow for navigated laparoscopic liver resection was tested using a liver phantom. It demonstrated the navigation system's capacity to register preoperative and intraoperative images with a mean target registration error (TRE) of 3.7 mm and showed promising augmented reality views. Additionally, this test led to workflow enhancements related to liver sensor placement and visualization techniques.

The developed navigation workflow for laparoscopic liver resection integrated Aurora EM tracking, tracked laparoscopic instruments, and software for intraoperative liver 3D model visualization. While feasible in an operating setting during phantom tests, further enhancements in visualization and accuracy are needed. A clinical study will be conducted to determine intraoperative feasibility, providing valuable experience to technical physicians and surgeons. In the near future, the presented navigation method may enhance laparoscopic resection accuracy and reduce disease recurrence. A clinical study at NKI-AvL will soon validate this navigation system for clinical use.

Keywords: Image-guided Surgery, Surgical navigation, Laparoscopy, Liver cancer

Acknowledgments

This master's thesis is the result of 8 months of research and with that it concludes my Master's degree in Technical Medicine at the TU Delft, the Leiden University, and the Erasmus University Rotterdam. Throughout my master's program, I had the privilege of gaining valuable experiences in various areas that engaged my interest, including 3D printing, 3D planning, and 3D visualization techniques. This research project allowed me to combine all these interests and further expand my knowledge and skills. Since I had not previously completed an internship at this department, I began this project with relatively little prior experience in the field of surgical navigation. Nevertheless, my supervisors provided me with a comprehensive understanding of this technique at an impressive pace, allowing me to delve into it with hands-on experience. They encouraged me to work independently while remaining readily available for insightful brainstorming sessions, which was the supervisory style that really fits my way of working.

First of all, I would like to thank my daily supervisor, Karin Olthof, for her helpful guidance throughout these months. I truly appreciated our collaborative working style and her patience and support during the extensive testing phases, sometimes extending into late hours. As the saying goes, "Je kunt testen tot je een ons weegt" (You can test until you're blue in the face); she also showed me the invaluable skill of research efficiency. Thanks for not only guiding me in the right direction but also encouraging me to reflect on my results, enhancing my critical attitude. As a true expert in the field, she demonstrated how a physician-technician can work both clinically and technically, highlighting the need and added value of this interdisciplinary domain.

Secondly, I want to thank Matteo Fusaglia, whose door was always open for quick questions. Thanks for providing me with clear explanations whenever I struggled to grasp the underlying reasons for those ever-present errors, and for guiding me in the right direction by sometimes only asking the right questions. He introduced me to the incredible possibilities of 3D visualizations, expanding my horizons in the technical aspects of this technique.

A critical viewpoint was provided during update meetings by Koen van Dongen, whom I would like to sincerely thank for being on my assessment committee. Also, I want to thank the hepatobiliary surgeons from this institute for their helpful clinical insights regarding my research and for their enthusiasm about technical innovations in surgery. In particular, I would like to express my gratitude to my clinical supervisor, Professor Theo Ruers, for his expertise and for reminding me to keep the clinical end goal in mind.

Besides, I extend my thanks to everyone from the "Vide" for letting me join the team outing and for all the coffee breaks and brainstorming sessions, which also extended beyond just work-related discussions. Lastly, I need to thank my friends and family for always providing encouraging words and motivation, and for patiently listening to my endless complaints about the trains.

I can honestly say I enjoyed doing this thesis and I am grateful for the opportunity to contribute, even in a small way, to the ongoing mission of improving clinical care for cancer patients. I have witnessed how navigation techniques have already demonstrated their added value by helping surgeons overcome challenges in locating lesions, which left a strong impression on me.

Julia Greeven
Rotterdam, September 2023

Contents

List of Figures	1
List of Tables	3
List of Abbreviations	4
1 Introduction	5
1.1 Clinical background	5
1.1.1 Liver cancer	5
1.1.2 Options in diagnostics	5
1.1.3 Liver anatomy	6
1.1.4 Treatment options for liver cancer	6
1.1.5 Laparoscopic liver surgery	7
1.1.6 Image guidance during laparoscopic surgery	8
1.1.7 Rationale	8
1.2 Technical background	9
1.2.1 Tracking system	9
1.2.2 Image registration	10
1.2.3 Standard clinical care	12
1.3 Research objectives	13
1.3.1 Primary objective	13
1.3.2 Secondary objectives	13
2 Tracking of laparoscopic instruments	14
2.1 Introduction	14
2.1.1 Laparoscope	15
2.1.2 Laparoscopic ultrasound	15
2.1.3 Laparoscopic sealer/divider	15
2.2 Methodology	16
2.2.1 Adapter design and production	17
2.2.2 Calibration	19
2.2.3 Validation	20
2.3 Results	23
2.3.1 Adapter design and production	23
2.3.2 Validation	23
2.4 Discussion	24
2.4.1 Adapter location	24
2.4.2 Calibration, tracking and registration	25
3 Fast calibration method LUS adapter	26
3.1 Introduction	26
3.2 Methodology	26
3.2.1 Design and production of the calibration tool	26
3.2.2 Calibration of the calibration tool	26
3.2.3 Use of the calibration tool	28
3.2.4 Validation	28
3.3 Results	30
3.3.1 Validation of reproducibility of attachment process	30
3.3.2 Validation of calibration accuracy	30
3.4 Discussion	31
4 Clinical implementation	32
4.1 Introduction	32
4.2 Methodology	33
4.2.1 Navigation system description	33
4.2.2 User interface	33
4.2.3 Liver sensor attachment	34
4.2.4 Validation of navigation workflow and accuracy	34

4.3 Results	36
4.3.1 Liver sensor attachment.	36
4.3.2 User interface	36
4.3.3 Validation navigation workflow and accuracy	37
4.4 Discussion.	39
5 Conclusion	41
5.1 Clinical relevance.	41
5.2 Future directions	42
Reference list	43
Appendices	
A Literature Review	1
B Technical Drawing Adapter	ii
C Summary study protocol	iii

List of Figures

1.1	Couinaud's classification of liver segments [1]	6
1.2	Laparoscopic liver surgery [2]	7
1.3	On the left side the Aurora NDI planar field generator, with on the right its EM field (cube and dome volume) [3].	9
1.4	On the left side the Aurora NDI tabletop field generator, with on the right its EM field (cube and dome volume) [3].	9
1.5	(a) The six degrees of freedom in 3D space: three translations (X,Y,Z) and three rotations (roll, pitch, yaw) (b) Aurora 6DoF cable sensor (c) Aurora 6DoF Probe [3, 4]	10
1.6	Overview of registration steps from preoperative imaging modality to intraoperative ultrasound	11
1.7	Surgical navigation workflow during standard clinical care for open liver surgery	12
2.1	Laparoscopic instruments used during laparoscopic surgery	14
2.2	In-house developed adapter of the laparoscope	15
2.3	Adapter of laparoscopic ultrasound (LUS) probe	15
2.4	Accuracy of sensor tested at different locations attached to the laparoscopic instrument	17
2.5	Adapter design with a parallel location of the sensor [5]	17
2.6	Tip-to-tip test with surgical pointer to assess calibration accuracy	18
2.7	Different locking mechanisms for the adapter enclosing the shaft	18
2.8	Coordinate systems with corresponding transformations for the LigaSure adapter calibration	19
2.9	Calibration device used for calibration of the LigaSure adapter with a red circled divot	20
2.10	Actual and 3D Slicer view of the tracked calibration device and tracked LigaSure before (a) and after (b) calibration of the adapter	20
2.11	Testing the reproducibility of attaching the adapter	21
2.12	Indicating divots on calibration device. The top images depict the 3D environment in 3D Slicer software, while the bottom images show actual views	22
2.13	Adapter attached on shaft of Laparoscopic Pointer	22
2.14	Final design of LigaSure adapter	23
2.15	Results of four calibration accuracy tests using the LigaSure, Pointer, Laparoscopic pointer and the Laparoscopic pointer with the adapter. Boxplots shows the median, quartiles and the cross indicates the mean	24
3.1	(a) LUS probe tip featuring a hole to click the adapter on. (b) 3D model of calibration tool with a hole for the EM sensor and a holder. (c) 3D-printed calibration tool with the attached EM sensor and adapter	27
3.2	Coordinate systems with corresponding transformations used for calibration of the calibration tool	27
3.3	Coordinate systems of EM sensor attached on calibration tool and the EM sensor attached on the adapter with corresponding transformation	28
3.4	Coordinate systems and corresponding transformations for tracked ultrasound probe calibration	29
3.5	Two ultrasound (US) images show an electromagnetic (EM) pointer positioned on the right side of each image. The pointer tip is situated in front of the US plane in (a) and precisely within the US plane in (b) The correct pointer tip is indicated by a red dot	29
3.6	Results of LUS calibration accuracy tests. Boxplot shows the median, quartiles and the cross indicates the mean	30
3.7	Calibration evaluation in two directions of golden standard adapter using a surgical pointer. The left image in both subfigures displays the 3D view, and the right image shows the 2D US plane with an overlaid virtual model of the pointer.	31
4.1	Possible errors during navigated laparoscopic liver resection [6]	32
4.2	(a) Liver phantom used during the phantom test and (b) a segmented 3D model of the phantom in 3D Slicer	34
4.3	Operating room test set up. 1) Laparoscope monitor 2) Laparoscopic tower 3) Tracked LigaSure Maryland 4) EM field generator 5) Tracked laparoscope 6) Patient tracker 7) Tracked laparoscopic ultrasound probe 8) BK Ultrasound system 9) Navigation monitor with preoperative 3D model	35
4.4	Schematic overview of all transformations required for registration	35
4.5	Experimental setup for testing adhesion of the Glubran2 glue on a (a) cow and (b) human liver specimen and (c) testing the laparoscopic use of the catheter	36

4.6	Navigation environment in Unity software, with on the left a view with the 3D models and on the right the view with the 3D model overlaying the 2D-US image	36
4.7	Various options in the AR software	37
4.8	Results of augmented reality view. (a) Alignment of the liver edge (b) Validation overlay with US image (c) Diminishing overlay at the liver's periphery	37
4.9	Results of accuracy phantom tests. Boxplot shows the median, quartiles and the cross indicates the mean	37
4.10	Overview of laparoscopic navigation workflow. 1) Liver sensor placement 2) LUS probe orientation 3) Landmark-based registration 4) Loading the registration into AR software 5) Visual assessment of the 3D model overlay onto the laparoscope image 6) Calculation of the TRE between tumor centers in US volume (C_{US}) and its co-registered preoperative counterpart (C_M)	38
C.1	Clinical workflow steps for navigated laparoscopic liver resection	iii

List of Tables

- 2.1 Root Mean Squared (i.e. RMS) errors of Aurora 6DoF sensor in orientation and position, alongside two volumes of the field generator (FG) [3] 14
- 2.2 Risk assessment and requirements list 16
- 2.3 Results of three different calibrations for different sensor location 18
- 2.4 Standard deviations (SD) of Euclidean distance and Euler angels of difference between adapter sensor and reference sensor after repeatedly reattaching the adapter by three individuals 23

- 3.1 Standard deviations of repeated LUS clip attachment on calibration tool 30

List of Abbreviations

- 2D** Two-dimensional.
- 3D** Three-dimensional.
- CNC** Computer numerically controlled.
- CPI** Clinical Physics and Informatics.
- CRC** Colorectal cancer.
- CRLM** Colorectal liver metastases.
- CSD** Central sterilization department.
- CT** Computed tomography.
- DoF** Degrees of freedom.
- EM** Electromagnetic.
- EMTS** Electromagnetic tracking system.
- FDG** 18F-fluorodeoxyglucose.
- FG** field generator.
- FRE** Fiducial registration error.
- HCC** Hepatocellular carcinoma.
- ICP** Iterative closest point.
- IGS** Image guided surgery.
- IOUS** Intraoperative ultrasound.
- LUS** Laparoscopic ultrasound.
- MDR** Medical Devices Regulation.
- METC** Medisch ethische toetsings commissie.
- MR** Magnetic resonance.
- MRI** Magnetic resonance imaging.
- NKI-AvL** Netherlands Cancer Institute – Antoni van Leeuwenhoek.
- PET** Positron emission tomography.
- RMSE** Root mean square error.
- SCU** System Control Unit.
- TRE** Target registration error.
- US** Ultrasound.

1.1. Clinical background

1.1.1. Liver cancer

Liver cancer is the seventh most common cancer and the third leading cause for cancer death worldwide (8.3%) with a relative 5-year survival rate of approximately 18% [7, 8]. Liver cancer can be categorized into two types: primary liver cancer and secondary liver cancer, which is also known as hepatic metastasis. The most prevalent liver malignancies include primary hepatocellular carcinoma (HCC) and metastatic colorectal cancer. HCC is more prevalent in Asia and Africa compared to western countries. Nevertheless, the incidence rates of HCC in Western countries have shown a gradual increase in recent years [9]. In the Netherlands, incidence has increased, from approximately 200 new diagnoses in 1990 to around 1000 in 2021 of which HCC represents more than 90% of primary liver cancers [10, 11]. Colorectal liver metastases (CRLM) are more prevalent, representing the most common type of secondary liver cancer, often due to their spread through the portal circulation [12]. In 2022, 12.000 new cases of colorectal cancer (CRC) were diagnosed in the Netherlands [13]. Up to 50% of patients diagnosed with CRC present with CRLM or develop liver metastasis within 5 years after diagnosis [14].

1.1.2. Options in diagnostics

The diagnosis of liver cancer involves a comprehensive evaluation, including a detailed medical history, physical examination, radiological tests, and pathological analysis. Primary liver cancer usually develops in the setting of chronic liver disease, particularly in patients with cirrhosis due to alcohol use, chronic hepatitis B or C virus infections, or nonalcohol-associated steatohepatitis [15, 16]. These preexisting liver conditions can lead to the rapid onset of symptoms such as weight loss, fatigue, jaundice, and upper abdominal pain, indicating possible HCC [17]. During a physical examination, an enlarged, irregular, and tender liver may be detected. Additionally, an elevated tumor marker, α -fetoprotein, can potentially indicate the presence of liver cancer. However, this marker alone is not highly indicative, as one-third of patients exhibit normal levels. Additionally, it lacks specificity for HCC, as its levels can also elevate in cases of acute or chronic hepatitis and during pregnancy [18].

Radiological assessment plays an essential role in primary liver cancer detection. Initially, ultrasound (US) is commonly utilized as the primary diagnostic tool due to its cost-effectiveness, non-invasiveness, and lack of radiation exposure. US has a variable sensitivity ranging from 58% to 89% and a specificity of over 90% [19]. Given that its sensitivity can be affected by lesion size and the presence of conditions such as cirrhosis and obesity, computed tomography (CT) or magnetic resonance imaging (MRI) are often used to confirm diagnoses and assess the tumor's spatial relationship with adjacent critical structures [20–23].

For secondary liver lesions, the standard diagnostic procedure involves contrast-enhanced CT, particularly in cases where a primary tumor like CRC is suspected. The use of iodine contrast enhances the contrast-to-noise ratio between healthy liver tissue and malignant lesions on CT. Additionally, considering the use of fluorodeoxyglucose positron emission tomography combined with CT (FDG-PET-CT) or chest CT can help identify potential extrahepatic tumor activity, potentially indicating a change in treatment. FDG-PET is not considered as the primary diagnostic method because it has limited resolution for detecting small lesions ($\varnothing < 1\text{cm}$).

MRI is frequently obtained as an additional imaging modality due to its superior sensitivity in detecting liver lesions, particularly in cases involving small lesions ($\varnothing < 1\text{ cm}$). Furthermore, the inclusion of diffusion-weighted MRI enhances diagnostic accuracy by showing proton diffusion discrepancies between malignant and benign tissues. The integration of liver-specific MRI contrast agents further enhances MRI's capability to identify and characterize small lesions [24]. The Netherlands Cancer Institute – Antoni van Leeuwenhoek (NKI-AvL) acquires standard diagnostic MR scans using multi-phase MR sequences enhanced with a liver-specific gadolinium-based contrast agent (Gd-EOB-DTPA, Primovist, Bayer AG, Germany) [25]. This scan offers a comprehensive view of hepatic vasculature, biliary tree anatomy, and small lesion sizes, facilitating early detection of liver malignancies, especially in cases of colorectal metastases. At NKI-AvL, Primovist serves as the standard MRI contrast agent for all liver metastases, except in cases of neuroendocrine (NET) tumors, where Dotarem contrast is used [6, 26].

1.1.3. Liver anatomy

The liver, which constitutes approximately 2% of the average body weight, is the largest internal human organ [27]. It is positioned in the right upper quadrant of the abdominal cavity below the diaphragm and above the stomach and the gallbladder. It is protected by the rib cage and maintains its position through ligamentous attachments [28]. The liver plays a vital role in a multitude of physiological processes. Major functionalities of the liver include nutrient storage, detoxification, protein synthesis and hormone production. It is the only internal human organ with the natural ability to regenerate lost tissue. A complete liver can be regenerated from as little as 25% of the remaining tissue, while this percentage increases in cases where chemotherapy is performed and when the liver is affected by cirrhosis [29]. Additionally, the liver is unique due to its dual blood supply from the portal vein (approximately 75%) and the hepatic artery (approximately 25%) [30]. The liver can be anatomically divided into four lobes and eight smaller segments, first described by the anatomist Claude Couinaud (Figure 1.1). Couinaud's segments are defined by their vascular supply, their biliary drainage, and their venous drainage via the hepatic veins [27]. The lobes are divided into anterior, posterior, lateral, and medial segments by branches of the hepatic veins. Similarly, the left and right branches of the portal vein divide the liver into superior and inferior segments.

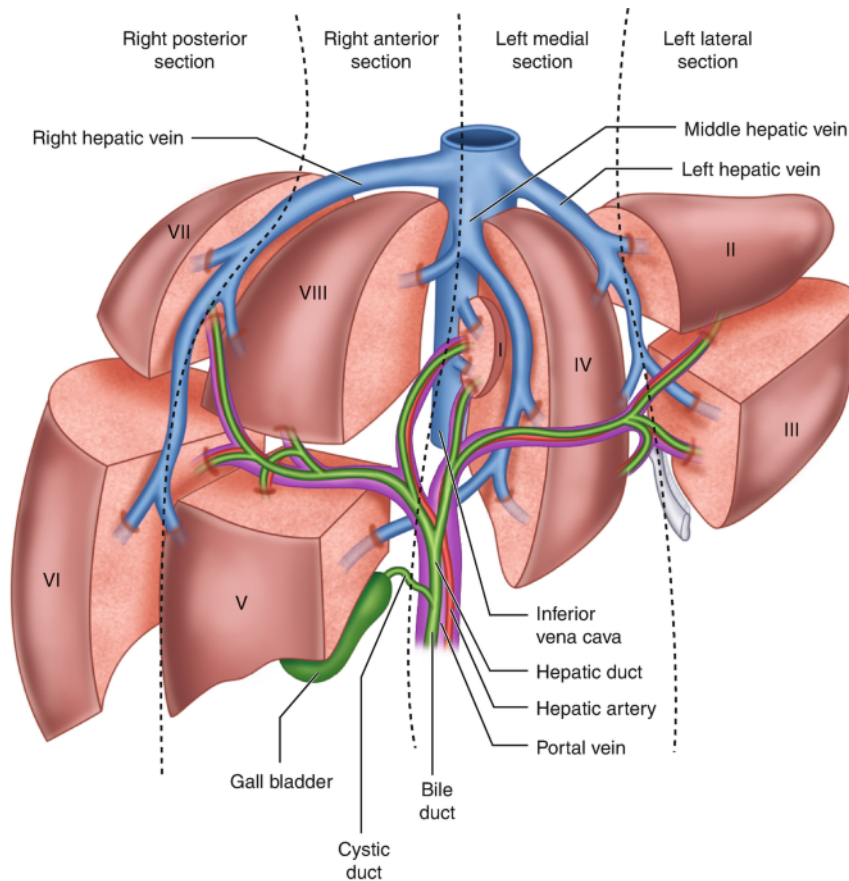


Figure 1.1: Couinaud's classification of liver segments [1]

1.1.4. Treatment options for liver cancer

Liver cancer treatment options vary depending on factors such as tumor location, stage, and patient eligibility. The main treatment options include surgery, local ablation techniques, liver transplantation and neoadjuvant therapy.

Surgical resection, commonly known as hepatectomy, is the most effective treatment for liver malignancies and considered the gold standard. It involves the surgical removal of a portion of the liver containing the tumor, a procedure that can follow the Couinaud segments or take the form of a non-anatomical wedge resection. Anatomical resection refers to following the anatomical boundaries of these segments during the resection process. Both the tumor and a significant portion of healthy liver tissue are removed. While the anatomical representation aids in surgical resection planning, it may not always align precisely with the liver's functional anatomy. However, it enables the removal of individual segments without impacting adjacent ones [31]. Conversely, a non-anatomical resection focuses on sparing healthy liver tissue by removing only the tumor with a 5–10 mm safety margin. This resection type provides the advantage of preserving more healthy liver tissue, although achieving a clear resection margin can be more challenging without the use of anatomical landmarks. The choice to perform this type of resection depends on factors such as preoperative chemotherapy, pre-existing liver conditions, the risk of recurrence, and the tumor's location and size [32].

To successfully perform a hepatectomy, surgeons must accurately interpret the intrahepatic vasculature to ensure sufficient blood flow to and from the remaining liver. Due to the liver's natural regenerative capacity, up to 80% of the total liver volume can be resected, with variability depending on patient conditions and lesion location [33]. Currently only 10-20% of patients with liver malignancies are eligible for surgical resection [34]. However, advancements in surgical techniques, anesthesia, chemotherapy, imaging technology, and the broadening of resectability criteria by surgeons have led to an increased number of patients undergoing surgery. In the past, resections were performed with a minimal resection margin of 10 mm, but over the years it has been indicated that smaller margins of 1 mm result in similar survival and local recurrence rates [35].

Patients become eligible for hepatic resection when complete removal of the lesion can be achieved with clear margins, and the remaining functional liver volume ensure proper postoperative liver function [36]. However, when a tumor reaches an advanced stage or becomes too large, surgical intervention may no longer be feasible. In exceedingly rare instances, a liver transplant might be a viable option. This involves the replacement of the diseased liver with a healthy one from a donor. Although highly successful, the limited availability of donor organs remains a challenge. An alternative treatment, such as systemic chemotherapy can be employed for palliative purposes as well as in a neoadjuvant setting prior to surgery. It can be used to downstage tumors, making them resectable, or to convert non-resectable metastases into resectable ones. It may also achieve complete radiological disappearance in some cases. The majority of patients receiving systemic therapy also undergo local treatment. Microwave ablation (i.e. MWA) and radio-frequency ablation (i.e. RFA) are local treatment options that are becoming more common and can be performed percutaneously. These procedures utilize high temperatures to induce tumor cell necrosis.

Other local treatment possibilities include stereotactic radiotherapy, vascular treatment as transarterial chemo embolization and radio embolization.

1.1.5. Laparoscopic liver surgery

Although open surgery remains the conventional approach for abdominal procedures, there has been a notable shift in recent decades toward minimally invasive techniques. This transition is driven by the potential for reduced trauma for patients [37]. Laparoscopic liver surgeries offer significant advantages over open surgery, as they eliminate the need for extensive abdominal incisions, leading to reduced postoperative discomfort, lower costs, and faster recovery times [38, 39]. Additionally, this type of surgery may present a viable alternative for specific patients with medical comorbidities or limited physical capabilities when open surgery is not a feasible option.

Laparoscopic surgery typically involves creating two to four small incisions. The first incision is utilized to introduce carbon dioxide gas into the abdominal cavity, inducing pneumoperitoneum, facilitating the surgical workspace. This is achieved through the insertion of specialized surgical tubes called trocars, which act as access points for elongated surgical instruments (Figure 1.2a). After the trocar makes the initial incision, a plastic cannula is introduced, providing a stable entry point for the surgical instruments. Cannulas are equipped with a flexible valve designed to maintain a consistent internal pressure by effectively sealing the pneumoperitoneum while inserting and removing the instruments [40]. Once the cavity is adequately inflated, a laparoscope is introduced via one of the trocars. This laparoscope provides real-time video images displayed on a monitor, serving as a visual guide during the surgery (Figure 1.2b). Depending on the specific procedure, additional incisions may be created, and more trocars are positioned as necessary to accommodate the use of surgical instruments.



(a) Laparoscopic instruments through trocars inside patient's abdomen



(b) Live video of laparoscopic procedure on a monitor

Figure 1.2: Laparoscopic liver surgery [2]

1.1.6. Image guidance during laparoscopic surgery

Challenges in laparoscopic liver surgery lies in the inability to physically palpate the liver tissue, resulting in difficulties in identifying a resection margin that achieves oncological clearance. Intraoperative imaging is the only source of information regarding the surgical situs. Due to the liver's complex three-dimensional (3D) anatomy, caused by its highly variable vascular anatomy, difficulties arise in maintaining the correct anatomical orientation within the two-dimensional (2D) laparoscopic view, which lacks depth perception. This orientation challenge can result in incomplete oncological resections and unintended vascular or biliary injuries [41]. Laparoscopic ultrasound (LUS) can be used prior to liver tissue resection to locate liver lesions and determine their margins in relation to healthy tissue and critical structures, such as blood vessels. Therefore, it plays a crucial role in identifying the precise resection plane. LUS is the preferred imaging technique in laparoscopic liver surgery due to its real-time capabilities and non-invasiveness.

Once resection has started, utilizing LUS becomes challenging due to its provision of 2D images, making it difficult to interpret along with the laparoscopic camera's orientation. Furthermore, the diagnostic accuracy of LUS is compromised when dealing with liver cirrhosis or small, barely visible liver lesions e.g. due to positive response of neoadjuvant systemic treatment [42–44]. Localizing such lesions and mapping 2D-US images into the physical 3D anatomical scene is demanding. To address these challenges, a potential solution lies in image-guided surgery (IGS) or surgical navigation. This technique relied on a process called registration, where preoperative imaging, such as MRI and CT scans, are mapped to the patient's actual intraoperative anatomy. This enables surgeons to visualize tumor locations and critical structures from the preoperative image in real-time during surgery, relative to the patient's body.

In addition, 3D volume rendering can be employed to generate a more intuitive 3D representation of the liver. These methods focus on reconstructing a 3D volume of the liver from preoperative image scans, allowing the surgeon to interact with it and explore various perspectives of the anatomy. As a laparoscopic image gives a 2D view of the liver, the correlation with the 3D model can be difficult to interpret. Therefore, augmented reality (AR) emerges as a promising technique to enhance the spatial comprehension with underlying anatomy [45]. It superimposes the 3D model onto the laparoscopic screen, enabling the integration of both the intraoperative laparoscopic view and 3D visualization of patient-specific anatomy within a single environment. Furthermore, it can incorporate LUS imaging, enhancing its usability and intuitiveness [5, 46].

1.1.7. Rationale

Accurate lesion localization and a comprehensive understanding of patient-specific vascular and biliary structures not only assist in planning complex liver surgeries but also enhance the success of tumor resections while preserving a greater amount of functional liver tissue [35, 41]. In addition, difficulties in localizing lesions, prolongs the overall duration of the surgery, posing potential risks to the patient. Hence, the implementation of surgical navigation is crucial in liver resection, particularly in laparoscopic procedures, addressing concerns like spatial awareness, depth perception, and haptic feedback. This thesis therefore focuses on developing and clinically implementing surgical navigation for laparoscopic liver resection.

Surgical navigation has found its place in various medical fields like orthopedics, facial surgery, and neurosurgery [47–49]. However, its implementation for highly deformable organs remains limited as it may cause imprecise navigation [50, 51]. The flexibility of the liver complicates the alignment of the 3D model with the intraoperative reality. Factors such as respiratory motion, pneumoperitoneum, and surgical manipulation, result in the altering of the liver and its shape and position [33]. However, under the hypothesis that precise and controlled mobilization could achieve a satisfactory level of accuracy for local navigation by rigidly aligning preoperative data, this research does not address liver deformation for navigation.

1.2. Technical background

Surgical navigation techniques aim to integrate preoperative and intraoperative images within the same coordinate system, alongside the tracked surgical instruments. To perform surgical navigation successfully, specialized hardware and software are essential. This includes tracking sensors, imaging devices, and a navigation system responsible for processing and presenting the collected data in a user-friendly way. A technical background of tracking, registration and visualization will be given in the following subsections.

1.2.1. Tracking system

Tracking can be achieved through optical or electromagnetic (i.e. EM) methods. Active optical tracking involves the use of cameras to monitor the position and orientation of instruments fitted with flashing light-emitting diodes. Passive optical tracking relies on cameras detecting near-infrared light, with instruments equipped with retro-reflective markers reflecting the incoming light back to the cameras. While these systems are wireless and offer large working volumes compared to EM systems, they require direct line-of-sight between markers and cameras. In laparoscopic settings, where maintaining a line-of-sight is impossible when tracking inside the patient's abdomen, EM tracking is preferable over optical tracking. Nevertheless, EM tracking is sensitive to interference from ferromagnetic surgical equipment near the field generator, potentially affecting tracking accuracy [52, 53].

EM tracking systems are composed by a field generator, control electronics, and EM sensors. At the NKI-AvL, two types of field generators (FG) are used: the Aurora planar (Figure 1.3) and the tabletop field generator (Figure 1.4). These field generators offer a unique measurement volume (cube and dome), physical design, and mounting choices that suit various EM navigation system workflows and procedures. During surgery, the field generator emits a known EM field geometry, inducing unique voltages within the sensors placed in this field. These voltages are then amplified by the Sensor Interface Unit (SIU), and digitized by the System Control Unit (SCU). The SCU calculates the sensors' positions and orientations, transmitting this data to the host computer [3].

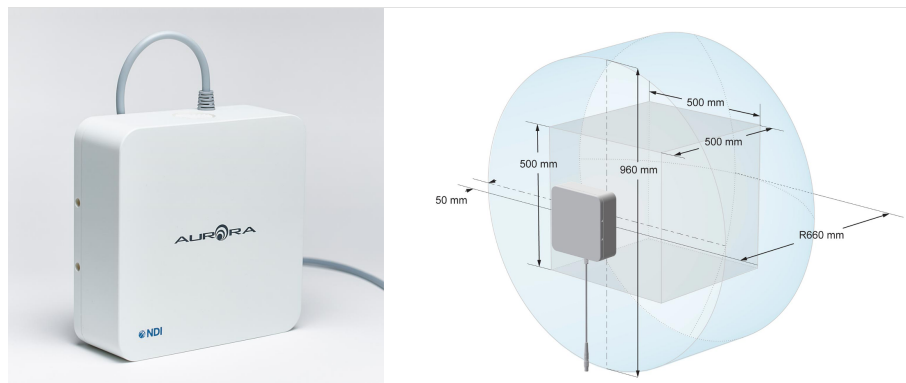


Figure 1.3: On the left side the Aurora NDI planar field generator, with on the right its EM field (cube and dome volume) [3].

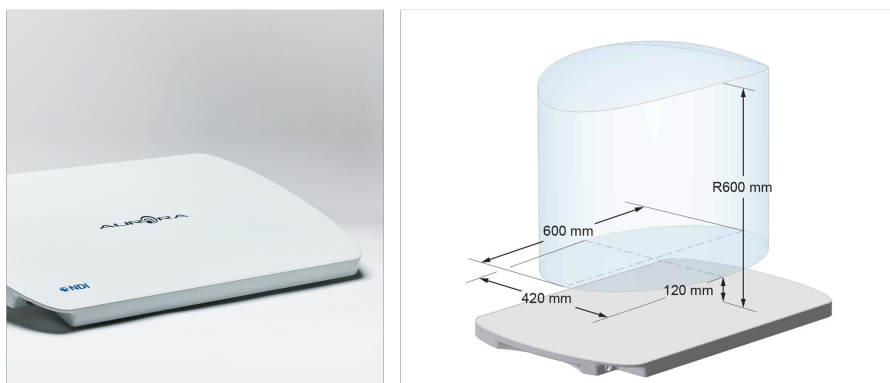


Figure 1.4: On the left side the Aurora NDI tabletop field generator, with on the right its EM field (cube and dome volume) [3].

There are two types of EM sensors: five degrees of freedom (5DoF) and six degrees of freedom (6DoF) sensors. Degrees of freedom represent the number of axes in which changes in position or rotation can be detected. In the case of 5DoF sensors, they provide information on translation in X-, Y-, and Z- positions, along with two orientations in yaw and pitch. On the other hand, 6DOF sensors include an additional orientation measurement (i.e. roll) (Figure 1.5a). 6DoF sensor are preferred when the complete attitude of an instrument needs to be tracked (Figure 1.5b). Due to its compact size, the sensors can be integrated into medical instruments, thereby functioning as localization points in 3D space. In this research, these sensors are embedded into adapters, which are clip-on tools designed

to fit onto surgical instruments in a univocal way. An additional tool that is used during navigation is the Aurora 6DoF Probe, also called surgical pointer (Figure 1.5c). This is a digitizing probe with a rigid, straight metal tip that determines the 3D location of a fiducial in a reference coordinate system. It has an embedded EM sensor, and the position and orientation of the tip are tracked with high accuracy [3, 4].

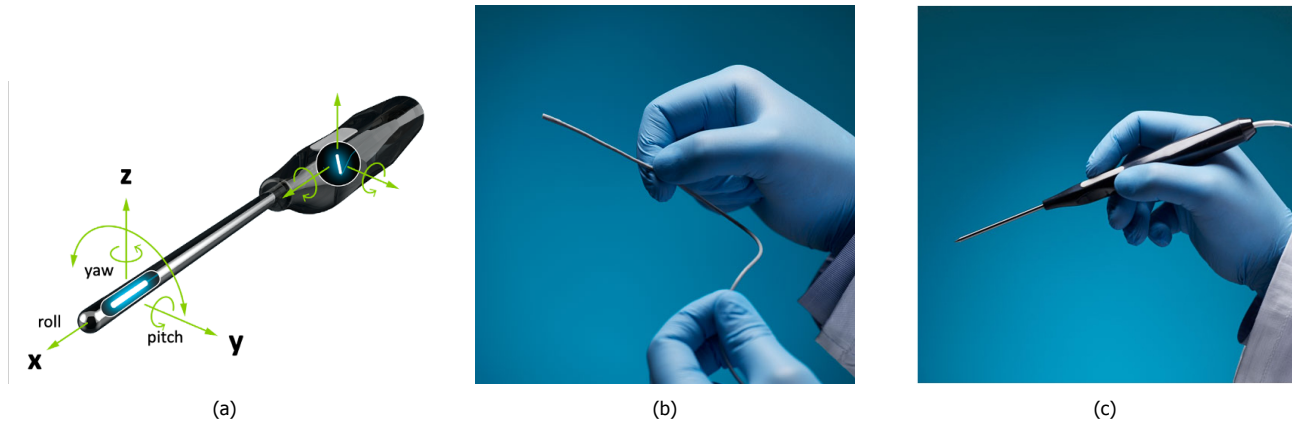


Figure 1.5: (a) The six degrees of freedom in 3D space: three translations (X,Y,Z) and three rotations (roll, pitch, yaw) (b) Aurora 6DoF cable sensor (c) Aurora 6DoF Probe [3, 4]

Electromagnetic tracking systems (EMTS) can be subject to various sources of error. Inaccurate or distorted measurements can have an impact on the overall accuracy of the navigation system, as they propagate through the registration procedure. These inaccuracies can be broadly classified into two distinct types: jitter and error. Jitter refers to the variations or fluctuations in a static measurement over time, which reflect the precision of the measurement. On the other hand, error indicates the accuracy of the measurement and highlights any systematic differences between the measured values and the actual values. A common source of error arises from the presence of ferromagnetic or electrical objects and the limitations of the operating volume. The strength of the EM field is at its highest near the reference point (field generator) but decreases rapidly with the inverse cube of the distance from this point. This characteristic has a significant impact on the positional accuracy of tracking sensors within the measurement volume. In essence, sensors tend to provide more accurate positions when they are closer to the FG, where the induced current is stronger [54].

1.2.2. Image registration

Registration is the process that maps data coordinates, such as images or point locations, from one specific coordinate system to another. This is a crucial step in merging spatial data obtained from different sources. Mathematically, rigid image registration involves finding a 4×4 transformation matrix, denoted as T , that for instance, optimally maps a source image (A) into a target image (B). This transformation matrix comprises a translation vector (${}^B t_A$) and a rotation matrix (${}^B R_A$), which can be combined as the transformation matrix ${}^B T_A$ following Equation 1.1. ${}^B T_A$ describes the transformation from coordinate system A to B, enabling the conversion of points from A (${}^A p$) to B coordinates (${}^B p$) using Equation 1.2. Solving this problem is complex due to the fact that A encompasses seven degrees of freedom (DoF). These include three degrees from the rotation matrix, three from the translation vector, and one attributed to the scaling factor. However, it is important to note that scaling is typically not applied in medical image registration since medical images often share corresponding dimensions (in millimeters) [55].

$${}^B T_A = \begin{bmatrix} {}^B R_A & {}^B t_A \\ 0 & 1 \end{bmatrix} \quad (1.1)$$

$${}^B p = {}^B T_A {}^A p \quad (1.2)$$

In surgical navigation at the NKI-AvL, a similar technique is employed to establish the relationship between the tracked intraoperative ultrasound (IOUS) image coordinate system and the pre-operative coordinate system. The IOUS provides real-time visuals of the organ's position and orientation during surgery. However, a registration is necessary because the coordinate system's origin and axis orientations in the preoperative scan differ from those in the IOUS. The aim is to establish a correspondence between pixel positions in the ultrasound images (p_{US}) and voxel positions within the MR (or CT) volume (p_{MR}). This involves carrying out two registration processes: one from the US probe to the EMTS and another from the EMTS to MR. First, a calibration transformation must be computed that finds the relation between the coordinate system of the US image and that of the tracked US probe, denoted as ${}^{Probe} T_{US}$. This calibration step will be explained later on in this thesis. Subsequently, the EM field generator detects the tracked probe, leading to the transformation ${}^{EM} T_{Probe}$. However, as described earlier, the liver, being a highly deformable organ, moves during the surgical procedure due to respiratory motion and surgical manipulation. To account for

these movements, an electromagnetic sensor is placed, serving as a reference point on the liver's surface. This marker can be positioned near a liver metastasis, allowing for tracking the local movement of the metastatic lesion during surgery. The relationship between the tracked probe and the reference sensor is continually updated through the transformation matrix ${}^B T_A$. Finally, image registration maps the preoperative imaging to the EM field (${}^{MR} T_{EM}$). Figure 1.6 provides an overview of the steps involved in this registration process, while Equation 1.3 illustrates the transformation of a point ${}^{US} p$ to the registered point ${}^{MR} p$ in the preoperative scan.

$${}^{MR} p = {}^{MR} T_{EM} \cdot {}^{EM} T_{Probe} \cdot {}^{Probe} T_{US} \cdot {}^{US} p \quad (1.3)$$

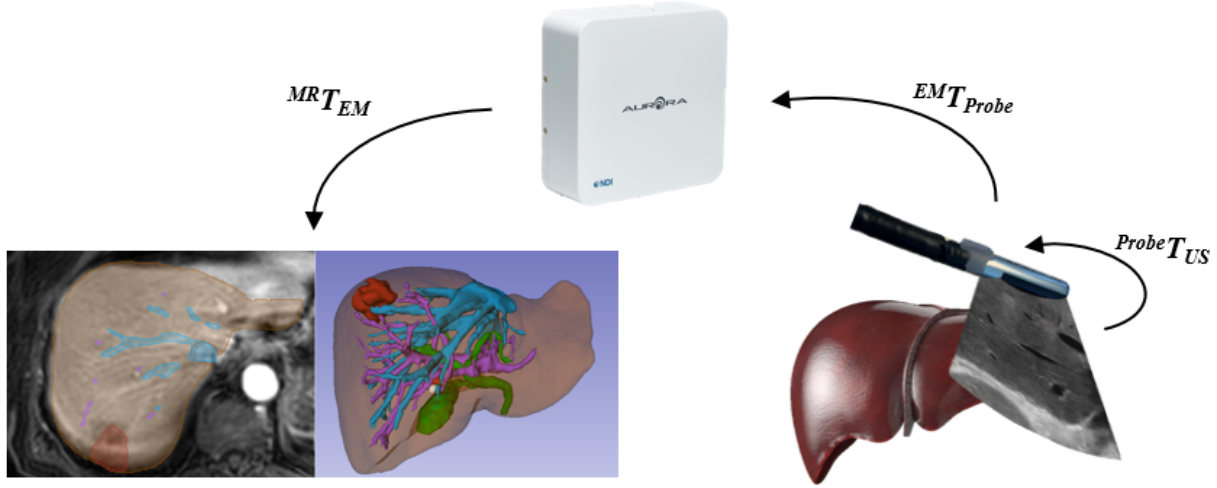


Figure 1.6: Overview of registration steps from preoperative imaging modality to intraoperative ultrasound

To establish ${}^{MR} T_{EM}$ and achieve alignment between the two modalities, mutual information extracted from both the US and preoperative images is needed. Various registration methods can be employed, with a common emphasis on hepatic vessels, which are prominent in both types of imaging. In this institute, landmark-based registration is frequently utilized. Surgeons identify vascular bifurcations (where a vessel divides) in intraoperative US and align them with corresponding points on the preoperative 3D model through rigid registration.

To ensure the safe and reliable implementation of MR-US co-registration, it is essential to assess its accuracy. Several factors can influence the accuracy of image co-registration at various stages of the registration process. In different phases of this study, the reasons for inaccuracies vary, depending on the type of experiment conducted. While qualitative validation of co-registered images relies on subjective evaluation, it is also important to use quantitative methods for evaluating registration accuracy.

Image registration accuracy is commonly defined as the fiducial registration error (FRE), which is, in other words the root mean square error (RMSE) of the mean distances between point-correspondences:

$$FRE = \sqrt{\frac{1}{N} \sum_{i=1}^N (p_{1,i} - p_{2,i})^2} \quad (1.4)$$

Here, the average Euclidean distance between a point $p_{1,i}$ and a transformed point $p_{2,i}$ with sample size N is calculated. This is performed by the iterative closest point (ICP) algorithm that matches the closest points. Nonetheless, the FRE lacks objectivity since the same fiducials used for determining the transformation are also employed to assess the registration. A more impartial measure involves employing distances between points not involved in the registration process, known as targets. This difference between points is directly relevant to the purpose of registration and providing more clinical relevance, indicated by the target registration error (TRE). The TRE is defined as the distance between any point, which is not employed for registration, and its corresponding transformed point. A frequently selected target is a lesion, with the center of mass serving as the basis for this distance calculation. The registration accuracy of these target points is influenced by their positions in relation to the used fiducials, where larger distances usually result in higher TRE values. As a result, the TRE is calculated individually for each point without averaging. To get a single performance measure, the root mean square of the found TREs can be calculated following [55]:

$$TRE_{RMS} = \sqrt{\frac{1}{N} \sum_{m=1}^N TRE_m^2} \quad (1.5)$$

1.2.3. Standard clinical care

At the NKI-AvL, an IGS navigation technique has been developed and is currently applied as standard clinical care for open liver surgery. A study has been published that aimed to assess this navigation workflow and demonstrated an accuracy in landmark-based registration, resulting in a mean FRE of 10.3 ± 4.3 mm and a mean TRE of 8.5 ± 4.2 mm [56, 57]. The current surgical navigation workflow for open liver surgery at this institute can be divided into various preoperative and intraoperative steps. Figure 1.7 visualizes an overview of this workflow.

Preoperatively, 3D models of the liver parenchyma, lesions, hepatic, and portal veins were semi-automatically segmented from diagnostic MR or contrast-enhanced CT scans. Segmentation is performed within the open-source software 3DSlicer (<https://slicer.org>). Image segmentation involves the process of transforming an image into a set of pixel regions, each represented by a mask or labeled image. This enables selective processing of significant image segments, minimizing the need to process the entire image at once. Intraoperatively, ultrasound images are tracked with the assistance of an electromagnetic tracking system. A different open-source software (CustusX, <https://custusx.org>) is employed for the registration process and for presenting the navigation environment.

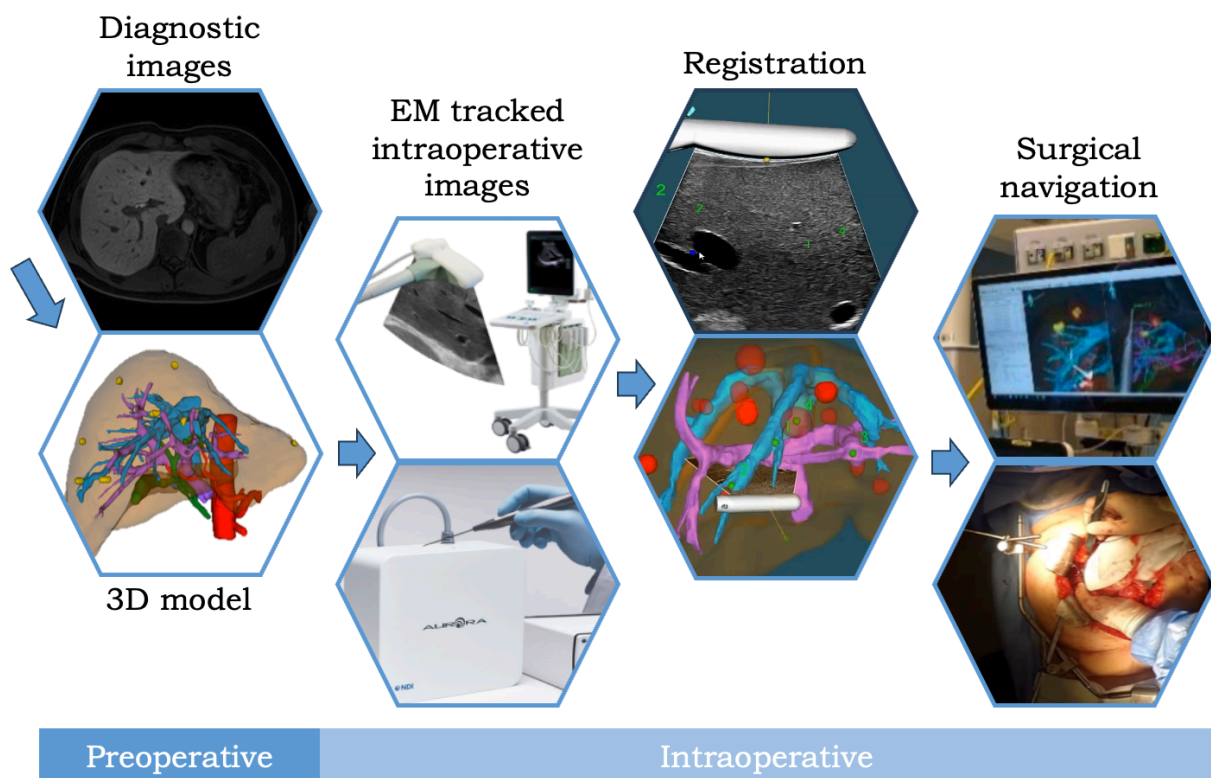


Figure 1.7: Surgical navigation workflow during standard clinical care for open liver surgery

Non-CE marked medical devices involved in clinical research

Surgical navigation systems incorporating in-house developed software and hardware components fall under the category of non-CE-marked medical devices. When such a navigation system is intended for a clinical investigation involving human participants to evaluate its safety and performance, formal approval from a Medical Ethics Review Committee (MERC), also known as the Medisch Ethische Toetsings Commissie (METC) in Dutch, is essential prior to initiating the study. This committee is tasked with ensuring the trial's proper design and ethical acceptability. Compliance with the regulatory framework set by the European Union for medical devices, particularly the Medical Devices Regulation (MDR, 2017) [58], is important in this context. The MDR outlines the requirements for providing information related to clinical investigations that involve medical devices without CE marking.

Under the MDR, medical devices are categorized into four risk-based classes, ranging from Class I (lowest risk) to Class III (highest risk) [59]. This classification system aids regulators, manufacturers, and healthcare professionals in guaranteeing that medical devices adhere to the required safety and performance standards for their intended purposes. It takes into account the vulnerability of the human body and the potential risks associated with the devices.

In brief, these four classes include:

- Class I (low risk) – Medical devices with minimal potential to compromise patient safety. Examples consist of items such as bandages, wheelchairs, and non-powered surgical instruments.
- Class IIa (medium risk) – Medical devices that necessitates periodic evaluation conducted by a recognized regulatory body, such as certain diagnostic devices or surgical clamps.
- Class IIb (medium/high risk) – Medical devices that represent a moderate to higher risk category such as bone fixation devices. Regulatory authorities mandate regular conformity assessments for these devices, which are conducted by recognized bodies.
- Class III (high risk) – These medical devices play a critical role in patient health and life support. This category encompasses equipment vital to the well-being and survival of patients, such as heart valves or neurostimulators.

To ensure a structured presentation of all essential information, the researcher compiles a standard Investigational Medical Device Dossier (IMDD), which is submitted to the METC alongside the research protocol and other pertinent documents.

An important criterion for gaining approval to use the navigation system involves close collaboration with the institution's Clinical Physics and Informatics (CPI) department and the Central Sterilization Department (CSD) department. CPI oversees the safe and effective utilization of the medical device, assessing it for potential technical or mechanical risks associated with its software and hardware components. CSD, on the other hand, ensures the proper cleaning, disinfection, and sterilization of medical devices before their application on patients and evaluates the risks related to the transmission of infections caused by these devices [60]. To secure approval from CSD, medical devices must demonstrate complete sterilizability and therefore follow certain design criteria. Small lumen must be minimized and materials must be resistant to high autoclave temperatures and Sterrad sterilization [61, 62].

1.3. Research objectives

A navigation workflow is already standard clinical practice for open liver resection at this institute. The goal is to extend this approach to laparoscopic procedures. However, before achieving successful implementation, adjustments to the workflow are required, as the laparoscopic setting differs significantly from open surgery in factors such as accessibility to the surgical field and the various instruments to be tracked. Furthermore, approval from the METC must be obtained to allow the start of a clinical research in this field of surgery.

1.3.1. Primary objective

The primary objective of this thesis was to establish a surgical workflow for electromagnetically guided laparoscopic liver resection at the NKI-AvL to be implemented into clinical practice.

1.3.2. Secondary objectives

To achieve this aim, several specific objectives have been identified, taking into consideration the existing navigated liver surgery workflow at this institution. These objectives are outlined below:

- Development of a tracking method for the laparoscopic sealer/divider (Chapter 2).
- Development of a fast calibration method for the laparoscopic ultrasound probe (Chapter 3).
- Establishing a validation procedure to assess navigation accuracy and workflow in navigated laparoscopic liver resection (Chapter 4).

Tracking of laparoscopic instruments

This chapter describes the tracking of the instruments used during laparoscopic surgery to achieve surgical navigation. These instruments include a laparoscopic ultrasound (i.e. LUS) probe, a laparoscope and a laparoscopic sealer/divider. Adapters to electromagnetically track the LUS probe and the laparoscope have been developed in previous research. This chapter focuses on the design, calibration, and validation of an adapter specifically for tracking the laparoscopic sealer/divider. Calibration was performed using a calibration device, and the validation process includes the evaluation of its usability, sterilizability, reproducibility in attachment, and calibration accuracy.

2.1. Introduction

Laparoscopic instruments are extended surgical tools that are inserted in the patient's abdomen through a trocar. Tracking provides information on the location and orientation of the laparoscopic instruments in the operating room. These instruments have different appearance and therefore require unique designed adapters containing the EM sensor for tracking. 3D printing provides the advantage of in-house developing and rapid prototyping of an adapter that is compatible both with the laparoscopic instruments and the EM sensors currently employed at the NKI-AvL for surgical navigation, specifically the Aurora 6DoF cable sensor (NDI, Waterloo, ON) (as depicted in Figure 1.5b). The tracking accuracy of these EM sensors, is reported in Table 2.1 [3, 4].

Table 2.1: Root Mean Squared (i.e. RMS) errors of Aurora 6DoF sensor in orientation and position, alongside two volumes of the field generator (FG) [3]

	Cube Volume FG (RMS)	Dome Volume FG (RMS)
<i>Position (mm)</i>	0.48	0.70
<i>Orientation (°)</i>	0.30	0.30



(a) Laparoscope (Endoeye 0°, Olympus) [63]



(b) Laparoscopic Ultrasound probe (BK5000, I12C4f) [64]



(c) LigaSure Maryland (Covidien, Medtronic) [65]

Figure 2.1: Laparoscopic instruments used during laparoscopic surgery

2.1.1. Laparoscope

The laparoscope is an instrument utilized to visualize the abdominal cavity, and at the NKI-AvL, the Endoeye with a 10 mm diameter 0° viewing angle (Olympus, Tokio, Japan) is used in the clinical routine (Figure 2.1a). It comprises an optical system, consisting of a high-resolution camera and a light source, resulting in high-quality video-feed of the abdominal cavity [66]. The video feed from the camera is displayed on a monitor, allowing surgeons to perform the surgery.

An adapter has been developed in a previous project at the NKI-AvL [67]. The 3D model of the design is shown in Figure 2.2a. The 3D-printed adapter consists of an upper and lower part, the former containing an EM sensor, and fits on the handle of the instrument, as shown in Figure 2.2b and 2.2c. The sensor is placed in the extended part of the adapter, closer to the laparoscope's tip, enabling freedom of movement around the trocar. By locating the sensor closer to the laparoscope's tip, tracking accuracy is expected to improve, since calibration errors will be less magnified by the tracking errors. During laparoscopic surgery, this instrument is placed inside a sterile cover, eliminating the need for sterilization and consequently simpler biocompatibility validations are required.

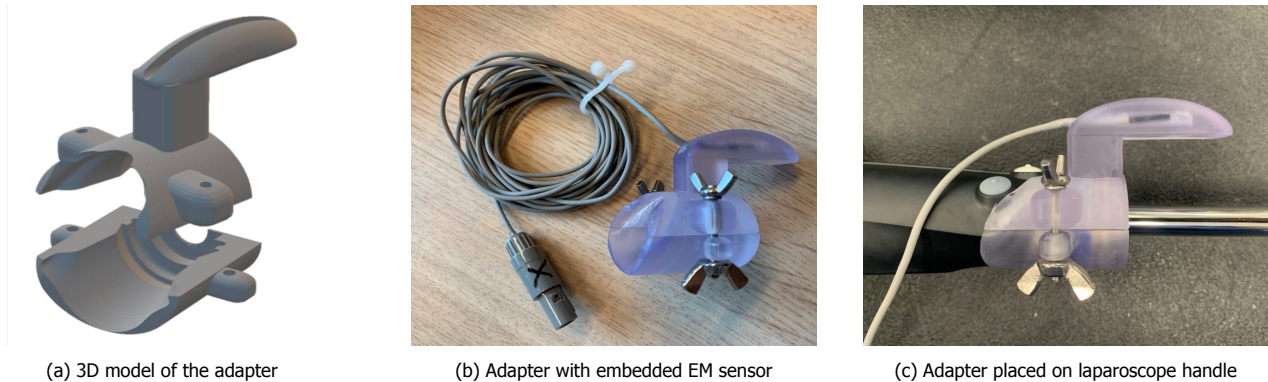


Figure 2.2: In-house developed adapter of the laparoscope

2.1.2. Laparoscopic ultrasound

During laparoscopic surgery, the laparoscopic ultrasound probe (model I12C4f) and a BK5000 Ultrasound system (BK Medical, Herley, Denmark) are used as intraoperative imaging modality for the assessment of the hepatic anatomy (Figure 2.1b). To track the LUS, an adapter containing an EM sensor which attaches to the flexible tip was developed at the NKI-AvL. The 3D model and final 3D-printed adapter containing an EM sensor are shown in Figure 2.3a and 2.3b. The adapter is placed on the tip of the US probe using a click-fastener mechanism (Figure 2.3c). As for the laparoscope, this adapter is enclosed within a sterile cover during laparoscopic liver surgery.

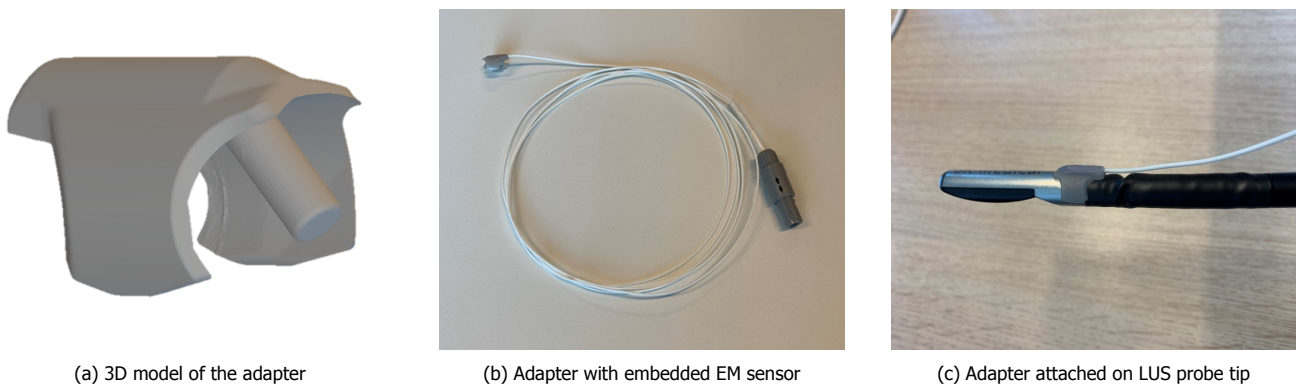


Figure 2.3: Adapter of laparoscopic ultrasound (LUS) probe

2.1.3. Laparoscopic sealer/divider

An adapter containing an EM sensor for the laparoscopic sealer/divider, also referred to as "LigaSure Maryland" or "LigaSure" (Medtronic, Minneapolis, USA) (Figure 2.1c) was developed and validated. This instrument allows surgeons to grasp, seal and cut liver tissue during laparoscopic surgery. The shaft of the instrument can be rotated to change the orientation of the tip. Additionally, when using the handle to engage the tip, the shaft moves back and forth. Its cylindrical shaft is inserted into the trocar.

Electromagnetic tracking of the instrument offers two viable options: monitoring either its tip or its proximity to the handle. Optimal tracking occurs at the tip, where any shaft bending exerts minimal influence on the tip's position, ensuring limited lever-arm effect and enhanced precision in tracking and navigation. This advantageous approach mitigates the amplified impact of tracking and calibration errors on points distant from the tracked frame, in contrast to nearby points [68]. However, challenges arise when aiming to track the instrument's tip. An adapter affixed to the tip must traverse the trocar's opening, a task similarly faced by the wired EM sensor. Consequently, the adapter's design cannot significantly increase the shaft's diameter. Additionally, heat generated at the tip poses a concern, potentially affecting the adapter's material. These complexities result in a preference to position the adapter closer to the handle of the instrument. Nevertheless, this adjusted location is unlikely to substantially compromise navigation accuracy, as the primary objective is to ascertain the tip's spatial position for navigation purposes. Thus, evaluating calibration accuracy across various positions became necessary to pinpoint the adapter's final placement. The subsequent section delves into the development process and the validation techniques employed for tracking the laparoscopic sealer/divider adapter.

Table 2.2: Risk assessment and requirements list

Hazards	Causes	Risk estimated	Requirements
Infection	Contaminated/ unsterile adapter	Sepsis	<i>Materials</i> Adapter should be made from a sterilizable material. The glue used for attaching the sensor is suitable for the material of the adapter as well as the silicon of the Aurora cable. <i>Design</i> The design does not contain any lumen except for the opening for sensor placement. The remaining space should be filled entirely with glue to avoid unsterile areas.
Toxic reaction contact materials	Sensitive to contact materials	Toxic reaction	<i>Materials</i> Material should be selected on biocompatibility.
Incorrect attachment to LigaSure	Human error	Calibration is not valid	<i>Design</i> The design ensures that the adapter can be securely attached to the instrument to ensure accurate calibration. The attachment should be reproducible.
High tracking error	Distortion of EM field	Incorrect visualization in software	<i>Materials</i> The material of the adapter is non-ferromagnetic (does not influence EM field).
	Movement of adapter or sensor	Calibration is not valid	<i>Design</i> The design allows for the containment of the Aurora 6DOF EM sensor (NDI, Waterloo, ON) and ensures no sensor movement No movement between adapter and LigaSure shaft after attachment to ensure accurate calibration.
Breaking	Material failure	Debris in surgical field	<i>Materials</i> Should not break during attachment or detachment. Adequate material should be used (stainless steel).
Influence on workflow	No causes foreseen/ design failure	Failure of LigaSure, new tool required Damaging trocar, gloves, sterile covers	<i>Usability</i> Adapter position does not hinder the standard handling of the LigaSure. Assembling onto LigaSure takes less than one minute without extensive training. Easy to attach and detach without damaging sensor or LigaSure. Does not have sharp edges that could rupture surgical gloves, sterile covers or damage the trocar.

2.2. Methodology

A risk assessment was initially conducted to list a set of requirements that the adapter must meet. Subsequently, the requirement list was utilized to determine the adapter's design, taking into account aspects such as the material, design and usability. The risks, causes and requirements are listed in Table 2.2. To summarize the table, important aspects taken into consideration during the design process are:

- The material of the adapter should be sterilizable, biocompatible and non-ferromagnetic.
- The design of the adapter should be user-friendly and not significantly interfere with the clinical workflow.
- The adapter should be easy to attach in a univocal way and ensure that the sensor remains fixed to the instrument.

2.2.1. Adapter design and production

Location determination of adapter

The main hypothesis in determining the adapter's location on the sealer/divider is that the closer the EM sensor is to the instrument's tip, the higher its tracking accuracy. To test this hypothesis, the adapter was placed on three different locations: middle (Figure 2.4a), proximal (Figure 2.4b) and parallel (Figure 2.4c). The parallel location implies that the sensor is mounted at a distance from the shaft of the instrument with a stable construction. If it is determined that positioning the sensor in closer proximity to the tip results in improved accuracy without degradation in a parallel configuration, it may be feasible to consider a parallel design. In such a design, the sensor could be positioned near the tip without obstructing the instrument's movement through the trocar, similar to the design of the laparoscope adapter (Subsection 2.1.1). An intraoperative setting is demonstrated in a study by Liu et al. [5], as shown in Figure 2.5. It was decided not to test the location of the adapter at the very tip because it interferes with the surgical workflow. Eventually, a tip-to-tip measurement was performed to test the calibration accuracy where a pointer was used to touch the tip of the LigaSure (Figure 2.6).

First, the adapter was calibrated using the method that will be described in Section 2.2.2. To obtain a quantitative measure for the calibration accuracy, the CustusX software (SINTEF, Trondheim, Norway) was used to visualize the residual distance between the pointer and the tip of the LigaSure. At both tips a marker was placed within the software and a distance measure widget was selected. This process was repeated three times for each location, with the adapter recalibrated to ensure consistent calibration. The results are reported in Table 2.3. The different locations had no significant impact on accuracy, as the mean accuracies varied approximately within the range of the tracking error of the EM sensor (Table 2.1).

The adapter will be placed close to the handle, as it has the highest probability of not interfering with the surgical workflow. Based on this decision, the following subsection will show the design and development process of the adapter that will be located in proximity of the handle.

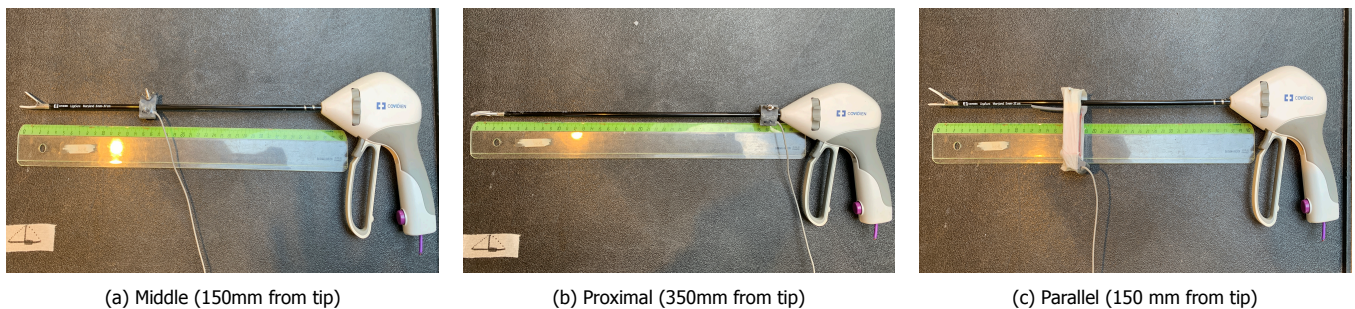


Figure 2.4: Accuracy of sensor tested at different locations attached to the laparoscopic instrument



Figure 2.5: Adapter design with a parallel location of the sensor [5]



(a) Pointer touching the tip of the LigaSure

(b) Distance visualized in CustusX software

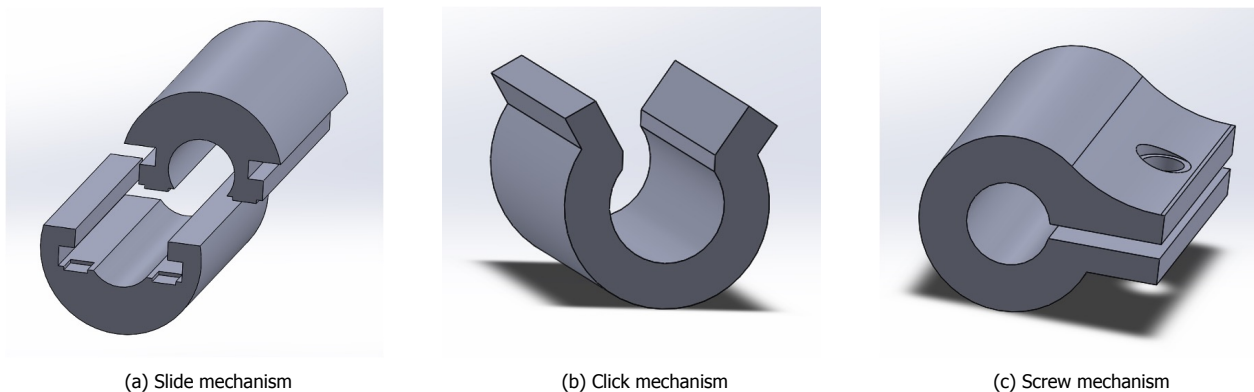
Figure 2.6: Tip-to-tip test with surgical pointer to assess calibration accuracy

Table 2.3: Results of three different calibrations for different sensor location

	Middle (mm)	Proximal (mm)	Parallel (mm)
Calibration 1	2.3	3.0	2.5
Calibration 2	2.9	1.7	3.4
Calibration 3	2.5	3.0	2.1
Mean \pm SD	2.6 \pm 0.3	2.6 \pm 0.8	2.7 \pm 0.7

Determination of the design

To design the adapter, Solidworks 2023 was used (Dassault Systèmes, <https://www.solidworks.com/>). To create prototypes, the Formlabs Form 3B 3D printer was used. This 3D printer employs the Stereolithography (SLA) technique, using a laser to solidify photopolymer resin. With the help of an ultraviolet (UV) laser, the printer accurately replicates the shape of the initial layer from the 3D model, and the photopolymers harden under UV light exposure. As each solidified layer detaches from the resin tank, a new layer forms, and the process is repeated until completion [69]. The different prototypes that were created and tested, each containing different locking mechanisms, are shown in Figure 2.7. A distinction was made between a slide (Figure 2.7a), click (Figure 2.7b), and screw mechanism (Figure 2.7c). The final design was determined in collaboration with technical physicians and surgeons. After consultation, it was decided that the closing system with a screw was preferred, with the assurance of stability being the decisive factor.



(a) Slide mechanism

(b) Click mechanism

(c) Screw mechanism

Figure 2.7: Different locking mechanisms for the adapter enclosing the shaft

Production of adapter

The final adapter was produced using a different technique from SLA, namely Computer Numerical Control (Computer numerically controlled) machining, performed by a medical instrument developer (Medex, Almere, The Netherlands). This manufacturing technique is a metal fabrication method where pre-programmed computer software controls machining instruments such as lathe and drills [70]. CNC machining involves a subtracting manufacturing approach that removes material from a substrate and achieves higher levels of accuracy than SLA [71]. Using this technique was decided due to sterilization requirements that were not met by using the resin accessible at the NKI-AvL.

The final adapter produced by Medex needed to obtain approval from the CSD of the NKI-AvL. The sterilization process involves gas plasma sterilization using the STERRAD™ system (Advanced Sterilization Products (ASP), CA, USA) [62]. This method utilizes a combination of hydrogen peroxide (H₂O₂) and low-temperature gas plasma that sterilizes medical devices and materials. The radiofrequency plasma breaks down the hydrogen peroxide, creating a plasma cloud consisting of UV light and free radicals. This combination effectively eliminates all bacteria, ensuring

sterilization. After sterilization, the plasma energy is deactivated, free radicals return to a stable state and recombine into non-toxic byproducts like oxygen and water vapor [62]. Compared to others, this sterilization method offers two advantages: the adapters can be sterilized within our institute, allowing them to be ready for use within a few hours, and the STERRAD™ system avoids high temperatures or pressure, minimizing the risk of potential damage to the sensor inside the adapter [6].

2.2.2. Calibration

To determine the instrument's location and alignment within the 3D environment, an initial calibration of the adapter must be performed. This implies determining the relationship between the sensor in the adapter and the tip of the instrument. Due to the fact that the EM sensors are affixed within the adapters with glue, each individual adapter required its own calibration, owing to variations in the sensor's orientation within the adapter. A schematic overview of the different coordinate systems and corresponding transformations for this calibration process is illustrated in Figure 2.8. Calibration matches the position and orientation between both coordinate systems by finding the static transformation between the tip of the instrument and the EM sensor attached to the adapter (${}^{EMsensor}T_{Tip}$ from Figure 2.8).

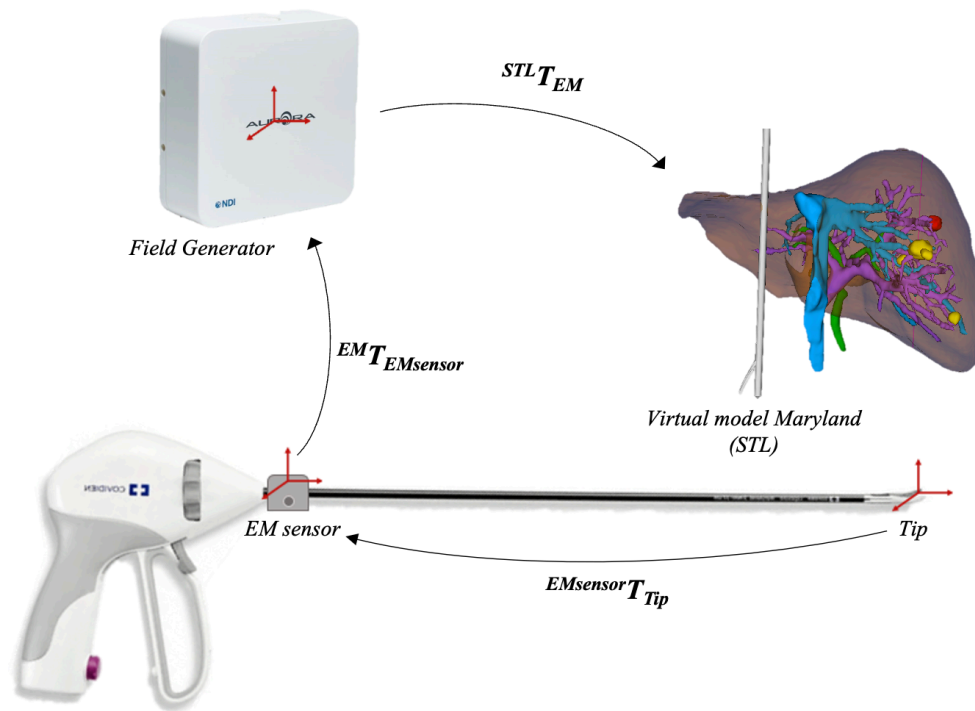


Figure 2.8: Coordinate systems with corresponding transformations for the LigaSure adapter calibration

The calibration process for the LigaSure adapter involved utilizing a calibration device (Figure 2.9). This is a 3D-printed tool which can be tracked due to an attached EM sensor. It was developed in a previous project at NKI-AvL and allows for the insertion of the tip of the instrument [72]. By placing the instrument in the calibration device, in a specific configuration, the transformation between the instrument's tip and the EM sensor can be calculated.

A software module was previously developed for integration within the 3D environment of the software 3D Slicer. This module enables the calculation of the transformation matrix by using a calibration button. The module utilizes the tracking data, calibration of the device itself and a tip location as described in Equation 2.1 [72]. In this equation, 'Maryland' refers to the adapter containing the EM sensor, and 'Sensor' refers to the sensor of the calibration device. Consequently, a new transformation matrix is added within the software. By assigning it to the virtual model (performing the transformations ${}^{EM}T_{EMsensor}$ and ${}^{STL}T_{EM}$) the integration within the software is possible so that it can be used for navigation. Figure 2.10 illustrates the calibration process, where the top view displays the 3D environment before (Figure 2.10a) the calibration button was pressed, and the bottom image displays the 3D view after the calibration (Figure 2.10b).

$${}^{Maryland}T_{Tip} = {}^{Maryland}T_{EM} \cdot {}^{EM}T_{Sensor} \cdot {}^{Sensor}T_{Tip} \cdot \begin{bmatrix} 0 \\ 0 \\ 0 \\ 1 \end{bmatrix}_{Tip} \quad (2.1)$$

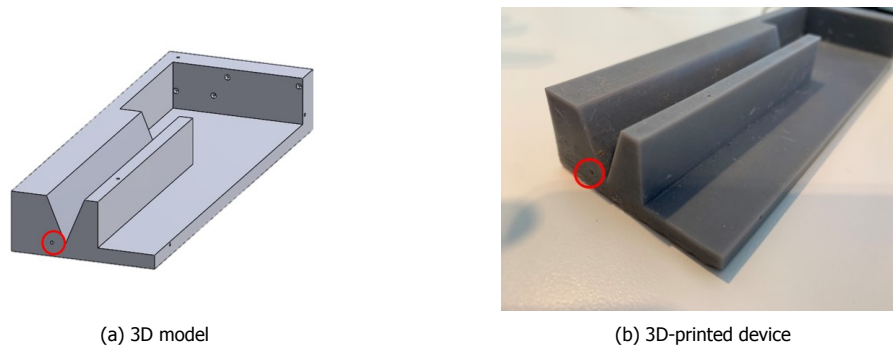


Figure 2.9: Calibration device used for calibration of the LigaSure adapter with a red circled divot

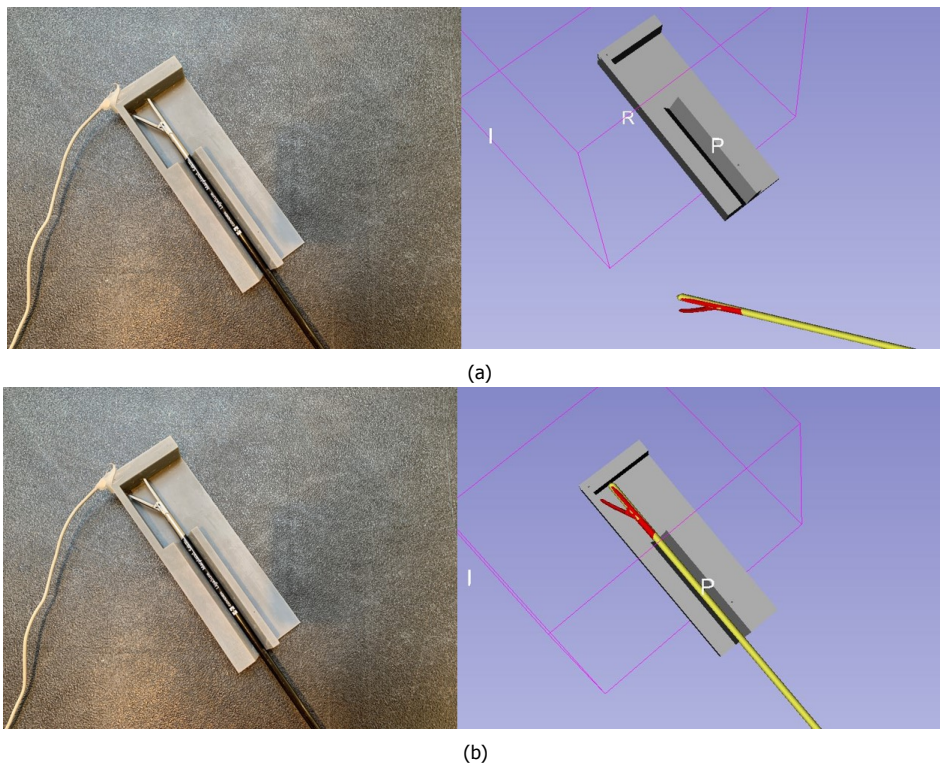


Figure 2.10: Actual and 3D Slicer view of the tracked calibration device and tracked LigaSure before (a) and after (b) calibration of the adapter

2.2.3. Validation

Reproducibility of attaching the adapter

To use the same calibration matrix for an adapter without having to recalibrate it every time it is reattached to the laparoscopic instrument, it is crucial to ensure that the adapter consistently attaches to the same position each time. To verify this, a reference sensor was attached to the handle of the LigaSure. The aim of this experiment is to find the transformation (${}^{EM_{sensorReference}}T_{EM_{sensorAdapter}}$) between the reference sensor and the sensor of the adapter (Figure 2.11). If the transformation between this reference sensor and the sensor of the adapter remains consistent each time the adapter is reattached, it can be concluded that repeating the calibration is unnecessary.

Given the cylindrical nature of the instrument's shaft, achieving a univocal attachment of the adapter can pose a challenge. To address this, an user guide has been devised to optimize this process, comprising the following steps:

1. Rotating the instrument's tip completely to the left using the turning wheel.
2. Fixating the adapter onto the shaft while aligning its center with a slot on the handle.
3. Tightening the screw to secure the adapter in place.
4. Engaging the handle, causing the shaft to move, and resulting in a slight forward movement of the adapter.
5. Reaffirming the tightness of the adapter screw to ensure secure fixation.

To test the reproducibility of attaching the adapter, a test was conducted by three individuals, with each person attaching the adapter to the instrument ten times. Of these three individuals, two were inexperienced in attaching the adapter and received instructions beforehand.

The test comprised the following steps:

1. Attachment of the adapter on the shaft of the instrument.
2. Positioning of the instrument in the center of the electromagnetic field.
3. Recording of the position and orientation of both sensors for five seconds.
4. Detachment of the adapter.

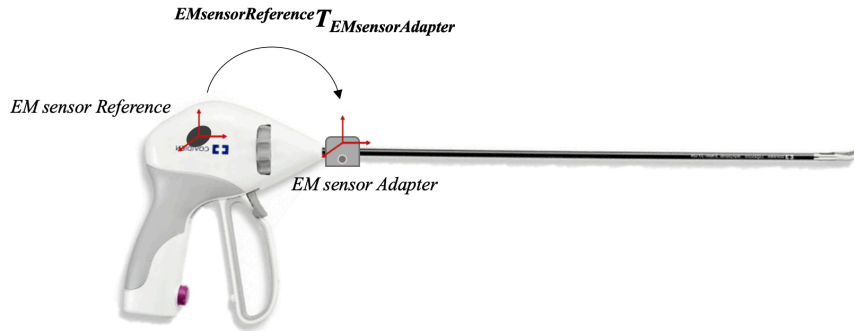


Figure 2.11: Testing the reproducibility of attaching the adapter

These steps were repeated ten times. The sensors' position and orientation were averaged over a five-second recording period to filter jitter errors. The averaging of transformations was achieved by calculating the mean of translations and averaging quaternions for rotations [73]. A quaternion represents a 3D orientation and rotation by coding the axis-angle representation. It has the advantage of enabling quaternion multiplication, which allows for the easy accomplishment of sequences of rotations [55]. Subsequently, standard deviations were calculated to assess the variations in transformations among the ten measurements, utilizing both Euclidean distances and Euler

angles as measures. The Euclidean distance between a point $p_1 = \begin{bmatrix} x_1 \\ y_1 \\ z_1 \end{bmatrix}$ and point $p_2 = \begin{bmatrix} x_2 \\ y_2 \\ z_2 \end{bmatrix}$ can be calculated using Equation 2.2. Euler angles represent rotation around one of the three axes in 3D space (R_x, R_y, R_z) [55].

$$d(p_1, p_2) = \sqrt{(x_1 - x_2)^2 + (y_1 - y_2)^2 + (z_1 - z_2)^2} \quad (2.2)$$

Calibration accuracy

The calibration accuracy of the adapter was evaluated and compared to the Aurora 6DoF surgical pointer (NDI, Waterloo, Ontario, Canada). The accuracy obtained with the pointer was used as a gold standard. Because an in-house developed laparoscopic pointer will be used during laparoscopic procedures, its accuracy was also assessed. This device functions similarly to a surgical pointer, featuring an EM sensor at its tip to achieve accurate tracking. Nonetheless, it has a longer length, a sensor located slightly beyond the tip and a less sharply pointed tip.

For accuracy assessment, the calibration device described in the previous subsection was used (Section 2.2.2). This tracked device contains ten small divots that are defined as landmarks for registration (Figure 2.9). Then, the surgical pointer, the calibrated LigaSure and the laparoscopic pointer were used to digitize these divots (Red divots in Figure 2.12) on the calibration device and new landmarks were defined when the instruments touches the actual divots (Blue divots in Figure 2.12). Subsequently, the "fiducial registration wizard" module in 3D Slicer was utilized to perform an iterative closest point registration, aiming to minimize the difference between the two point clouds. The registration process resulted in a RMSE expressed in millimeters for all instruments.

Error management

Numerous factors can contribute to inaccuracies in assessing calibration precision. To address this concern, supplementary measurements were conducted to facilitate the formulation of definitive conclusions, accounting for these influential variables. To ensure the robustness of various calibration approaches, the LigaSure instrument underwent three separate registration procedures. In each iteration, the adapter was recalibrated following reattachment. However, complications arose due to the significant spatial separation between the calibration tool and the LigaSure adapter. This discrepancy caused the sensors to traverse the outer boundaries of the Planar field generator's measurement volume. Consequently, a phenomenon akin to 'flickering' was evident, wherein the tracking data exhibited oscillations even when the sensor was held stationary. This introduced complexities in the registration process, as the 3D Slicer instrument model failed to remain fixed. This instability bore the potential to induce substantial deviations in locating the blue divot, consequently influencing the RMSE. Given that the planar field generator has the most extensive measurement volume, alternative field generators were unsuitable. Despite employing the tabletop

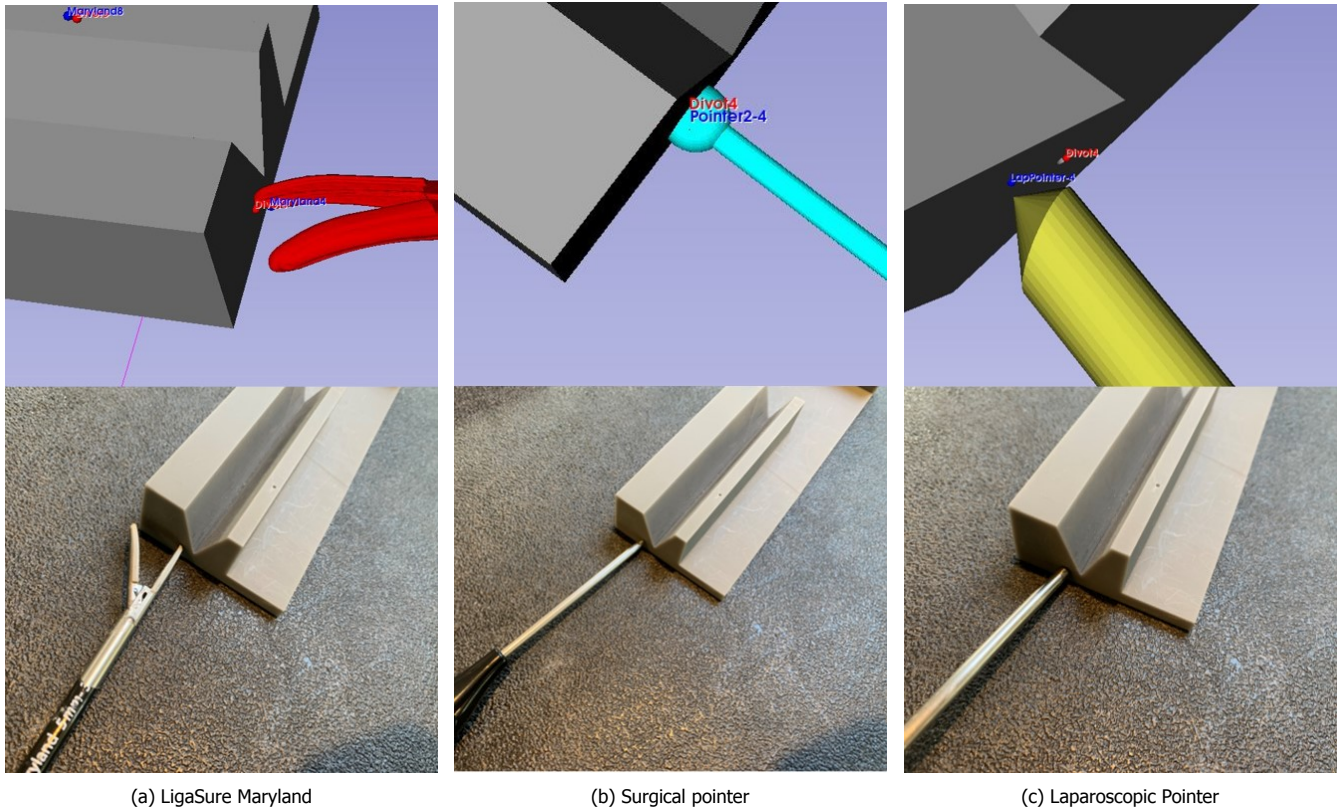


Figure 2.12: Indicating divots on calibration device. The top images depict the 3D environment in 3D Slicer software, while the bottom images show actual views

field generator in an attempt to mitigate the issue, the results proved inconclusive.

To investigate the hypothesis that sensor placement within the measurement volume caused the ‘flickering,’ adjustments were made. By positioning the adapter nearer to the tip, the two sensors were aligned more centrally within the electromagnetic field. Consequently, the identification of divots displayed reduced flickering, attributed partially to the mitigation of the lever-arm effect. This experiment indicated that locating sensors at the periphery of the electromagnetic field could indeed give rise to the observed instability.

Another issue that could increase the error is the fact that the tip of the LigaSure is not completely straight and has a slight curve. Therefore, the calibration accuracy could show a deviation between the actual tip position and the divots on the calibration device used to calculate the transformation between the tip and the adapter. This deviation might be due to practical challenges in measuring non-symmetric instruments with a caliper (measuring instrument for cylindrical shafts). To investigate whether a perfectly straight instrument could yield better accuracy, the accuracy of the laparoscopic pointer was evaluated. The adapter was attached to the shaft and calibrated using the calibration device as described in Section 2.2.2 (Figure 2.13). Subsequently, the fiducial registration was repeated for this setup and the root mean squared error was calculated.



Figure 2.13: Adapter attached on shaft of Laparoscopic Pointer

2.3. Results

2.3.1. Adapter design and production

The final design of the adapter is shown in Figure 2.14 and a technical drawing of the final design can be found in Appendix B. The adapter was CNC-machined by Medex (Almere, The Netherlands) from stainless steel 360L, which is a sterilizable, biocompatible, and non-ferromagnetic material. The decision was made to glue the EM sensor within an opening in the adapter. This opening fills up the available space for the sensor. As a result, the entry of bacteria and microorganisms is prevented, addressing challenges related to sterilization. The design features a cylindrical hole that needs to be slid over the instruments' shaft first and then tightened with a screw. The design was adjusted by adding two holes above the part that encloses the shaft of the LigaSure (Figure 2.14a). This was done because it allows the rigid material to be more flexible and fit more tightly around the shaft, preventing any movement once the screw is tightened. The EM sensor is positioned at the top side of the adapter. The smooth finish ensures no inconvenience to the surgeon during the attachment process and while using the laparoscopic instrument.



Figure 2.14: Final design of LigaSure adapter

2.3.2. Validation

Sterilization and usability

The adapter was approved for sterilization by the CSD of the NKI-AvL. Following a brief instruction, both a surgical nurse and a surgeon were able to securely attach the adapter to the LigaSure. This attachment process was completed in less than ten seconds and repeating resulted in a steep learning curve.

Reproducibility of attaching the adapter

The standard deviations calculated for the three measures over the reproducibility tests are shown in Table 2.4. The inaccuracy in position of the adapter attached by the three individuals is within the tracking accuracy range of the sensor, as indicated in Table 2.1. This suggests that the position of the adapter remain consistently similar with each attachment. The SD for rotation exhibited greater deviations along two axes (y and z). These deviations resulted from challenges in aligning the adapter with the handle visually and variations in how the tip is positioned when placing the instrument on the table. However, considering that the tip's position is of more importance than its orientation, the result of deviation in position holds greater significance.

Table 2.4: Standard deviations (SD) of Euclidean distance and Euler angles of difference between adapter sensor and reference sensor after repeatedly reattaching the adapter by three individuals

	Individual 1	Individual 2	Individual 3
SD Euclidean distance (mm)	0.15	0.18	0.13
Euler angles			
SD Rx (°)	0.08	0.2	0.5
SD Ry (°)	2.3	1.1	4.5
SD Rz (°)	1.31	0.8	3.1

Calibration accuracy

The boxplots in Figure 2.15 depict the results of the fiducial registration using the LigaSure adapter, the surgical pointer, the laparoscopic pointer and the laparoscopic pointer with the adapter attached for indicating the divots on the calibrated device. Registration was repeated three times for each device. The adapter of the LigaSure demonstrated an accuracy of 2.5 mm, which was higher than the accuracy of the surgical pointer (1.1 mm) or the laparoscopic pointer (1.4 mm). This could indicate that the calibration method or the location of the adapter on the

instrument, which might influence the tracking accuracy, could be contributing factors affecting the accuracy. However, the transformation matrix from the calibration device's sensor to the tip of the LigaSure is significantly smaller, resulting in less influence if computed incorrectly, compared to the transformation from the tip to the Ligasure's adapter, which covers a distance of approximately 35 mm. A minor tracking error of the EM sensor can result in a significant error in the tip's position, which can be attributed to the lever-arm effect.

In Subsection 2.2.1, a tip-to-tip measurement was conducted to evaluate the calibration accuracy of the adapter at various locations along the shaft of the Ligasure instrument. One limitation of this test is the presence of a systematic error. This error encompasses the challenge of consistently indicating the tip of the LigaSure with the surgical pointer. Consequently, the method described in subsection 'Calibration Accuracy' (2.2.3) is more reliable. To evaluate the impact of the adapter's location, this calibration method was repeated for a position closer to the tip. Eventually, the calibration accuracy at this location was similar to the accuracy of the surgical pointer (1.7 mm). Therefore, the distance of the adapter is a determining factor that influences the calibration accuracy. However, the exact accuracy could not be established because of the distance between the sensor of the calibration device and the sensor of the adapter, exceeding the measurement volume of the field generator.

Another observation apparent from the boxplots in Figure 2.15, is that the mean registration error of the LigaSure was comparable to the accuracy achieved when the adapter was attached to the laparoscopic pointer. This suggests that the curved tip of the LigaSure does not significantly impact the calibration accuracy. Furthermore, the large standard deviation in the registration error of the laparoscopic pointer with the adapter could suggest that in combination with the significant flickering issue, precise indication of the divots is challenging due to the less sharp tip of the laparoscopic pointer.

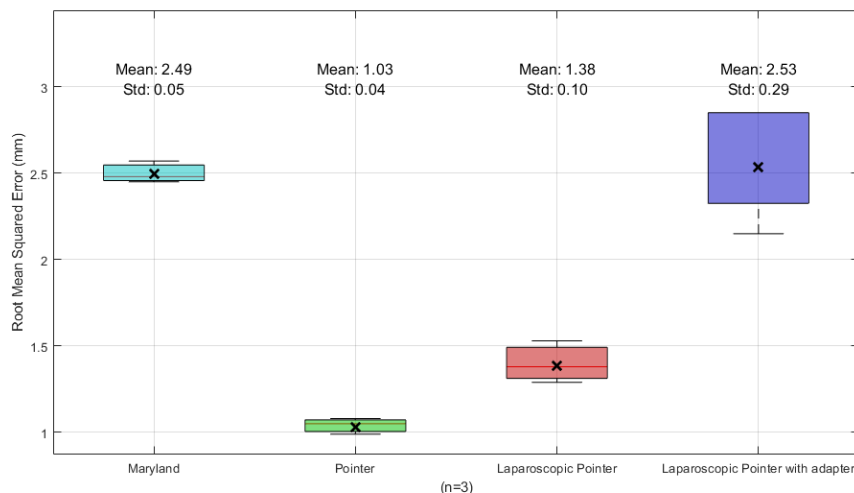


Figure 2.15: Results of four calibration accuracy tests using the LigaSure, Pointer, Laparoscopic pointer and the Laparoscopic pointer with the adapter. Boxplots shows the median, quartiles and the cross indicates the mean

2.4. Discussion

An adapter was developed to track the resection tool LigaSure. The adapter meets the design requirements as it is made from a non-ferromagnetic material, is sterilizable, and can be easily attached to the instrument by the surgeon and surgical nurse. Additionally, the reproducibility of attachment showed positive results. The calibration accuracy was not within the range of the tracking error of the EM sensor, nor was it comparable with the gold standard. Therefore, it requires further improvement to be effectively used for guidance of laparoscopic liver resection. However, this discrepancy can be influenced by various factors. Consequently, it is essential to recognize limitations related to the adapter's location, calibration method and accuracy assessment.

2.4.1. Adapter location

The development of an adapter for the LigaSure posed multiple challenges. These challenges arose from its cylindrical shape, rotational movement, and back-and-forth motion, along the requirement to navigate through a trocar. Developing an adapter that can securely attach to the instrument without disrupting the workflow proved to be a demanding task. As described in Subsection 2.2.1, locating the sensor in a parallel position was considered. This approach could offer the advantage of positioning the adapter closer to the tip without significantly disrupting the clinical workflow. However, due to the extended arm, it could potentially result in reduced stability and increased mobility during surgery, which might adversely affect navigation accuracy. Therefore, the decision was made not to opt for such a design; however, it should be noted that the location could have influenced the navigation accuracy.

2.4.2. Calibration, tracking and registration

Regarding the calibration of the adapter, it is important to take into account that there are various calibration methods, each with its own advantages and disadvantages. It was decided to utilize the in-house developed calibration device due to its fast measurement, ease of use and accuracy. Additionally, an advantage is that this method provides the orientation with respect to the sensor, in addition to just the tip location. The LigaSure is a non-symmetrical device, making it necessary to calibrate the orientation in addition to the translation. One drawback is that the calibration method does not address jitter error due to its reliance on a single data point. Utilizing multiple data points for calibration could enhance accuracy. In addition, the calibration method is limited by its inapplicability during surgery. The current version lacks sterilization capability, making it unsuitable for surgical use. The next step is creating a version of this device using a sterilizable material. However, since the reproducibility test yielded positive results, it is also feasible to pre-calibrate the adapter and subsequently use this calibration during surgery without the need for recalibration. Nevertheless, it should be taken into account that the sensors glued in different adapters can also have varying orientations. As a result, different calibration matrices should be determined for different adapter versions.

Furthermore, tracking inaccuracies significantly impact the navigation accuracy. One factor contributing to errors is damaged electromagnetic sensors. Nonetheless, detecting damage resulting from excessive bending or cracking of receiver wires can be challenging [54]. Additionally, the distance between the sensor and transmitter plays a significant role in system performance. Increasing the gap between the receiver and field generator results in a decrease in tracking accuracy. These considerations highlight the need for careful attention to sensor and field generator placement and handling to ensure optimal tracking accuracy [54]. As described earlier, the large distance between the sensor of the calibration device and the sensor of the adapter during calibration evaluation was unavoidable. Placing the sensor on the calibration device closer to the adapter sensor could potentially mitigate this problem and consequently reduce the registration error. Another consideration is that the calibration evaluation method utilized the same device used for the adapter's calibration. If there are errors in the calibration device itself, these errors will be replicated when the device is used to evaluate the calibration accuracy.

Lastly, the ICP registration used for assessing the calibration also has limitations. It is sensitive to outliers, which could considerably affect the alignment quality of point clouds, resulting in incorrect matches [74]. So, if a divot was wrongly indicated during the test, it could have a substantial impact. Therefore, it should be considered that this registration method led to a remaining registration error for the pointer of approximately 1 mm, which serves as a golden standard. Additionally, it is important to note that using RMSE as a measure of accuracy may not directly correspond to the tracking accuracy. Reducing landmarks for registration can lower the RMSE but worsen tracking accuracy by making it too specific for one location on the calibration device. To enhance tracking accuracy, more landmarks can be used, even if it increases RMSE.

In conclusion, it is necessary to note that tracking the LigaSure involves a trade-off between two crucial aspects: interfering with the clinical workflow or compromising calibration accuracy. While the calibration accuracy improves when the adapter is positioned closer to the tip, this could potentially disrupt the clinical workflow. Therefore, it is important to focus on error management to optimize calibration accuracy rather than altering the adapter design. Despite the fact that calibration accuracy deviates by around 1mm from the surgical pointer (golden standard), the adapter can still be utilized to visualize the instrument within the navigation environment and show the live position and orientation of the instrument with respect to relevant anatomical structure. However, it is crucial to consider these factors for future goals to ensure optimal performance during navigated resection.

Fast calibration method LUS adapter

A calibration method was developed for the adapter of the laparoscopic ultrasound probe. The method involved the use of a calibration tool for calibrating a new adapter. It was subjected to validation tests for both reproducibility and accuracy.

3.1. Introduction

Ultrasound transducers convert electric signals into ultrasonic waves using piezoelectric crystals. These waves penetrate the tissue, and based on tissue properties, varying amounts of waves are reflected and detected by the transducer. The speed of sound in tissue (about 1540 m/s) is used to calculate distances, providing real-time, non-invasive imaging of different structures within the organ, such as vessels and tumors [75].

For EM navigation within this institute, tracked ultrasound systems involve a sensor attached to a probe, with the tracking device continuously calculating its position and orientation. In the case of the laparoscopic ultrasound probe within this study, the adapter contains the EM sensor that is attached to the probe. The real-time obtained tracking data is used to determine the 3D coordinates of each pixel of the ultrasound images. Integrating these US images into the tracker coordinate system has the benefit of enabling registration with the preoperative images. However, it is important to note that the device tracks the position and orientation of the sensor on the probe, not the US image plane itself. Therefore, an additional step is necessary: computing the transformation between the adapter's sensor and the image plane itself [76].

Calibration of tracked US devices has been extensively explored in the literature, leading to the development of various solutions [73]. These solutions typically involve using a tracked phantom with known geometry to correlate specific phantom features identified in captured US images with the known geometric properties of the phantom. However, such calibration methods are time-consuming. It is convenient to have a faster calibration method for new LUS adapters. To achieve this, a calibration tool was developed to provide a quick calibration method when an uncalibrated adapter is attached to it.

3.2. Methodology

3.2.1. Design and production of the calibration tool

The top side of the probe's tip contains a small hole intended for purposes such as inserting an ablation needle (Figure 3.1a). During this study, this hole is used to fix the adapter, resulting in a convenient click-on mechanism (Figure 2.3). A 3D scan of the laparoscopic ultrasound probe tip was used in order to a design 3D model in Solidworks (Dassault Systèmes, Educational Edition, available at <https://www.solidworks.com/>). A hole was created in the model to make it possible to glue the EM sensor in it, shown at the red arrow in Figure 3.1b. Additionally, an extension that serves as a holder was attached in the design, allowing it to remain stable on a table during use (Figure 3.1c). Thereafter, the model was 3D-printed at the NKI-AvL with the Formlabs Form 3B printer using a SLA technique and a photopolymer resin.

3.2.2. Calibration of the calibration tool

Before the calibration tool can be employed to calibrate a LUS adapter, the relation between the tool itself and the attached EM sensor must be determined. This is done by attaching a calibrated adapter onto the calibration tool and establishing the different coordinate systems and corresponding transformations, as illustrated in Figure 3.2. The transformation of the calibration tool, which is defined as the transformation from the coordinate system of the EM sensor attached on the calibration tool to the coordinate system of the calibration tool itself (${}^{EMsensorTool}T_{Tool}$), was separated into two parts:

$${}^{EMsensorTool}T_{Tool} = {}^{EMsensorAdapter}T_{Tool} \cdot {}^{EMsensorTool}T_{EMsensorAdapter} \quad (3.1)$$

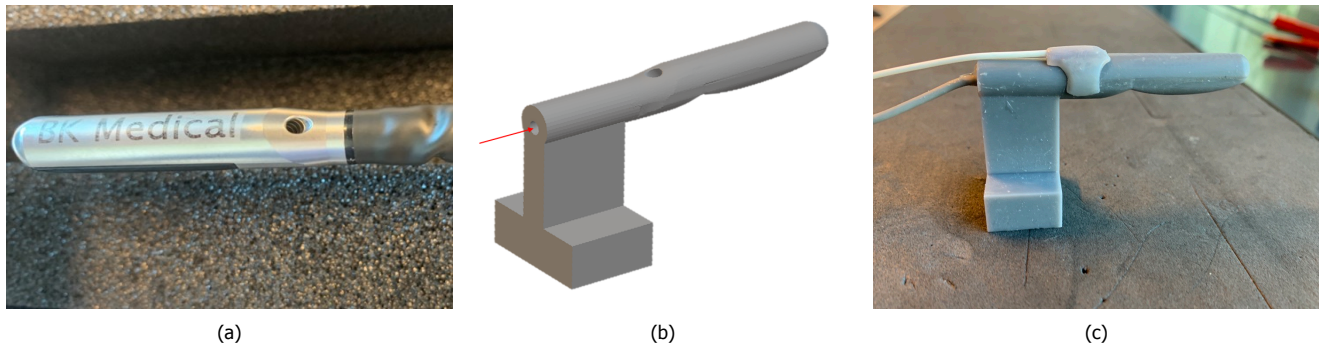


Figure 3.1: (a) LUS probe tip featuring a hole to click the adapter on. (b) 3D model of calibration tool with a hole for the EM sensor and a holder. (c) 3D-printed calibration tool with the attached EM sensor and adapter

First, a transformation was defined for the calibration of the calibrated adapter, which is the already known relation between the coordinate system of the adapter itself and the coordinate system of the EM sensor attached to the adapter. Since the adapter is attached on the calibration tool, we assume the relation of the adapter sensor with respect to itself is similar as with respect to the calibration tool (${}^{EMsensorAdapter}T_{Adapter} = {}^{EMsensorAdapter}T_{Tool}$). The second transformation between both EM sensors is continually updated through the transformation matrix ${}^{EMsensorTool}T_{EMsensorAdapter}$. This transformation is obtained via the EM field generator and was separated following Equation 3.2:

$${}^{EMsensorTool}T_{EMsensorAdapter} = {}^{EMsensorTool}T_{EM} \cdot {}^{EM}T_{EMsensorAdapter} \quad (3.2)$$

The open-source software 3D Slicer was used to compute the final transformation and obtain a calibration matrix of the calibration tool. By aligning the virtual model together with the tracking data of the sensor and the calibration matrix, it can be visualized within the navigation environment.

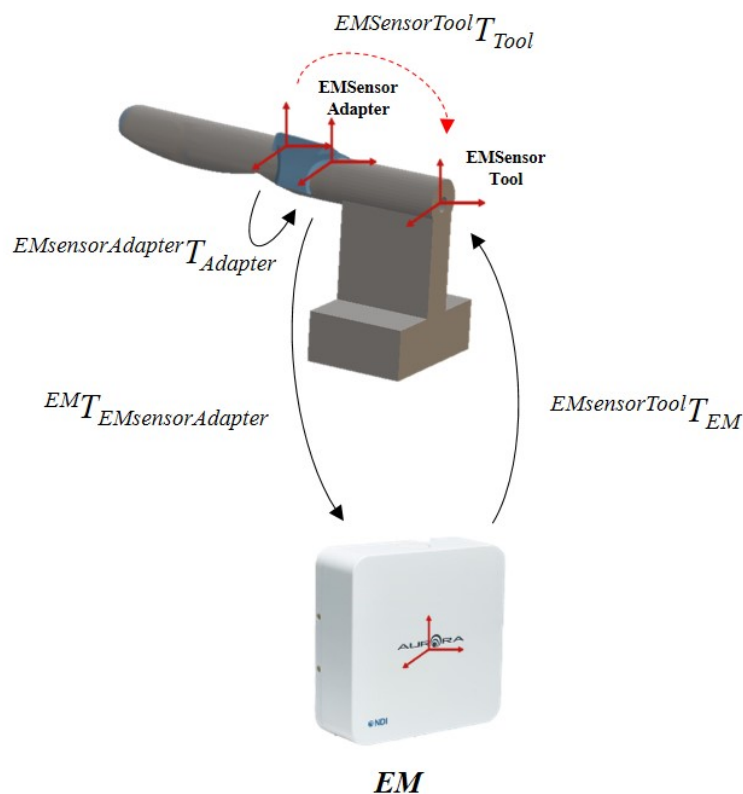


Figure 3.2: Coordinate systems with corresponding transformations used for calibration of the calibration tool

3.2.3. Use of the calibration tool

After calibrating the calibration tool, this transformation matrix can be used for calibrating a new LUS adapter without performing additional steps. The desired calibration, referred to as the transformation ${}^{EMsensorAdapter}T_{Adapter}$, was computed in the 3D Slicer software. This was accomplished by first attaching an uncalibrated LUS adapter onto the calibration tool. Then, the difference in position and orientation between both EM sensors was computed (${}^{EMsensorTool}T_{EMsensorAdapter}$). This was repeated ten times by placing the calibration tool with the attached LUS adapter in different position and orientation to limit jitter and tracking errors arising from sub-optimal positions of the sensor within the EM field. Subsequently, the average between these ten transformations was computed to limit jitter. To compute the calibration matrix of this LUS adapter, this average transformation was multiplied to the calibration of the calibration tool (Equation 3.3). As the LUS adapter is attached on the calibration tool, the desired transformation ${}^{EMsensorAdapter}T_{Adapter}$ can be similar denoted as ${}^{EMsensorAdapter}T_{Tool}$.

$${}^{EMsensorTool}T_{Adapter} = {}^{EMsensorTool}T_{Adapter} \cdot {}^{EMsensorAdapter}T_{EMsensorTool} \quad (3.3)$$

3.2.4. Validation

Reproducibility of attachment process

Given that the same calibration method will be applied to all adapters, it must be tested to ensure consistent orientation and position when attached to the calibration tool. A reproducibility test was performed by attaching the adapter ten times. Additionally, the calibration tool was placed in different position and orientation within the EM field. The tracking data was recorded for five seconds and averaged to limit jitter and calculations were made to find the transformation between both EM sensors (${}^{EMsensorAdapter}T_{EMsensorTool}$) in Figure 3.3. The variation in position and orientation between the two sensors was determined by calculating the standard deviations of both the Euclidean distance and Euler angles.

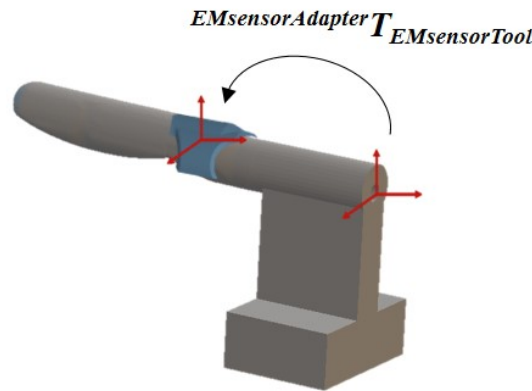


Figure 3.3: Coordinate systems of EM sensor attached on calibration tool and the EM sensor attached on the adapter with corresponding transformation

Calibration accuracy

Probe calibration plays a critical role in a tracked ultrasound system, directly affecting the accuracy of the navigation. Therefore, it is crucial to quantify the calibration accuracy achieved with the calibration tool. This employed calibration method was proposed by Bo et al. [77], in which the tip of the EM-tracked surgical pointer was utilized for landmark-based registration. The pointer will be used for digitizing, equipped with an internal calibration that achieves tracking accuracy within submillimeters, thus serving as the gold standard. Four coordinate systems are involved, visualized in Figure 3.4. 1) The US image coordinate system, originating from the left lower corner of the US image, 2) The LUS probe coordinate system, originating from the center of the US probe imaging array, 3) The US sensor coordinate system, originating from the EM sensor in the clip-on tool, and 4) the coordinate of the EM system. US calibration aims to find the 4×4 transformation matrix describing the rotation and translation from pixels in the US images to the EM sensor attached on the US probe, following the equation:

$${}^{USsensor}T_{USpixel} = {}^{USimage}T_{USpixel} \cdot {}^{USprobe}T_{USimage} \cdot {}^{USsensor}T_{USprobe} \quad (3.4)$$

Initially, a transformation was defined that includes rotation and translation, determined by the probe's origin on the US screen, along with a scaling factor based on the current zoom factor of the US device (${}^{USimage}T_{USpixel}$). The second transformation matrix translates points from the US image coordinate system to the US probe coordinate system (${}^{USprobe}T_{USimage}$). A final transformation matrix translates points from the US probe coordinate system to the coordinate system of the EM sensor attached to the US probe (${}^{USsensor}T_{USprobe}$).

To evaluate the calibration of the adapter, the EM pointer's tip was scanned with the LUS device in a basin with a 9.5% ethanol/water solution, with a speed of sound of 1540 m/s mimicking soft tissue. The pointer tip was consistently directed toward the scanning part of the LUS probe and positioned at 13 different locations in relation to the US image. These locations were evenly distributed across the image's field of view. For each position, the orientation of the US probe was adjusted until the most prominent artifact emerged at the pointer tip on the ultrasound image. This confirmed that the pointer tip was positioned in the 2D-US image plane. Figure 3.5 illustrates the variation in artifact intensity. The left image shows nearly no artifact, indicating that the pointer is not exactly in the 2D-US plane. The right image shows the artifact with the highest intensity, with the pointer tip's location marked by a red dot.

Throughout the measurements, the US images were recorded along with their respective tracking information. This information comprised the transformation data from the EM sensor (USsensor) to the EM (${}^{EM}T_{USsensor}$) and the transformation from the EM pointer to the EM coordinate system (${}^{EM}T_{EMpointer}$). This tracking information was utilized to evaluate the ${}^{USsensor}T_{USprobe}$ transformation.

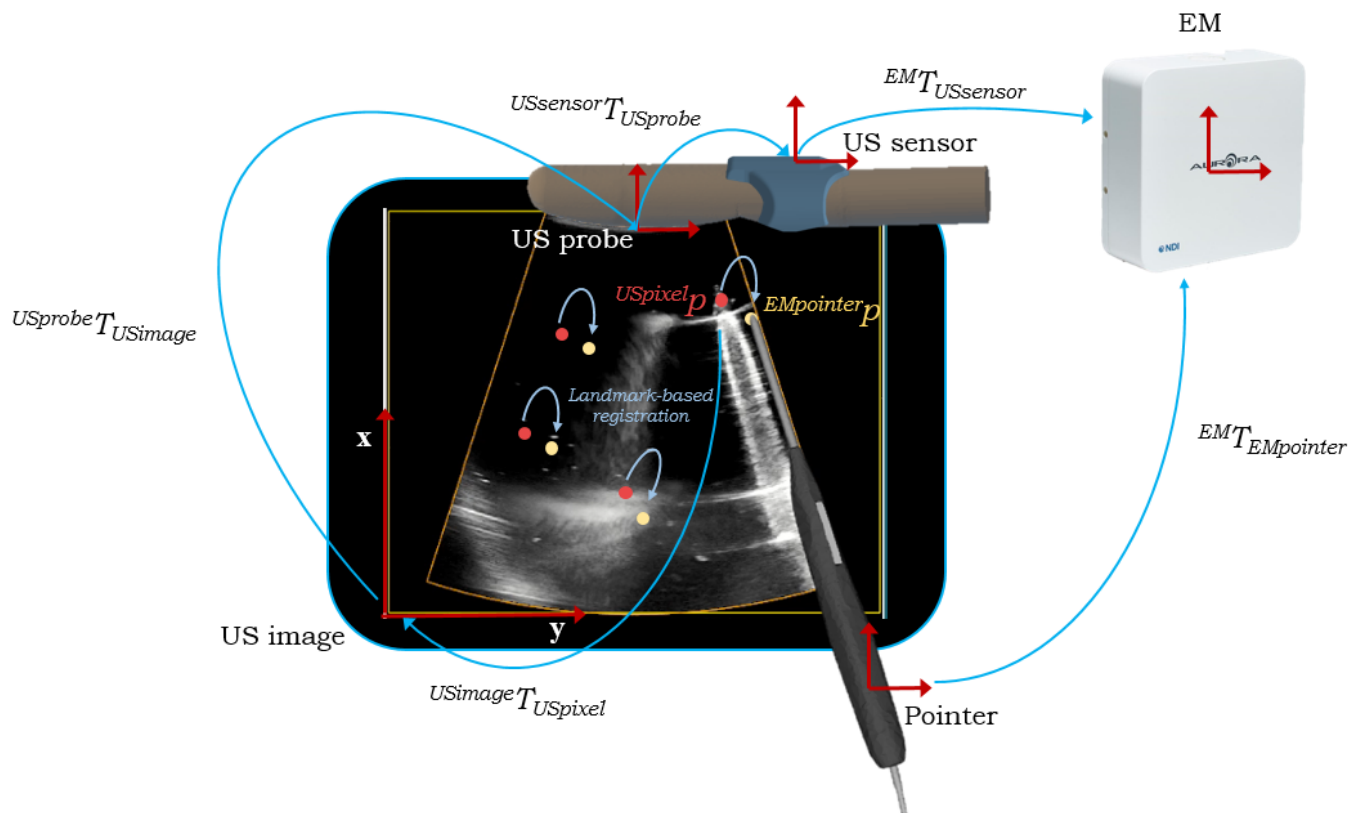


Figure 3.4: Coordinate systems and corresponding transformations for tracked ultrasound probe calibration

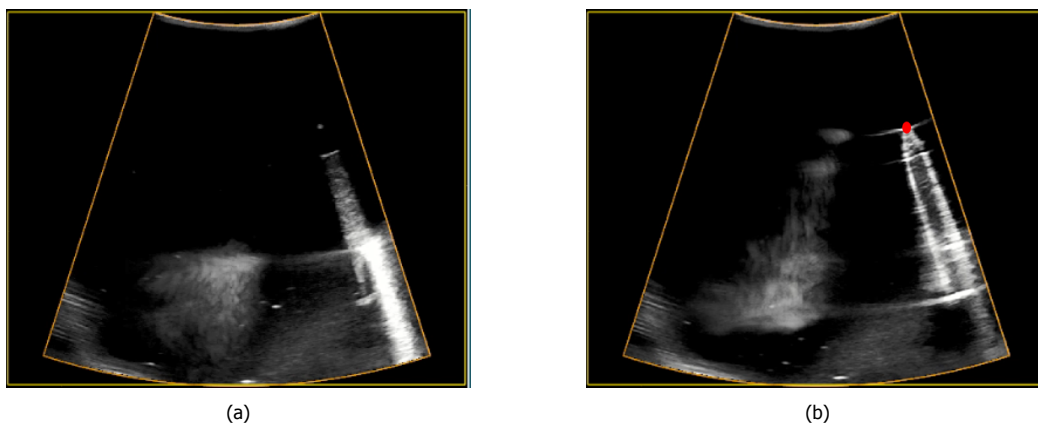


Figure 3.5: Two ultrasound (US) images show an electromagnetic (EM) pointer positioned on the right side of each image. The pointer tip is situated in front of the US plane in (a) and precisely within the US plane in (b). The correct pointer tip is indicated by a red dot.

For each EM pointer location, two matching points were chosen, resulting in two sets of 13 points each. The initial set of points was manually chosen on the US image, precisely at the location of the pointer tip (as indicated by the red dots in Figure 3.4). These points were defined within the US probe coordinate system, following Equation 3.5:

$${}^{USprobe}p = {}^{USprobe}T_{USimage} \cdot {}^{USimage}T_{USpixel} \cdot {}^{USpixel}p \quad (3.5)$$

$${}^{USsensor}p = ({}^{EM}T_{USsensor})^{-1} \cdot {}^{EM}T_{EMpointer} \cdot {}^{EMpointer}p \quad (3.6)$$

The second set of points was determined using tracking data from the EMTS (as indicated by the yellow dots in Figure 3.4). In this case, the EM pointer's recorded position was established within the US sensor coordinate system using Equation 3.6. When calibrating this adapter, or finding ${}^{USsensor}T_{USprobe}$, these point sets undergo a landmark-based registration process utilizing an iterative closest point algorithm through the 'fiducial registration wizard' module within 3D Slicer (blue arrows in Figure 3.4). However, since the aim was to assess the existing calibration, the points indicated by the pointer (${}^{EMpointer}p$) were transformed into the coordinate system of the US probe, just as the points ${}^{USpixel}p$ are defined, using this calibration matrix.

A RMSE was computed that showed the Euclidean distances between the point pairs following Equation 1.4, allowing for evaluation of the transformation ${}^{USsensor}T_{USprobe}$ obtained with the calibration tool.

3.3. Results

3.3.1. Validation of reproducibility of attachment process

The standard deviations calculated for orientation (Euler angles) and position (Euclidean distance) differences resulting from the reproducibility tests are shown in Table 3.1. The inaccuracy of the adapter attached onto the calibration device is within the tracking accuracy range of the sensor, as reported in Table 2.1. This suggests that the position and orientation of the adapter remain consistently similar with each attachment.

Table 3.1: Standard deviations of repeated LUS clip attachment on calibration tool

SD Euclidean distance (mm)	0.14
Euler angles	
SD R_x ($^\circ$)	0.23
SD R_y ($^\circ$)	0.12
SD R_z ($^\circ$)	0.19

3.3.2. Validation of calibration accuracy

Figure 3.6 shows the results of the calibration accuracy evaluation, with a mean RMSE of 3.67 ± 0.74 mm.

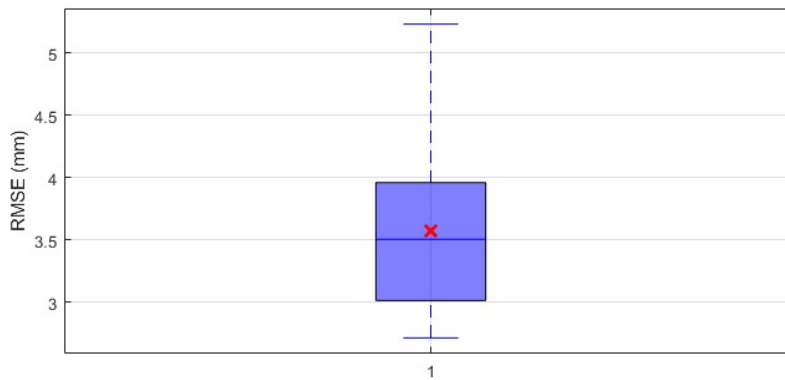


Figure 3.6: Results of LUS calibration accuracy tests. Boxplot shows the median, quartiles and the cross indicates the mean

3.4. Discussion

A calibration tool was developed to facilitate fast calibration of the LUS adapter. This tool demonstrated consistency in attaching the adapter, and the calibration accuracy obtained with this tool was assessed using a surgical pointer.

Calibrating the probe using the dedicated calibration tool yielded a relatively high inaccuracy, compared with results reported in the literature [77, 78]. Additionally, using the described pointer method to calibrate the adapter resulted in a higher calibration accuracy (RMSE = 0.57 mm). Given that probe calibration significantly directly impacts the performance of an US-based navigation system, it is essential to enhance this accuracy. However, before making conclusive judgments regarding this accuracy, several limitations associated with this rapid calibration method must be considered.

Firstly, the accuracy of calibration may be influenced by the design of the calibration tool. If the scan used to create the model lacks precision, the calibration may not be reliable for the actual LUS probe. This limitation could additionally be caused by the choice of material used for 3D printing the tool, as corrosion or material quality issues might decrease reliability. To mitigate this influence, a more robust 3D printing resin could be employed.

Furthermore, it is essential to note that the calibration tool was calibrated using a LUS adapter that was already calibrated with the described pointer method. Given that the calibration of a new adapter is reliant on this initial calibration, it is of great importance to note the potential limitations in the accuracy of this foundation calibration. The accuracy of this initial calibration was evaluated solely through visual inspection using the surgical pointer. During this assessment, the alignment between the virtual 3D pointer model and the physical pointer seen in the US image was verified, utilizing a similar principle involving the appearance of an artifact. While this visual inspection suggested accurate calibration, as depicted in Figure 3.7, it is important to note that this evaluation lacked a quantified measurement approach. To gain a more precise understanding of the calibration accuracy of this initial adapter, employing a method based on calculating the RMSE between the indicated points could offer a more precise assessment. Additionally, exploring iterative calibration methods may be beneficial in striving for the most accurate calibration feasible for the calibration tool.

The calibration evaluation method involving a tracked pointer proved to be relatively straightforward to apply, and with practice, visualizing the pointer tip on the US image became feasible. However, there are limitations to this method. Firstly, a manual selecting method of the points in the US image was employed. Results of this evaluation method, showed relatively a high standard deviation (0.7 mm) in comparison to the findings of Bø et al. (<0.1 mm) [77]. This might suggest that the accuracy of manually selecting pointer tip locations result in significant variability among points as they used motorized method to align the ultrasound plane and the pointer.

Another factor that could contribute to an inaccurate calibration method is the discrepancies in the speed of sound between the water in the basin used during measurements and the assumed value by the ultrasound device. It has been proposed by Fontanarosa et al. [79] that applying a correction method might enhance the positional accuracy in ultrasound images.

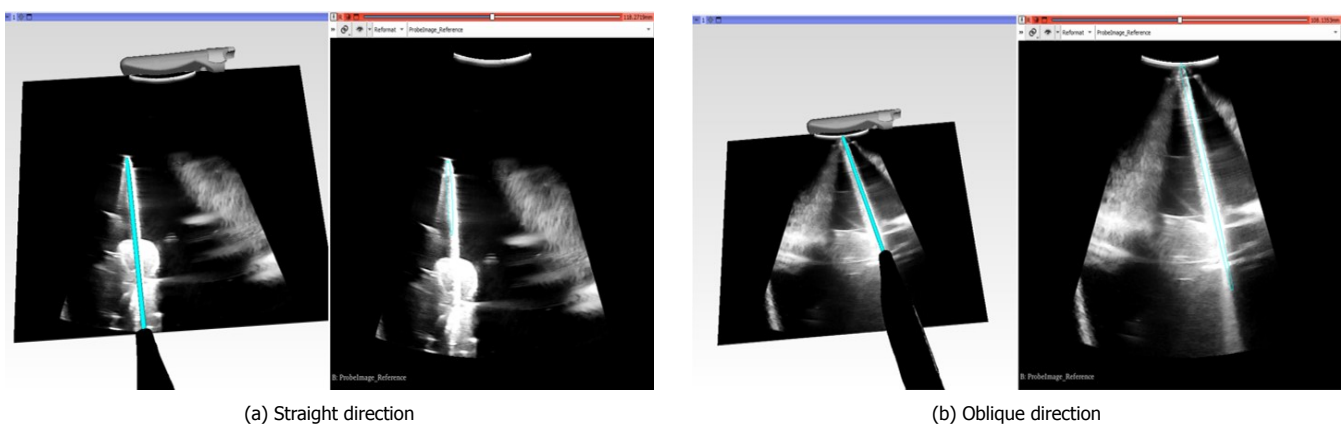


Figure 3.7: Calibration evaluation in two directions of golden standard adapter using a surgical pointer. The left image in both subfigures displays the 3D view, and the right image shows the 2D US plane with an overlaid virtual model of the pointer.

Clinical implementation

This chapter describes the process of implementing the navigation technique for laparoscopic liver resection in a clinical setting. To achieve this, a method for intraoperative validation of navigated laparoscopic liver resection was performed with a phantom test.

4.1. Introduction

Before this navigation technique can be used as standard clinical care for laparoscopic liver surgery, in vivo validation is necessary. Surgical navigation is accomplished by integrating instrument tracking and registration procedures, often involving surgeon input. Prior research has highlighted that inaccuracies in navigation systems stem from factors such as user dependence, instrument tracking errors, registration imprecision, and liver deformation. The degree of inaccuracy can vary due to diverse setups, algorithms, and organs of interest. Schneider et al. (2021) reported accuracies ranging from 8 to 15 mm [41]. However, comparing accuracy metrics between different systems is challenging due to variations in evaluation methods. Figure 4.1 illustrates potential sources of errors in using navigation during laparoscopic liver surgery. While factors like registration errors and the impact of organ deformation on navigation accuracy are significant, they are not within the scope of this research. To validate the developed laparoscopic navigation method, it is important to understand the contributions of instrument calibration errors and tracking errors to the overall navigation error.

In advance of this research, a literature review was conducted of ten studies (Appendix A) describing the current state of the art of accuracy evaluation and visualization methods for US-based navigated laparoscopic liver surgery. As there are no established gold standard methods for evaluating navigation accuracy, the evaluation methods within this limited amount of studies exhibited variability. Only three small clinical studies have evaluated a similar registration principle, aligning preoperative images with intraoperative images. Among these, one study reported an accuracy measure, resulting in a TRE of 10 mm in dissection planes [80]. Several studies showed results of testing navigation workflows without any registration, focusing on overlaying intraoperative ultrasound onto a laparoscopic video. These articles describe extensive options for visualizing the navigation environment, including multi-view displays on a single monitor and additional features such as color-coding and instrument trajectories [53, 81, 82]. However, many of these studies lacked quantitative evaluation methods. The feasibility study following this project will include this.

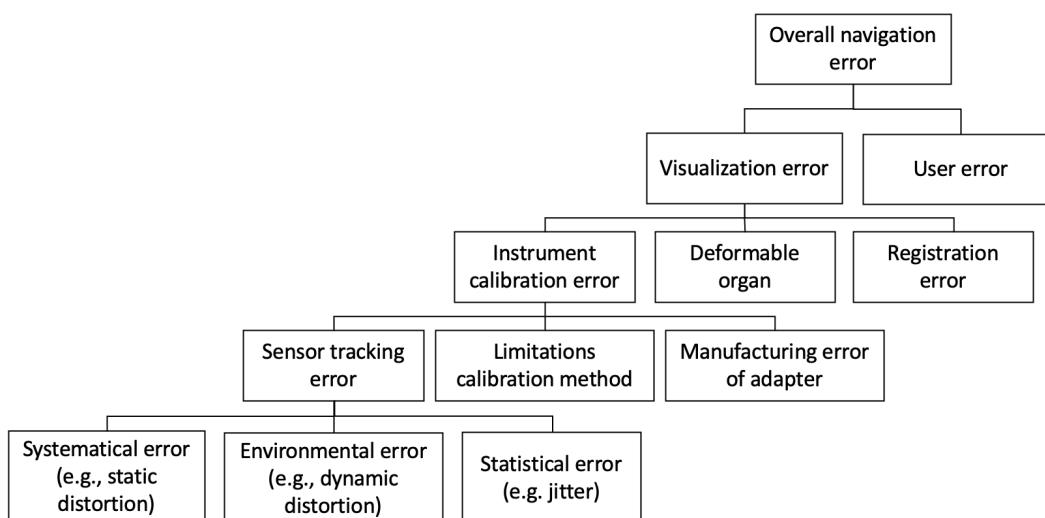


Figure 4.1: Possible errors during navigated laparoscopic liver resection [6]

An amendment was submitted to the METC for the study described in Chapter 1, with the objective of developing and evaluating an innovative ultrasound-based navigation system for guiding the resection and ablation of liver lesions in open liver surgery. This amendment involved the evaluation of a navigation workflow during a laparoscopic procedure and included multiple documents covering information of the developed adapters, software, hardware, and the study protocol. The feasibility and accuracy of this navigation system will be assessed during in vivo laparoscopic liver procedures at the NKI-AvL. This study aims to validate navigation accuracy by evaluating the registration between a preoperative 3D model and intraoperative ultrasound, as well as visualizing a virtual resection tool and overlaying a 3D preoperative model onto the real-time image of the laparoscope.

4.2. Methodology

The clinical workflow for navigation during laparoscopic liver resection will consist of several steps for which either the researcher or the surgeon will be responsible. Before research this technique in an actual clinical setting, these steps were simulated in a phantom test to mimic the clinical scenario. The aim of this test is to validate the navigation accuracy, optimize the workflow, and provide experience for the surgeon, surgical assistant, and technical physicians. Additionally, since a new software that incorporates augmented reality will be utilized, it was important to thoroughly evaluate the various options. Decisions regarding visualization were made in consultation with hepatobiliary surgeons at this institute. The assessment of these views was also conducted through the phantom test. The following subsections describe the execution of this phantom test.

4.2.1. Navigation system description

The US-based navigation system that is evaluated comprises the following components:

- An EMTS (Aurora, NDI[3]) is assembled with a FG, a SIU, a SCU), a 6DoF Cable Tool sensor, and a host computer. These components are all contained within a navigation trolley.
- A BK5000 US system (BK Ultrasound Systems, Analogic Corp., Peabody, MA, USA), with an EM-tracked LUS transducer
- Adapters for the laparoscopic sealer/divider and laparoscope
- A laparoscopic pointer
- Dedicated software designed for preoperative planning (3D Slicer), real-time intraoperative visualization (CustusX and Unity), and post-operative analysis (3D Slicer).

4.2.2. User interface

The software to be used for navigated laparoscopic liver resection is Unity, a real-time 3D development platform developed by Unity Technologies (San Francisco, USA). Generally, the majority of the user interface is kept consistent with the navigation user interface used in open liver surgery to minimize any confusion for the surgeons. However, because the augmented reality aspect is new, this will need to be evaluated further.

A 3D scene designed for navigated laparoscopic liver surgery was developed by a Post-doc from this institute. This scene facilitates the integration of EM tracking and the registration of imaging modalities. It enables the visualization of a tracked liver model alongside laparoscopic instruments and the creation of augmented reality using a preoperative liver model. This involves overlaying a 3D model onto the laparoscope image. As it is self-developed, the software allows for custom functionalities to be implemented. The visualization of laparoscopic instruments can take on different appearances, and the overlay can vary in transparency. Additionally, various imaging modalities can be combined on one screen to assist the surgeon, including the laparoscope video, ultrasound image, and preoperative imaging. A technical physician will control the software during laparoscopic surgery. The general 3D view displays the preoperative model, including blood vessels, bile ducts, and tumors, alongside models of the tracked surgical instruments. Combining the US image view with the registered 3D model provides immediate feedback on the registration accuracy. This is crucial as the 3D model's anatomy should align with that of the US image, making it a vital visualization tool. Furthermore, the registration accuracy of the laparoscope image and the preoperative model can be evaluated by ensuring that the liver contour in both images is aligned. Different visualization options were further evaluated through the phantom test.

4.2.3. Liver sensor attachment

An initial step in the navigation workflow is placing an EM sensor near the target lesion to serve as a reference. Movement or rotation was limited by fixation with surgical glue. In a laparoscopic setting, this glue has to be deposited using a catheter as it has to be done through a trocar. For this purpose, Glubran2 glue and a laparoscopic glue depositing catheter was used (GDmedical, Eindhoven, The Netherlands). An EM sensor was first glued onto a cow liver surface and later onto a resected human liver specimen to ensure secure attachment. Subsequently, the procedure for preparing the glue was tested during the phantom test setup with a surgeon and a surgical nurse (Figure 4.5c).

4.2.4. Validation of navigation workflow and accuracy

The IOUSFAN (Kyoto Kagaku Co., Ltd., Japan) soft tissue abdominal phantom was used for evaluation purposes, consisting of mimicked tissue of the liver parenchyma, veins, and lesions. The phantom's preoperative images were acquired with a CT scan and a 3D model was made based on this scan in the software 3D Slicer (Figure 4.2b). A test setting was created in an operating room to simulate a laparoscopic liver surgery (Figure 4.3). This phantom test was conducted with a surgeon and a surgical nurse. The adapters were attached to the laparoscopic instruments and the liver phantom was positioned within the EM field of the field generator. An EM sensor was attached on the side of the phantom to serve as a reference sensor (patient tracker). Additionally, the 3D model was loaded into the CustusX software.

Next, the ultrasound probe was oriented in the caudal direction to provide the navigation system with an initial understanding of its position and relation to the patient. This aids in subsequent registration steps. Subsequently, vessel bifurcations visible in both the ultrasound image and the 3D model of the phantom were indicated for a landmark-based registration. This resulted in a registration that transformed the LUS probe coordinate system to that of the MR model (${}^{MR}T_{EM} \cdot {}^{EM}T_{LUS}$). Figure 4.4 shows an overview of the different coordinate systems and their corresponding transformations. To integrate the laparoscopic instruments into the virtual environment, their adapter sensor's position and orientation with respect to the EM field (${}^{EM}T_{LM}, {}^{EM}T_{LUS}, {}^{EM}T_{LAP}$) was multiplied with their calibration matrix. Since the instruments were expressed in the coordinate system of the patient tracker attached on the liver phantom, an additional transformation ${}^{EM}T_{PT}$ must be performed.

To assess navigation accuracy, an ultrasound sweep of a targeted lesion was performed and a 3D ultrasound volume was reconstructed. After performing the registration, both volumes are in the same coordinate system, allowing to compute the TRE using the center of mass of the tumor in the acquired US volume and its co-registered preoperative counterpart. These steps were repeated multiple times by technical physicians and a surgeon. This resulted in three registrations with their corresponding TREs.

After these steps, the registration matrix that registers the intraoperative imaging with the preoperative imaging was loaded into the AR software (Unity). Since the laparoscope and ultrasound are expressed in the same patient tracker coordinate system, together with the calibration of the laparoscope, this registration aligned the real-time video from the tracked laparoscope with the 3D liver model's coordinate system by performing the transformation ${}^{MR}T_{EM} \cdot {}^{EM}T_{LAP}$. This resulted in an overlay of the 3D model onto the laparoscope image, which was visually evaluated based on superficial landmarks, such as the liver contour and fissure. The registration accuracy of the veins and lesions was additionally assessed using the tracked ultrasound image.

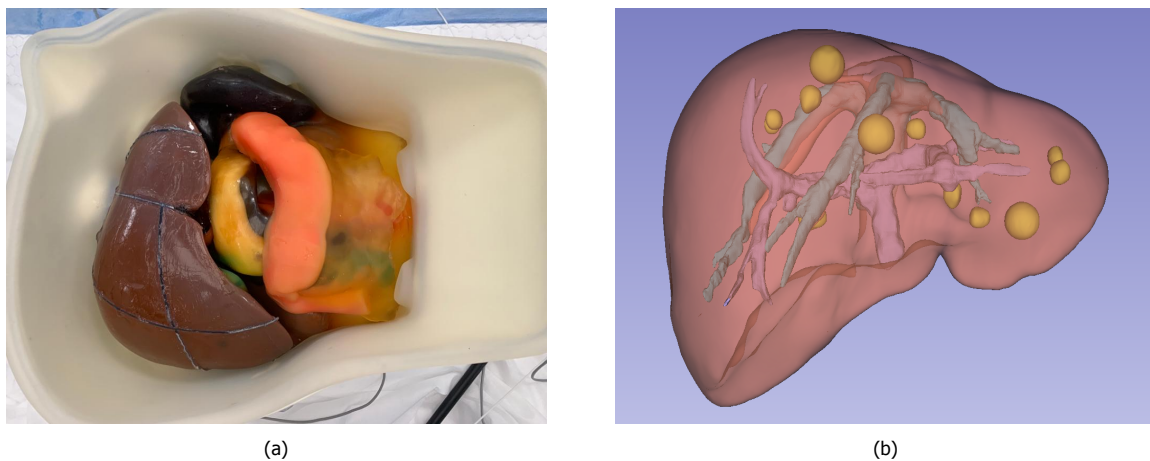


Figure 4.2: (a) Liver phantom used during the phantom test and (b) a segmented 3D model of the phantom in 3D Slicer

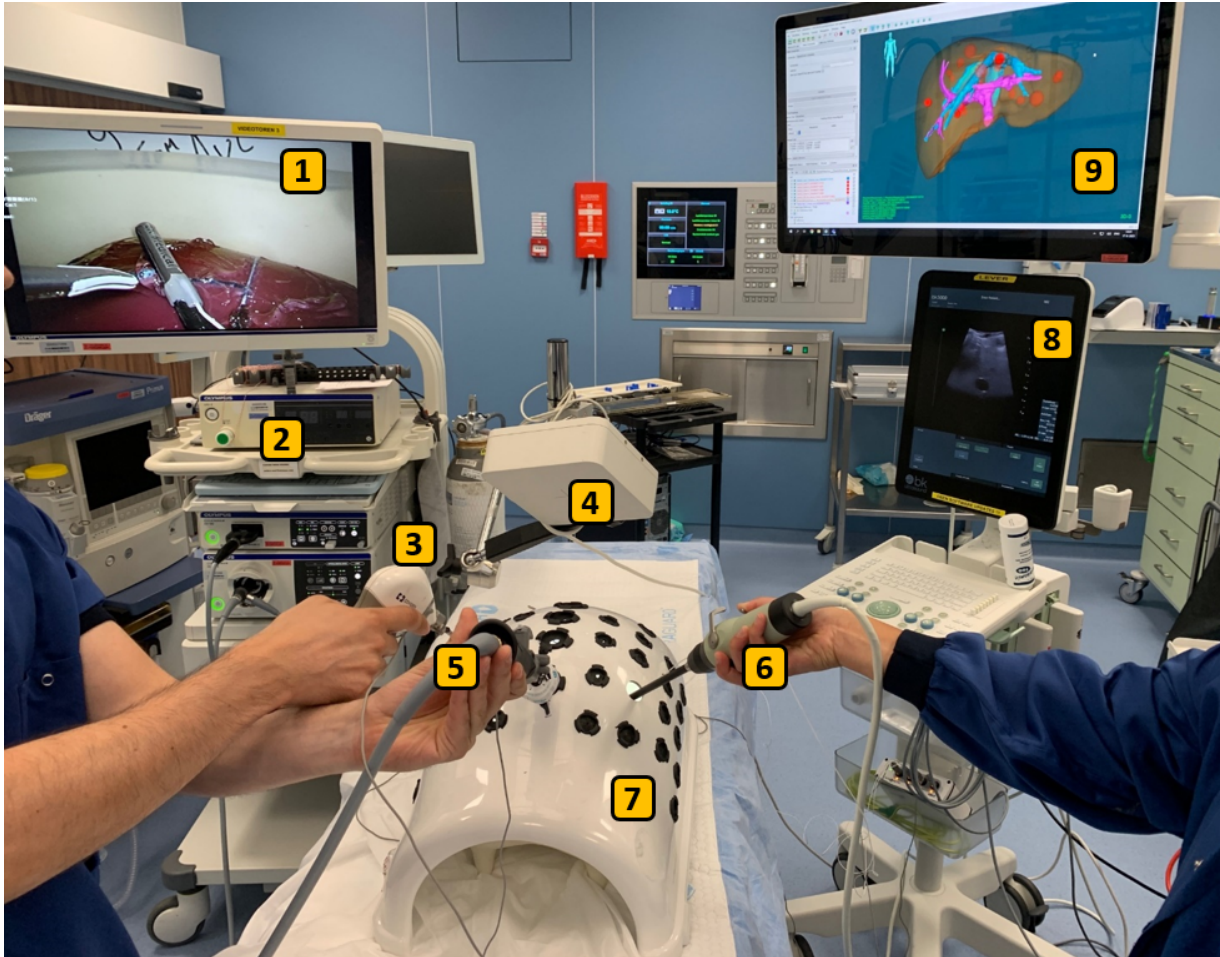


Figure 4.3: Operating room test set up. 1) Laparoscope monitor 2) Laparoscopic tower 3) Tracked LigaSure Maryland 4) EM field generator 5) Tracked laparoscope 6) Patient tracker 7) Tracked laparoscopic ultrasound probe 8) BK Ultrasound system 9) Navigation monitor with preoperative 3D model

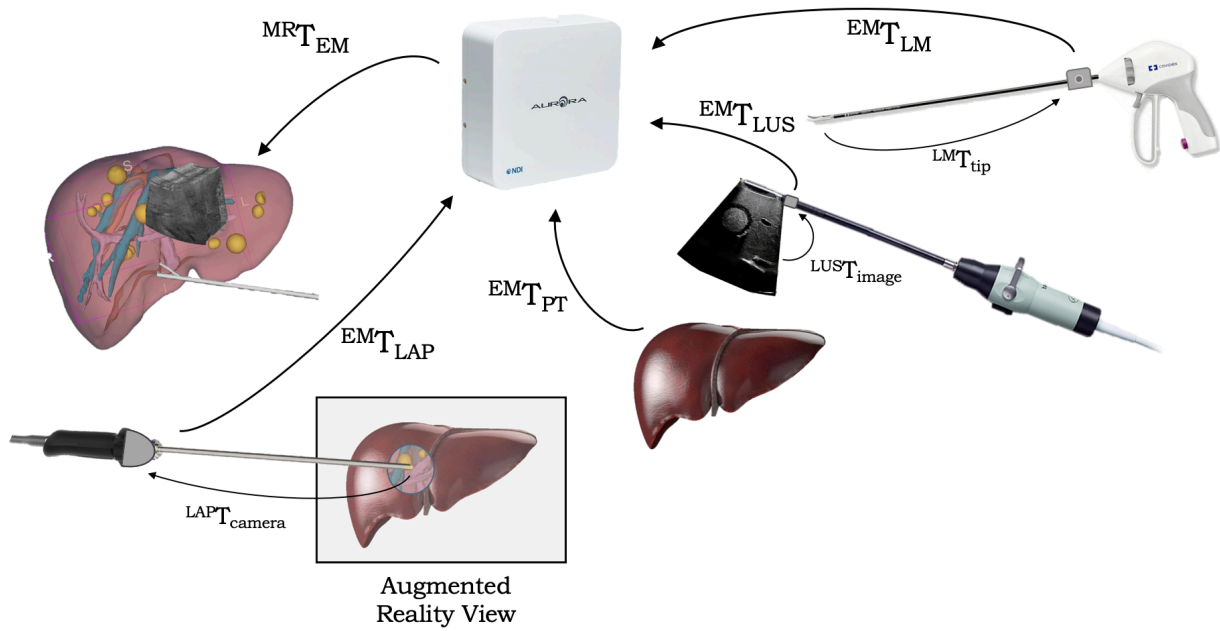


Figure 4.4: Schematic overview of all transformations required for registration

4.3. Results

The resulted steps of the navigation workflow are visualized in Figure 4.10.

4.3.1. Liver sensor attachment

Testing the glue on a cow liver and a human liver specimen showed strong adhesion (Figure 4.5a and Figure 4.5b). The glue was dry within one minute. The preparation and application of the glue was tested with a surgeon and a surgical nurse, where no problems were encountered (Figure 4.5c).

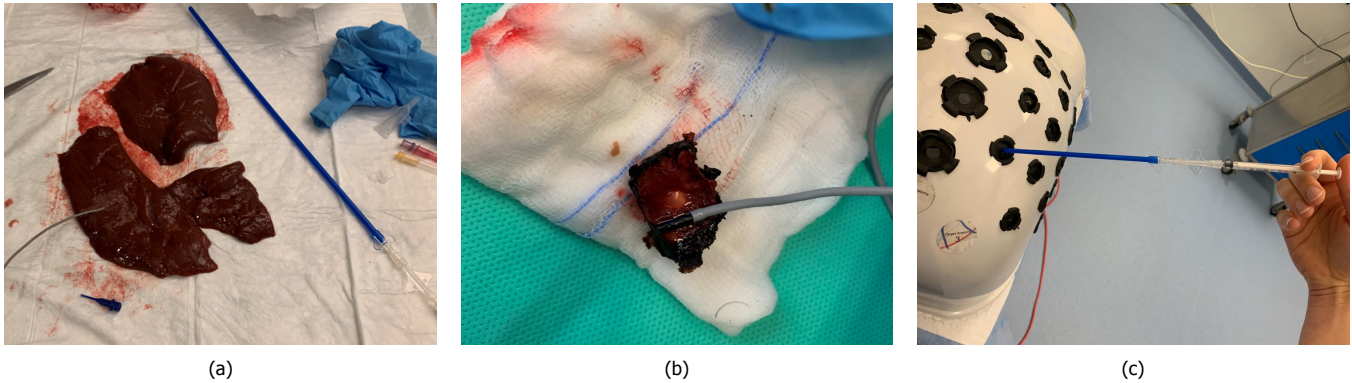


Figure 4.5: Experimental setup for testing adhesion of the Glubran2 glue on a (a) cow and (b) human liver specimen and (c) testing the laparoscopic use of the catheter

4.3.2. User interface

The phantom test showed the surgeon's preferences for the navigation visualization method, favoring a larger, highly transparent model AR overlay.

Varying options that are possible within the navigation software Unity include:

- A similar 3D view and 2D-LUS image with segmentation overlay as in CustusX alongside the virtual models of different instruments (Figure 4.6).
- Coloring a segment to indicate a planned resection region to the surgeon (Figure 4.7a).
- Different radius for overlay view (Figure 4.7b).
- Different transparency of the overlay (Figure 4.7c).

These adjustments will be further improved and determined during the initial phases of the clinical study.

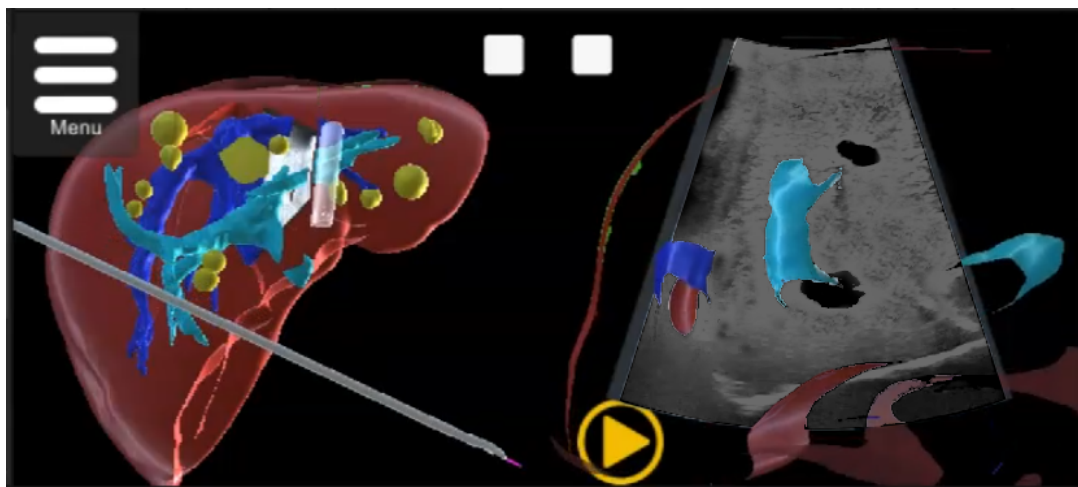


Figure 4.6: Navigation environment in Unity software, with on the left a view with the 3D models and on the right the view with the 3D model overlaying the 2D-US image

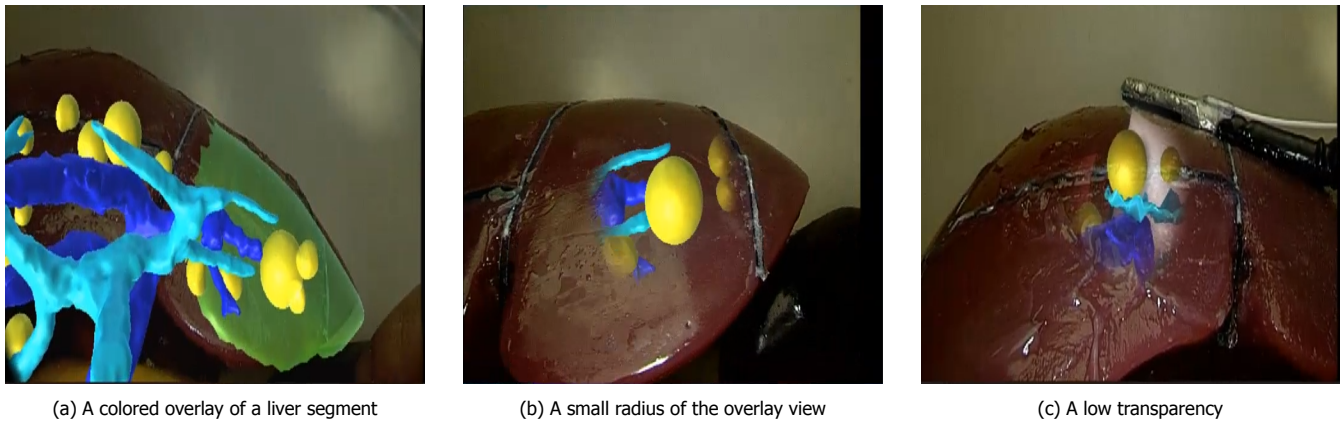


Figure 4.7: Various options in the AR software

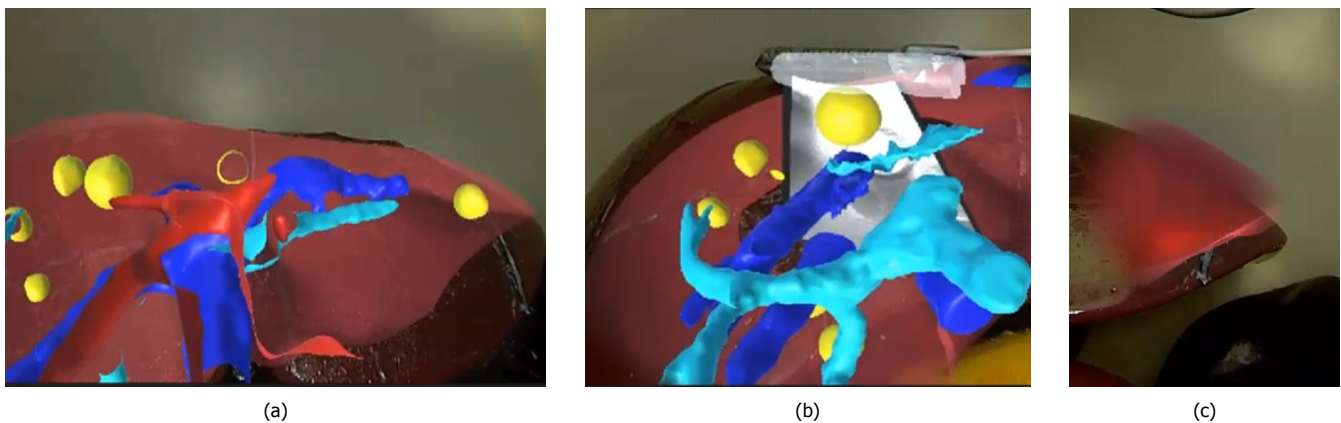


Figure 4.8: Results of augmented reality view. (a) Alignment of the liver edge (b) Validation overlay with US image (c) Diminishing overlay at the liver's periphery

4.3.3. Validation navigation workflow and accuracy

The TREs of three registrations during the phantom test are shown in Figure 4.9. The phantom test additionally demonstrated a satisfactory overlay of the 3D model onto the laparoscope image (Figure 4.8). For evaluation, the liver edge and the 2D-LUS image were used for reference. However, it is important to mention that the overlay accuracy diminishes at the liver's periphery (Figure 4.8c). This is primarily due to the fact that the registration landmarks were centered more on the targeted lesion rather than positioned at the liver's edge, resulting in the most accurate overlay in this particular region.

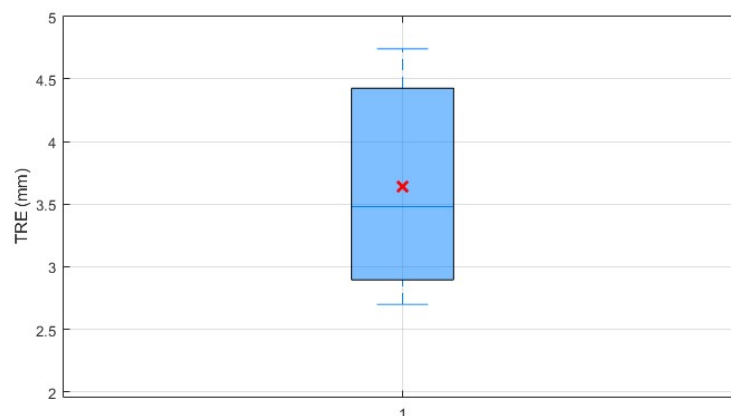


Figure 4.9: Results of accuracy phantom tests. Boxplot shows the median, quartiles and the cross indicates the mean

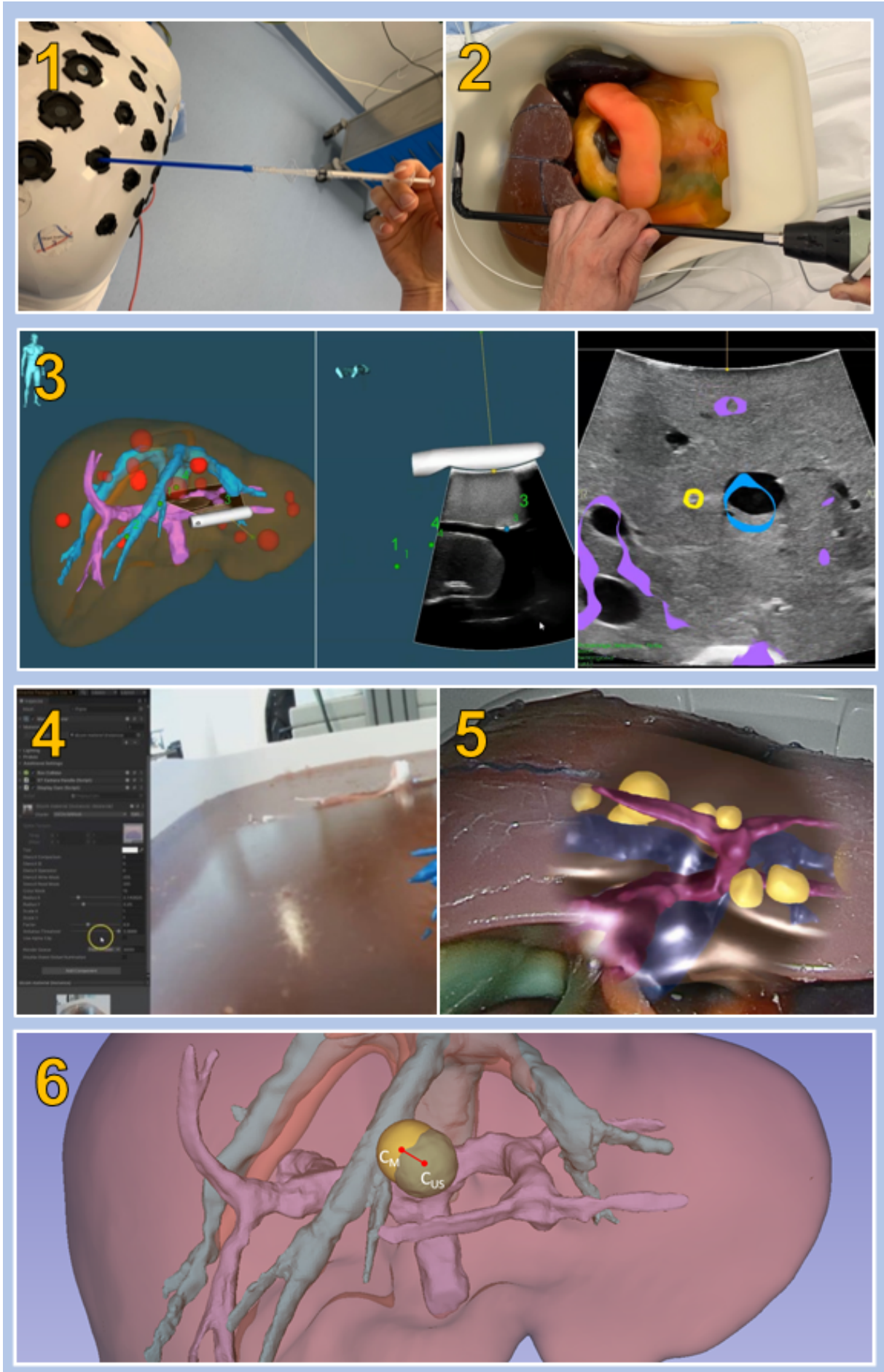


Figure 4.10: Overview of laparoscopic navigation workflow. 1) Liver sensor placement 2) LUS probe orientation 3) Landmark-based registration 4) Loading the registration into AR software 5) Visual assessment of the 3D model overlay onto the laparoscope image 6) Calculation of the TRE between tumor centers in US volume (C_{US}) and its co-registered preoperative counterpart (C_M)

4.4. Discussion

The EM navigation workflow underwent phantom tests to quantitatively assess navigation accuracy, enhance the workflow, gain experience, and evaluate the visualization approach. These tests indicated that the workflow is feasible, registers a target (TRE) with an accuracy of 3.7 mm and showed promising results with augmented reality.

Before drawing conclusions from these test results, it is essential to consider limiting factors. Firstly, potential errors, as described in Section 4.1, must be taken into account when evaluating navigation accuracy. The impact of calibration errors and tracking inaccuracies on navigation accuracy is discussed in detail in both Chapters 2 and 3. Furthermore, navigation accuracy depends on user actions, particularly how the adapters are attached to the instruments, which is crucial for achieving reliable calibrations. Additionally, the accuracy of registration is influenced by the manual selection of landmarks. Another factor to consider is the 3D model from the phantom used to assess navigation accuracy. This model was created based on CT scans acquired some time ago. Given that several tests have been performed on this phantom, there could have been alterations in its anatomical structure, potentially affecting registration errors and, consequently, navigation accuracy.

Overall, the phantom test demonstrated that this EM navigation workflow offers several advantages compared to the current standard practice. The navigation system enhances the understanding of the patient's anatomy by providing various 3D model views and 2D MRI slices within the navigation interface, allowing for interaction. Furthermore, augmented reality enables the surgeon to obtain a 3D view by looking at a single monitor. This aids in spatial comprehension, especially when only 2D images of the LUS and laparoscope are available during laparoscopic procedures. Additionally, real-time visualization of the laparoscopic sealer/divider within the navigation environment is achievable, enabling the determination of its position and orientation relative to anatomical structures. Nonetheless, these benefits need to be further confirmed through evaluation during a clinical study.

Also, it is important to note the difference between this phantom test and a clinical setting. In vivo, the registration accuracy is mostly affected by the differences between the intraoperative position and shape of the liver with respect to the preoperative situation. These discrepancies result from the time gap between the acquired MR/CT image and the surgery, as well as intraoperative changes in the liver due to surgical manipulation, pneumoperitoneum, and the patient's respiration. A possible solution to mitigate the registration error resulting from anatomical differences during and before surgery is to employ a navigation system solely reliant on IOUS imaging. In this approach, the virtual patient's anatomy is created only from intraoperative US images. Currently, at the NKI-AvL, it is attempted to create an automatic tumor segmentation algorithm from intraoperative US images. However, this approach remains challenging due to the complexity of tumor segmentation in US imaging. Tumors can vary significantly in size, shape, and echogenicity, making accurate segmentation difficult. Additionally, as one of the study's objectives is to visualize a 3D model of the entire liver using augmented reality, it is important to note that the current segmentation is limited to the region where the US sweep was performed. Models generated from intraoperative US images may not be ideal for achieving this goal.

Furthermore, clinical experience is essential because it is uncertain how the laparoscopic instruments will behave when manipulated by surgeons within the electromagnetic field. Since two adapters are positioned on the handles of the instruments, surgeons need to get use in keeping the adapters within the measurement volume of the field generator. Additionally, intraoperative experience is necessary for attaching the reference to the liver's surface in a sterile environment using the glue-depositing catheter and for removing the resected liver tissue from the patient's abdomen.

The phantom tests also demonstrated the feasibility of augmented reality implementation in the laparoscopic navigation workflow. However, the assessment of augmented reality was limited to visual evaluations based on superficial landmarks. A quantitative validation method could make the evaluation of navigation based on AR less subjective. However, evaluating AR technology poses significant challenges, particularly in comparing outcomes with and without the AR system. A possible method for evaluation AR was described by Teatini et al. [83], in which they quantified AR overlay error as the distance between a manual selected fiducial point on the 3D liver model and the centroids of cauterization marks on the liver surface. Nevertheless, they have demonstrated that user-induced errors can lead to notable discrepancies in AR accuracy.

A review by Malhotra et al. (2023) [84] regarding the evaluation and validation performed in this field revealed only one study that quantitatively assessed the accuracy of AR. This study utilized the reprojection error (RPE) for evaluation, which calculates the average Euclidean distance between projected 2D image points or lines and their true 3D positions during laparoscopy. To accomplish this, the researchers employed stereo image pairs from the laparoscope and used a CNN framework to estimate depth, creating a 3D representation of the liver surface during surgery. An ICP algorithm was then employed to register pre- and intraoperative models into a common coordinate space, enabling the superimposition of preoperative 3D models onto live laparoscopic images [85].

Furthermore, validation involves demonstrating that the navigation system functions as expected. This process

often focuses on confirming whether the implemented AR enhances comprehension within the operational domain. Validation can also rely on a variety of metrics, with one metric centered on user testing. In this context, feedback from surgeons regarding usability and effectiveness provides valuable insights into the AR navigation system's performance. Another metric explores how the technology impacts the entire medical team by enhancing situational awareness and influencing human factors. Additionally, the success of a procedure is determined not only by assessing its goals but also by evaluating the methods used to achieve these objectives, such as minimizing duration, cost, or standardization. These methods also serve as valuable metrics for evaluating the AR system. Lastly, the impact on patients can be investigated, including its effects on clinical scores, operating time, and recovery [84].

In this study, AR visualization during laparoscopic liver surgery will be extensively tested and, if necessary, optimized to the clinical setting. Surgeons will not rely on this visualization for surgical decision-making.

Lastly, it is important to note that the method used for calibrating the laparoscope adapter was specifically designed for the Endoeye with a 10 mm diameter and a 0° viewing angle. The laparoscope commonly used in our institute, however, features a 30° viewing angle. Therefore, intraoperative testing with the 0° angle laparoscope will be conducted solely for experimental purposes. Nevertheless, efforts should be directed towards calibrating this adapter for compatibility with the other laparoscope.

Conclusion

An adapter for tracking the laparoscopic sealer/divider was created, and its usability, sterilizability, and calibration reproducibility were validated. The calibration accuracy requires further enhancement. Nevertheless, the adapter can effectively visualize the instrument within the 3D navigation environment and indicate its position relative to critical anatomical structures, which was the initial goal for this method. Enhancements are needed in the calibration (evaluation) methods, if it is to be utilized for guided resection. When combined with the previously developed adapters for the other instruments, all three instruments can be tracked. While the calibration of the laparoscope was not addressed in this thesis, future steps involve adapting it for various laparoscopes and assessing its applicability. A rapid calibration method for the laparoscopic ultrasound adapter was developed and demonstrated its feasibility. However, calibration accuracy needs refinement for use during navigation, with a focus on improving the calibration tool design.

A phantom test demonstrated the feasibility of the entire workflow. The registration accuracy, measured as the target registration error (TRE), was found to be below 10 mm, a commonly suggested safety margin that is considered clinically acceptable [86]. However, it should be noted that during a laparoscopic procedure, registration is likely to be less accurate due to the deformable nature of the liver. Additionally, the practical feasibility of the workflow must be confirmed in an actual operating setting. The laparoscopic environment could present challenges related to performing an ultrasound sweep, conducting the registration process, and removing the reference sensor through a trocar. The surgeons have experience with these steps in open surgery; however, they need to acquire more expertise when performing these tasks in a laparoscopic setting. Ideally, achieving an accuracy below 3-5 mm with a navigation system would enable surgeons to make procedural adjustments based on the navigation-provided information. To assess the added value of this navigation system, both the registration accuracy and intraoperative qualitative assessments from the surgeons. Similarly, for augmented reality, a comprehensive evaluation, including both quantitative and qualitative aspects, is necessary to determine its benefits for the surgeon.

5.1. Clinical relevance

The clinical relevance of this project primarily lies in the reduction of complexity achieved through 2D view adaptation and lacking haptic feedback in laparoscopic procedures. Parenchyma-sparing liver resections aim to remove lesions while preserving maximum healthy liver tissue, providing sufficient margins around the lesions to reduce the chance of disease recurrence. While these procedures are relatively straightforward for small, superficial lesions, tackling complex cases like those in the posterior-superior segments demands extensive planning for laparoscopic procedures. This ensures both the removal of the pathological area and the maintenance of a safe resection margin [41]. Surgical navigation offers advantages during laparoscopic liver surgery by enhancing tumor localization accuracy and providing guidance for instruments in complex surgical situations. This could expand the indication criteria for patients for procedures that were initially not possible laparoscopically. Additionally, improved AR accuracy can enhance the precision of resection and potentially reduce the occurrence of unexpected bleedings and local recurrences [83].

A prospective feasibility study will be conducted at this institute to evaluate the practicality of using EM-navigation for laparoscopic liver resection. The literature lacks results of studies that have investigated non-commercial EM navigation systems in laparoscopic liver procedures while evaluating registration accuracy and augmented reality. This feasibility study aims to investigate whether this navigation method can enhance the accuracy of laparoscopic procedures. Quantitative assessment will be obtained using questionnaires based on the System Usability Scale (SUS) [87]. A summarized version of the study protocol can be found in Appendix C. During the clinical study, the system will undergo validation but will not be employed for the final laparoscopic resection, which will be carried out using IOUS and visual inspection of the AR view. Performing navigation during the first five included patients will be used to improve the navigation workflow. Approval for the amendment to the study protocol was obtained by the METC in August 2023.

5.2. Future directions

For the clinical implementation of navigation techniques during laparoscopic liver surgery, several directions for future research emerge, each addressing critical challenges. One obstacle in the laparoscopic navigation setup posed in this thesis lies in the tangle of wires of the electromagnetic sensors used. These wires could pose a challenge to the surgeons' freedom of movement, potentially leading to longer duration for performing surgical procedures. To mitigate this issue, a promising future direction could involve the exploration of wireless electromagnetic sensors, which would eliminate the need for cumbersome cables [88]. Also other tracking techniques for hepatic structures in clinical use, such as optical surface-based tracking or content-based image retrieval for registration, could eliminate the need for wired sensors. However, these have not yet become standard practice [57].

Moreover, the demand for more precise navigation within the dynamic context of laparoscopic liver surgery could benefit from deep learning techniques. Research in this area might focus on developing deep learning models to compensate for organ deformation and motion, thereby enhancing the accuracy of navigation [89]. Another approach of automatic featureless non-rigid registration for soft tissue registration in laparoscopic surgery, was reported by Reichard et al. [90]. However, this leads to a significantly more computation time, which is not feasible within the constraints of the operating room. Additionally, simultaneous localization and mapping (i.e. SLAM) [91] or Laser range scanners (i.e. LRS) [38] techniques allow performing a liver surface scan. This has the potential to eliminate liver deformation caused by physical contact during a US sweep, with LRS leading to high registration accuracy ($TR = 3.2 \pm 0.57$ mm). Besides, the obtained surface scan can subsequently be used for (continuous) deformable registration with the preoperative model. However, the additional equipment and increased computational time required for registration must be taken into account when considering this as a potential direction for future research.

Lastly, a promising direction is the integration of machine learning algorithms to predict and correct error propagation or magnetic distortion that may affect navigation accuracy during laparoscopic liver surgery. This innovation could significantly enhance the reliability of surgical navigation systems [54].

The potential for EM navigation extends beyond open and laparoscopic liver resection. In laparoscopic-assisted ablation, precise alignment of the tumor's center and the needle within the US image demands significant concentration and extensive expertise, particularly when tumors are poorly visible in the US image. Here, the adoption of image-guided surgical systems proves to be advantageous [86, 92]. Despite the additional aspect involved here, specifically the tracking of the ablation needle, the workflow developed in this thesis can partially be beneficial for this procedure. Furthermore, the use of robotic-assisted surgery may address the inherent limitations of laparoscopic procedures. This approach enhances surgical dexterity through the use of endo-wristed instruments with seven degrees of freedom. It eliminates the presence of unavoidable hand tremors and reduces the surgeon's vulnerability to fatigue during extended surgeries. Additionally, the routine adoption of stereoscopic laparoscopy further improves depth perception [41, 93]. However, this technique may lack comprehensive visualization without tactile feedback, necessitating a certain level of training and experience for successful execution [94]. Therefore, navigation could be beneficial for these procedures as it has the potential to enhance the surgeon's spatial awareness during the procedure, thereby improving the precision of tumor resection [95]. Additionally, patients may experience advantages from AR-assisted robotic liver resection as it facilitates more accurate tumor localization and enables the delineation of resection margins through a video-based augmented reality display [96]. Aspects of the workflow developed within this thesis can be applied to this type of surgery, including the use of a glue depositing catheter and augmented reality visualization. However, although several medical centers have gained experience in robotic liver surgery, further extensive studies are still required to define its true advantages over laparoscopy and standardize its clinical application [97].

This thesis describes the development of a surgical workflow for electromagnetically guided laparoscopic liver resection at the NKI-AvL. The navigation system integrated an Aurora EM tracking system, tracked laparoscopic instruments, and used the developed software for intraoperative visualization of a 3D model of the liver onto the laparoscopic video. Further improvements can be obtained regarding tracking accuracy, evaluation methods, and visualization techniques. Both technical and clinical experience must be obtained through testing this navigation system in a clinical study. In the future, navigation could improve the accuracy of laparoscopic resection and reduce the chance of disease recurrence.

Reference list

- [1] H. J. Paltiel and E. Y. Lee, *Pediatric ultrasound*, (2021).
- [2] *Learn about laparoscopic appendectomy and related surgeries*, [Online] Available: <https://www.vejthani.com/2021/05/pros-and-cons-laparoscopic-surgery/>, accessed: 2023-08-09.
- [3] *Northern digital inc. electromagnetic tracking that supports minimally invasive approaches*. [Online] Available: <https://www.ndigital.com/electromagnetic-tracking-technology/aurora/> (2020), accessed: 2023-08-09.
- [4] NDI (Northern Digital Inc.), *Electromagnetic Tracking Education Guide* (2021).
- [5] X. Liu, W. Plishker, T. D. Kane, D. A. Geller, L. W. Lau, J. Tashiro, K. Sharma, and R. Shekhar, *Preclinical evaluation of ultrasound-augmented needle navigation for laparoscopic liver ablation*, *International journal of computer assisted radiology and surgery* **15**, 803 (2020).
- [6] K. Olthof, *Towards the clinical implementation of navigated liver ablation*, M3 Technical Medicine Thesis, University of Delft, Erasmus, Leiden (2021).
- [7] H. Sung, J. Ferlay, R. L. Siegel, M. Laversanne, I. Soerjomataram, A. Jemal, and F. Bray, *Global cancer statistics 2020: Globocan estimates of incidence and mortality worldwide for 36 cancers in 185 countries*, *CA: a cancer journal for clinicians* **71**, 209 (2021).
- [8] A. Vogel, T. Meyer, G. Sapisochin, R. Salem, and A. Saborowski, *Hepatocellular carcinoma*, *Lancet* **400**, 1345 (2022).
- [9] J.-K. Li, X.-H. Liu, H. Cui, and X.-H. Xie, *Radiofrequency ablation vs. surgical resection for resectable hepatocellular carcinoma: A systematic review and meta-analysis*, *Molecular and Clinical Oncology* **12**, 15 (2020).
- [10] F. Eskens, K. Van Erpecum, K. De Jong, O. van Delden, H. Klumpen, C. Verhoef, P. Jansen, M. van Den Bosch, A. Méndez Romero, J. Verheij, et al., *Hepatocellular carcinoma: Dutch guideline for surveillance, diagnosis and therapy*, *Neth J Med* **72**, 299 (2014).
- [11] *Incidentie hpb-tumoren, integraal kankercentrum nederland*. [Online] Available: <https://iknl.nl/kankersoorten/hpb-tumoren/registratie/incidentie> (2021), accessed: 2023-09-03.
- [12] A. W. C. Kow, *Hepatic metastasis from colorectal cancer*, *Journal of gastrointestinal oncology* **10**, 1274 (2019).
- [13] *Incidentie darmkanker, integraal kankercentrum nederland*. [Online] Available: <https://iknl.nl/kankersoorten/darmkanker/registratie> (2021), accessed: 2023-09-03.
- [14] T. Shasha, M. Gruijs, and M. van Egmond, *Mechanisms of colorectal liver metastasis development*, *Cellular and Molecular Life Sciences* **79**, 607 (2022).
- [15] J. Llovet, R. Kelley, and A. e. a. Villanueva, *Hepatocellular carcinoma*. *Nature Reviews Disease Primers* **2**, 16018 (2016).
- [16] A. Shiani, S. Narayanan, L. Pena, and M. Friedman, *The role of diagnosis and treatment of underlying liver disease for the prognosis of primary liver cancer*, *Cancer control* **24**, 1073274817729240 (2017).
- [17] D. Dimitroulis, C. Damaskos, S. Valsami, S. Davakis, N. Garmpis, E. Spartalis, A. Athanasiou, D. Moris, S. Sakelariou, S. Kykalos, et al., *From diagnosis to treatment of hepatocellular carcinoma: An epidemic problem for both developed and developing world*, *World journal of gastroenterology* **23**, 5282 (2017).
- [18] N. C. Institute, *Liver (Hepatocellular) Cancer Screening (PDQ®) — cancer.gov*, https://www.cancer.gov/types/liver/hp/liver-screening-pdq#section_3.14 (Last updated: 01-09-2023), [Accessed 09-09-2023].
- [19] L. Bolondi, *Screening for hepatocellular carcinoma in cirrhosis*, *Journal of hepatology* **39**, 1076 (2003).
- [20] H. Tanaka, *Current role of ultrasound in the diagnosis of hepatocellular carcinoma*, *Journal of Medical Ultrasonics* **47**, 239 (2020).

- [21] J. M. Esfeh, K. Hajifathalian, and K. Ansari-Gilani, *Sensitivity of ultrasound in detecting hepatocellular carcinoma in obese patients compared to explant pathology as the gold standard*, *Clinical and molecular hepatology* **26**, 54 (2020).
- [22] D. V. Sahani and S. P. Kalva, *Imaging the liver*, *The oncologist* **9**, 385 (2004).
- [23] T. Vogl, K. Eichler, S. Zangos, M. Mack, and R. Hammerstingl, *Hepatocellular carcinoma: Role of imaging diagnostics in detection, intervention and follow-up*, *RoFo: Fortschritte auf dem Gebiete der Rontgenstrahlen und der Nuklearmedizin* **174**, 1358 (2002).
- [24] D. V. Sahani, M. A. Bajwa, Y. Andrabi, S. Bajpai, and J. C. Cusack, *Current status of imaging and emerging techniques to evaluate liver metastases from colorectal carcinoma*, *Annals of surgery* **259**, 861 (2014).
- [25] O. V. Ivashchenko, E.-J. Rijkhorst, L. C. Ter Beek, N. J. Hoetjes, B. Pouw, J. Nijkamp, K. F. Kuhlmann, and T. J. Ruers, *A workflow for automated segmentation of the liver surface, hepatic vasculature and biliary tree anatomy from multiphase mr images*, *Magnetic resonance imaging* **68**, 53 (2020).
- [26] J. Smit, *Ultrasound-based navigation for surgical removal of liver lesions*, M3 Technical Medicine Thesis, University of Twente (2017).
- [27] L. Campana, H. Esser, M. Huch, and S. Forbes, *Liver regeneration and inflammation: from fundamental science to clinical applications*, *Nature reviews Molecular cell biology* **22**, 608 (2021).
- [28] S. R. Abdel-Misih and M. Bloomston, *Liver anatomy*, *Surgical Clinics* **90**, 643 (2010).
- [29] F. Sheedfar, S. D. Biase, D. Koonen, and M. Vinciguerra, *Liver diseases and aging: friends or foes?* *Aging cell* **12**, 950 (2013).
- [30] A. Kalra, E. Yetiskul, C. J. Wehrle, and F. Tuma, *Physiology, liver*, (2018).
- [31] M. Fusaglia, *Design, integration and clinical investigations of image-guided laparoscopic liver surgery*, Ph.D. thesis, University of Bern, Biomedical Engineering (2015).
- [32] I. Paolucci, M. Schwalbe, G. A. Prevost, A. Lachenmayer, D. Candinas, S. Weber, and P. Tinguely, *Design and implementation of an electromagnetic ultrasound-based navigation technique for laparoscopic ablation of liver tumors*, *Surgical endoscopy* **32**, 3410 (2018).
- [33] J. S. Heiselman, L. W. Clements, J. A. Collins, J. A. Weis, A. L. Simpson, S. K. Geevarghese, T. P. Kingham, W. R. Jarnagin, and M. I. Miga, *Characterization and correction of intraoperative soft tissue deformation in image-guided laparoscopic liver surgery*, *Journal of Medical Imaging* **5**, 021203 (2018).
- [34] D. J. Bentrem, R. P. DeMatteo, and L. H. Blumgart, *Surgical therapy for metastatic disease to the liver*, *Annu. Rev. Med.* **56**, 139 (2005).
- [35] R. Eppenga, W. Heerink, J. Smit, K. Kuhlmann, T. Ruers, and J. Nijkamp, *Real-time wireless tumor tracking in navigated liver resections: An ex vivo feasibility study*, *Annals of surgical oncology* **29**, 3951 (2022).
- [36] C. Van de Velde, *Treatment of liver metastases of colorectal cancer*, *Ann Oncol* **16**, 144 (2005).
- [37] G. Andria, F. Attivissimo, A. Di Nisio, A. M. L. Lanzolla, and M. A. Ragolia, *Assessment of position repeatability error in an electromagnetic tracking system for surgical navigation*, *Sensors* **20**, 961 (2020).
- [38] M. Fusaglia, H. Hess, M. Schwalbe, M. Peterhans, P. Tinguely, S. Weber, and H. Lu, *A clinically applicable laser-based image-guided system for laparoscopic liver procedures*, *International journal of computer assisted radiology and surgery* **11**, 1499 (2016).
- [39] S. Vijayan, I. Reinertsen, E. F. Hofstad, A. Rethy, T. A. N. Hernes, and T. Langø, *Liver deformation in an animal model due to pneumoperitoneum assessed by a vessel-based deformable registration*, *Minimally Invasive Therapy & Allied Technologies* **23**, 279 (2014).
- [40] R. Mishra, *Textbook of practical laparoscopic surgery* (JP Medical Ltd, 2013).
- [41] C. Schneider, M. Allam, D. Stoyanov, D. Hawkes, K. Gurusamy, and B. Davidson, *Performance of image guided navigation in laparoscopic liver surgery—a systematic review*, *Surgical Oncology* **38**, 101637 (2021).
- [42] T. P. Kingham, S. Jayaraman, L. W. Clements, M. A. Scherer, J. D. Stefansic, and W. R. Jarnagin, *Evolution of image-guided liver surgery: transition from open to laparoscopic procedures*, *Journal of Gastrointestinal Surgery* **17**, 1274 (2013).

- [43] L. M. Pak, J. Gagnière, P. J. Allen, V. P. Balachandran, M. I. D'Angelica, R. P. DeMatteo, W. R. Jarnagin, M. I. Miga, A. L. Simpson, and T. P. Kingham, *Utility of image guidance in the localization of disappearing colorectal liver metastases*, *Journal of Gastrointestinal Surgery* **23**, 760 (2019).
- [44] S. Zalinski, E. K. Abdalla, A. Mahvash, and J.-N. Vauthey, *A marking technique for intraoperative localization of small liver metastases before systemic chemotherapy*, *Annals of surgical oncology* **16**, 1208 (2009).
- [45] B. Le Roy, E. Ozgur, B. Koo, E. Buc, and A. Bartoli, *Augmented reality guidance in laparoscopic hepatectomy with deformable semi-automatic computed tomography alignment (with video)*, *Journal of Visceral Surgery* **156**, 261 (2019).
- [46] L. W. Lau, X. Liu, W. Plishker, K. Sharma, R. Shekhar, and T. D. Kane, *Laparoscopic liver resection with augmented reality: a preclinical experience*, *Journal of Laparoendoscopic & Advanced Surgical Techniques* **29**, 88 (2019).
- [47] U. Mezger, C. Jendrewski, and M. Bartels, *Navigation in surgery*, *Langenbeck's archives of surgery* **398**, 501 (2013).
- [48] M. Anand and S. Panwar, *Role of navigation in oral and maxillofacial surgery: a surgeon's perspectives*, *Clinical, Cosmetic and Investigational Dentistry*, 127 (2021).
- [49] A. J. Karkenny, J. R. Mendelis, D. S. Geller, and J. A. Gomez, *The role of intraoperative navigation in orthopaedic surgery*, *JAAOS-Journal of the American Academy of Orthopaedic Surgeons* **27**, e849 (2019).
- [50] P. Gavriilidis, B. Edwin, E. Pelanis, E. Hidalgo, N. de'Angelis, R. Memeo, L. Aldrighetti, and R. P. Sutcliffe, *Navigated liver surgery: State of the art and future perspectives*, *Hepatobiliary & Pancreatic Diseases International* **21**, 226 (2022).
- [51] M. Falkenberg, M. Rizell, M. S. Eilard, A. Regensburger, R. Razazzian, and N. Kvarnström, *Radiopaque fiducials guiding laparoscopic resection of liver tumors*, *Surgical Laparoscopy, Endoscopy & Percutaneous Techniques* **32**, 140 (2022).
- [52] T. Langø, S. Vijayan, A. Rethy, C. Våpenstad, O. V. Solberg, R. Mårvik, G. Johnsen, and T. N. Hernes, *Navigated laparoscopic ultrasound in abdominal soft tissue surgery: technological overview and perspectives*, *International journal of computer assisted radiology and surgery* **7**, 585 (2012).
- [53] M. Kleemann, S. Deichmann, H. Esnaashari, A. Besirevic, O. Shahin, H.-P. Bruch, T. Laubert, et al., *Laparoscopic navigated liver resection: technical aspects and clinical practice in benign liver tumors*, *Case reports in surgery* **2012** (2012).
- [54] J. Much, *Error classification and propagation for electromagnetic tracking*, Ph.D. thesis, Techniscial University of Munich (2008).
- [55] F. Van Der Heijden, *Point registration* (University of Twente, April, 2020).
- [56] J. Smit, M. Fusaglia, B. Thomson, N. Kok, O. Ivashchenko, T. Langø, K. Kuhlmann, and T. Ruers, *Ultrasound-based navigation for open liver surgery with active tumor tracking and deformation compensation: Preliminary results*, *HPB* **24**, S105 (2022).
- [57] J. N. Smit, K. F. Kuhlmann, O. V. Ivashchenko, B. R. Thomson, T. Langø, N. F. Kok, M. Fusaglia, and T. J. Ruers, *Ultrasound-based navigation for open liver surgery using active liver tracking*, *International journal of computer assisted radiology and surgery* **17**, 1765 (2022).
- [58] *Regulation (EU) 2017/745 of the European Parliament and of the Council of 5 April 2017 on medical devices, amending Directive 2001/83/EC, Regulation (EC) No 178/2002 and Regulation (EC) No 1223/2009 and repealing Council Directives 90/385/EEC and 93/42/EEC (OJ L 117 5.5.2017, p. 1)* (2017), current consolidated version: <https://eur-lex.europa.eu/legal-content/EN/TXT/?uri=CELEX:02017R0745-20200424>.
- [59] *Guidance on classification of medical devices*, [Online] Available: https://health.ec.europa.eu/system/files/2021-10/mdcg_2021-24_en_0.pdf (October 2021), accessed: 2023-09-03.
- [60] L. Venix, *The feasibility of em navigation for gynecologic brachytherapy catheter insertion*, M3 Technical Medicine Thesis, University of Twente (2023).
- [61] "richtlijn beoordelingscriteria herbruikbare medische hulpmiddelen - vdsmh.", [Online] Available: <https://www.vdsmh.nl/publicaties/algemeen/richtlijn-beoordelingscriteria-herbruikbare-medische-hulpmiddele> (2022), accessed: 2023-09-12.

- [62] *Vaporized hydrogen peroxide gas plasma technology explained*, [Online] Available: <https://www.asp.com/en-gb/education/vaporized-hydrogen-peroxide-gas-plasma-technology-explained> (2023), accessed: 2023-08-11.
- [63] *Laparoscopen - alle medische specialisme -olympus medische systemen*, [Online] Available: <https://www.olympus.nl/medical/nl/Producten-oplossingen/Producten/Laparoscopen.html>, accessed: 2023-08-09.
- [64] *I12c4f (9066) 4-way laparoscopic transducer, bk medical holding company, inc.* (2023), [Online] Available: <https://www.bkmedical.com/transducers/i12c4f-4-way-laparoscopic/>.
- [65] *Ligasure maryland jaw open en laparoscopische sealer/divider met nanocoatingtechnologie*, [Online] Available: <https://www.medtronic.com/covidien/nl-nl/products/vessel-sealing/ligasure-maryland-jaw-sealer-divider.html>, accessed: 2023-08-08.
- [66] *A realistic 3d perception in laparoscopy - endoeye 3d*, [Online] Available: <https://www.olympus-europa.com/medical/en/Products-and-Solutions/Medical-Solutions/ENDOEYE-3D/>, accessed 27-08-2023.
- [67] K. Van Duren, *Augmented reality for laparoscopic liver navigation*, M3 Technical Medicine Thesis, University of Twente, p1-46 (2022).
- [68] G. Xiao, E. Bonmati, S. Thompson, J. Evans, J. Hipwell, D. Nikitichev, K. Gurusamy, S. Ourselin, D. J. Hawkes, B. Davidson, *et al.*, *Electromagnetic tracking in image-guided laparoscopic surgery: Comparison with optical tracking and feasibility study of a combined laparoscope and laparoscopic ultrasound system*, *Medical physics* **45**, 5094 (2018).
- [69] *Sla-stereolithography, dassault systèmes*, [Online] Available: <https://www.3ds.com/make/service/3d-printing-service/sla-stereolithography> (2023), accessed: 2023-08-01.
- [70] *What is computer numerical control (cnc)? entrepreneur media*, [Online] Available: <https://www.entrepreneur.com/science-technology/what-is-computer-numerical-control-cnc/439692> (2022), accessed: 2023-08-11.
- [71] X. Zhang and F. Liou, *Introduction to additive manufacturing*, in *Additive manufacturing* (Elsevier, 2021) pp. 1–31.
- [72] A. Nijman, *Development of an instrument calibration device for image guided surgery*, Master Biomedical technology and physics Thesis, VU Amsterdam (2023).
- [73] M. Hiep, *Tracked ultrasound for patient registration in surgical navigation during abdominal cancer surgery*, M3 Technical Medicine Thesis, University of Twente (2021).
- [74] J. Li, Q. Hu, Y. Zhang, and M. Ai, *Robust symmetric iterative closest point*, *ISPRS Journal of Photogrammetry and Remote Sensing* **185**, 219 (2022).
- [75] P. Hsu, R. W. Prager, A. H. Gee, and G. M. Treece, *Freehand 3d ultrasound calibration: a review*, *Advanced imaging in biology and medicine: technology, software environments, applications*, 47 (2009).
- [76] L. Mercier, T. Langø, F. Lindseth, and D. L. Collins, *A review of calibration techniques for freehand 3-d ultrasound systems*, *Ultrasound in medicine & biology* **31**, 449 (2005).
- [77] L. E. Bø, E. F. Hofstad, F. Lindseth, and T. A. Hernes, *Versatile robotic probe calibration for position tracking in ultrasound imaging*, *Physics in Medicine & Biology* **60**, 3499 (2015).
- [78] T. C. Poon and R. N. Rohling, *Comparison of calibration methods for spatial tracking of a 3-d ultrasound probe*, *Ultrasound in medicine & biology* **31**, 1095 (2005).
- [79] D. Fontanarosa, S. Van Der Meer, E. Harris, and F. Verhaegen, *A ct based correction method for speed of sound aberration for ultrasound based image guided radiotherapy*, *Medical physics* **38**, 2665 (2011).
- [80] K. Sakata, T. Kijima, and O. Arai, *Initial report: A novel intraoperative navigation system for laparoscopic liver resection using real-time virtual sonography*, *Scientific Reports* **10**, 6174 (2020).
- [81] T. Aoki, D. A. Mansour, T. Koizumi, Y. Wada, Y. Enami, A. Fujimori, T. Kusano, K. Matsuda, K. Nogaki, Y. Tashiro, *et al.*, *Laparoscopic liver surgery guided by virtual real-time ct-guided volume navigation*, *Journal of Gastrointestinal Surgery* **25**, 1779 (2021).

- [82] K. Konishi, M. Nakamoto, Y. Kakeji, K. Tanoue, H. Kawanaka, S. Yamaguchi, S. Ieiri, Y. Sato, Y. Maehara, S. Tamura, *et al.*, *A real-time navigation system for laparoscopic surgery based on three-dimensional ultrasound using magneto-optic hybrid tracking configuration*, *International Journal of Computer Assisted Radiology and Surgery* **2**, 1 (2007).
- [83] A. Teatini, E. Pelanis, D. L. Aghayan, R. P. Kumar, R. Palomar, Å. A. Fretland, B. Edwin, and O. J. Elle, *The effect of intraoperative imaging on surgical navigation for laparoscopic liver resection surgery*, *Scientific Reports* **9**, 18687 (2019).
- [84] S. Malhotra, O. Halabi, S. P. Dakua, J. Padhan, S. Paul, and W. Palliyali, *Augmented reality in surgical navigation: A review of evaluation and validation metrics*, *Applied Sciences* **13**, 1629 (2023).
- [85] H. Luo, D. Yin, S. Zhang, D. Xiao, B. He, F. Meng, Y. Zhang, W. Cai, S. He, W. Zhang, *et al.*, *Augmented reality navigation for liver resection with a stereoscopic laparoscope*, *Computer methods and programs in biomedicine* **187**, 105099 (2020).
- [86] M. Fusaglia, P. Tinguely, V. Banz, S. Weber, and H. Lu, *A novel ultrasound-based registration for image-guided laparoscopic liver ablation*, *Surgical innovation* **23**, 397 (2016).
- [87] J. Brooke, P. W. Jordan, B. Thomas, B. A. Weerdmeester, and I. McClelland, *Usability evaluation in industry*, (1996).
- [88] S. Sharma, A. Telikicherla, G. Ding, F. Aghlmand, A. H. Talkhooncheh, M. G. Shapiro, and A. Emami, *Wireless 3d surgical navigation and tracking system with 100 μ m accuracy using magnetic-field gradient-based localization*, *IEEE Transactions on Medical Imaging* **40**, 2066 (2021).
- [89] J. N. Smit, K. F. Kuhlmann, B. R. Thomson, N. F. Kok, T. J. Ruers, and M. Fusaglia, *Ultrasound guidance in navigated liver surgery: toward deep-learning enhanced compensation of deformation and organ motion*, *International journal of computer assisted radiology and surgery* , 1 (2023).
- [90] D. Reichard, D. Häntschi, S. Bodenstedt, S. Suwelack, M. Wagner, H. Kenngott, B. Müller-Stich, L. Maier-Hein, R. Dillmann, and S. Speidel, *Projective biomechanical depth matching for soft tissue registration in laparoscopic surgery*, *International Journal of Computer Assisted Radiology and Surgery* **12**, 1101 (2017).
- [91] R. Docea, M. Pfeiffer, S. Bodenstedt, F. R. Kolbinger, L. Höller, I. Wittig, R.-T. Hoffmann, E. G. Troost, C. Riediger, J. Weitz, *et al.*, *Simultaneous localisation and mapping for laparoscopic liver navigation: a comparative evaluation study*, in *Medical Imaging 2021: Image-Guided Procedures, Robotic Interventions, and Modeling*, Vol. 11598 (SPIE, 2021) pp. 62–76.
- [92] I. Paolucci, R.-M. Sandu, L. Sahli, G. A. Prevost, F. Storni, D. Candinas, S. Weber, and A. Lachenmayer, *Ultrasound based planning and navigation for non-anatomical liver resections—an ex-vivo study*, *IEEE open journal of engineering in medicine and biology* **1**, 3 (2019).
- [93] K. Wang, Y. Liu, H. Chen, W. Yu, J. Zhou, and X. Wang, *Fully automating li-rads on mri with deep learning-guided lesion segmentation, feature characterization, and score inference*, *Frontiers in Oncology* **13**, 1153241 (2023).
- [94] T. Okamoto, S. Onda, K. Yanaga, N. Suzuki, and A. Hattori, *Clinical application of navigation surgery using augmented reality in the abdominal field*, *Surgery today* **45**, 397 (2015).
- [95] N. C. Buchs, F. Volonte, F. Pugin, C. Toso, M. Fusaglia, K. Gavaghan, P. E. Majno, M. Peterhans, S. Weber, and P. Morel, *Augmented environments for the targeting of hepatic lesions during image-guided robotic liver surgery*, *Journal of surgical research* **184**, 825 (2013).
- [96] R. Tang, L.-F. Ma, Z.-X. Rong, M.-D. Li, J.-P. Zeng, X.-D. Wang, H.-E. Liao, and J.-H. Dong, *Augmented reality technology for preoperative planning and intraoperative navigation during hepatobiliary surgery: A review of current methods*, *Hepatobiliary & Pancreatic Diseases International* **17**, 101 (2018).
- [97] A. Ruzzenente, L. Alaimo, S. Conci, F. Bagante, T. Campagnaro, C. Pedrazzani, and A. Guglielmi, *Robotic liver surgery: literature review and current evidence*, *Mini-invasive Surg* **4**, 91 (2020).

Appendices contents

A Literature Review	1
B Technical Drawing Adapter	ii
C Summary study protocol	iii

A

Literature Review

This appendix contains a literature review, with the title:
Ultrasound-based navigation during laparoscopic liver surgery: a review of the state of the art.

Ultrasound-based navigation during laparoscopic liver surgery: a review of the state-of-the-art

Julia Greeven^a

^aMSc Student Technical Medicine, Technical University Delft, Leiden University Medical Center, Erasmus Medical Center, The Netherlands

May 19, 2023

Abstract

Laparoscopic camera and ultrasound (US) are standard imaging modalities used during laparoscopic liver surgery. Nonetheless, there are challenges due to the adaptation to two-dimensional (2D) imaging, the lack of depth perception and tactile feedback. A technique that can improve general localization of anatomical structures during laparoscopic procedures is surgical navigation combined with laparoscopic ultrasound (LUS). The purpose of this systematic review is to provide an overview of the literature on surgical navigation based on intraoperative LUS performed in laparoscopic liver surgery. The review highlights 10 key papers that discuss navigation, registration, visualization, and evaluation methods.

Keywords: liver, laparoscopy, image-guided surgery, surgical navigation, intraoperative ultrasound

1 Introduction

Primary and secondary liver cancer are one of the leading causes of cancer-related deaths worldwide [1, 2]. Surgical resection is the only curative treatment for patients with malignant liver tumors, hence it is considered the gold standard [1, 3]. While open surgery is the standard approach for abdominal surgeries, there has been a growing trend in the last decades towards switching to more minimally invasive methods. This shift is because minimally invasive procedures are associated with reduced trauma for patients. Laparoscopic liver procedures offer significant benefits over open surgery by eliminating the need for extensive abdominal incisions, resulting in decreased postoperative discomfort, reduced costs, and faster recovery times [4, 5]. However, there are certain factors that contribute to increased technical difficulty of the procedure compared to open surgery, which make laparoscopic approaches more challenging [6, 7]. The main challenge is the inability to palpate the liver parenchyma, resulting in difficulties in identifying resection margins [6, 7]. Other limitations of laparoscopy include limited instrument movement and adaptation to two-dimensional (2D) imaging [8]. The loss of tactile feedback and depth perception lead to reduced spatial understanding and an increased risk of unwanted contact between instruments and anatomical structures. As a result, performing laparoscopic liver procedures requires significant hand-eye coordination and extensive training [4]. Ultrasound (US) is the standard imaging modality during laparoscopic liver surgery as it is real-time, non-invasive and compensates for the loss of tactile feedback by providing imaging beyond the organs surface [9, 10]. US guidance is essential in planning the surgical approach and determining the exact resection planes [11]. Nevertheless, intraoperative ultrasound (IOUS) images, like laparoscopic images, are two-dimensional, which are challenging to interpret compared to the actual three-dimensional (3D) scene available in open surgery. Similar to laparoscopic surgery, ultrasonography has a steep learning curve in accurately visualizing and interpreting the subsurface anatomy due to the liver's complex 3D structure [12]. In addition, the effectiveness of LUS is hindered by the limitations imposed by the laparoscopic approach, which operates through a fixed port, has limited abdominal space and restricted probe positioning and angulation [13].

The use of surgical navigation can be beneficial in reducing the complexity of performing liver resection during laparoscopic surgery [14]. This technique aims to improve general localization of anatomical structures by integrating preoperative and intraoperative images with tracked surgical instruments by aligning them in the same coordinate system. This alignment process is known as registration, whereby the preoperative images are matched to the liver’s spatial location [15]. Displaying the highly variable vascular and tumor anatomy may aid in identifying tumor margins as well as blood vessels and bile ducts. Then, resection planes can be optimized to ensure adequate safety margins and the maximum amount of healthy liver tissue to be preserved [16]. Harms et al. (2001) [17] were the first to incorporate an electromagnetic (EM) tracking sensor into a conventional laparoscopic ultrasound (LUS) probe. By combining tracking and IOUS, it is possible to reconstruct a volume of the underlying anatomy, by defining each US image with its position in a 3D coordinate system. Surgical planning and identification of tumor locations can be aided by the creation of accurate 3D models of relevant anatomical structures through segmentation and reconstruction processes using preoperative Magnetic Resonance Imaging (MRI) or Computed Tomography (CT) scans [18]. These models can be used during surgery to guide decision-making and can be registered onto the patient’s anatomy [19]. To ensure the successful use of surgical navigation in laparoscopic liver procedures, it is crucial to obtain accurate patient-to-image registration [4]. The registration accuracy is affected by respiration motion, pneumoperitoneum, and surgical manipulation which causes the organ to change its shape and position with respect to its preoperative counterpart which is defined as a rigid 3D model [20, 21]. Therefore, it is important to perform intraoperative imaging throughout the surgery to provide updated information on the patient’s anatomy [18]. LUS imaging provides real-time imaging data that can be obtained throughout the course of a surgical procedure, and re-registering the liver’s position and orientation to the preoperative model is simpler and less time-consuming compared to CT or MRI imaging [6]. Given its low cost and standard availability during laparoscopy liver surgery, it is more valuable to rely navigation on IOUS for improving the accuracy and precision of the procedure [13, 9]. This systematic literature review aims to provide an overview of the current state of the art research in the use of US-based navigation technique to guide laparoscopic liver surgery. Different methods with their benefits and challenges associated with the use of this technique will be discussed and give insights into this area of study.

2 Methods

2.1 Search strategy

A systematic search was conducted in line with the PRISMA guidelines using multiple databases [22]. Medline, Embase and Web of Science were used as search engines. The search utilized both free-text and corresponding controlled vocabulary terms related to "liver" and "laparoscopy," as well as more technical terms such as "surgical navigation" and "intraoperative ultrasound". Additionally, the reference lists and forward-citations from the articles were consulted to identify additional relevant articles that were not found by using the search terms. Appendix A provides a detailed description of the search strategies used in all three databases.

2.2 Study selection procedure

The selection procedure of the articles comprised of screening and assessment for eligibility, performed by one observer. First, titles and abstracts were screened and included if they met the criteria of addressing liver laparoscopy and intraoperative US-based navigation. Articles were excluded according to the following criteria: 1) not written in English, 2) no full texts available through Erasmus Medical Center (EMC), Nederlands Kanker Instituut (NKI) or Leiden University Medical Center (LUMC) database searching, 3) not include relevant information on tracking method, registration method, and visualization methods of the surgical navigation, and 4) involving phantom and non-liver studies. Then, full articles were assessed for eligibility and included if their research covered 1) the liver, 2) laparoscopic surgery, 3) US-based surgical navigation.

2.3 Data extraction and study outcomes

Different aspects from the included studies were extracted to provide an overview of the methods that have been used for navigated laparoscopic liver surgery based on IOUS. This review describes the tracking methods, intraoperative visualization, and post-operative evaluation. In addition, results and limitations of the described techniques were useful to assess the extent of contribution in this field. A summary and a descriptive analysis of the included studies that discuss the use of IOUS to guide laparoscopic liver surgery was made. Whenever possible, objective measures like navigation accuracy and setup time were used to quantify the system's performance. However, due to significant variations in the research methodologies employed in the studies, a meta-analysis could not be conducted.

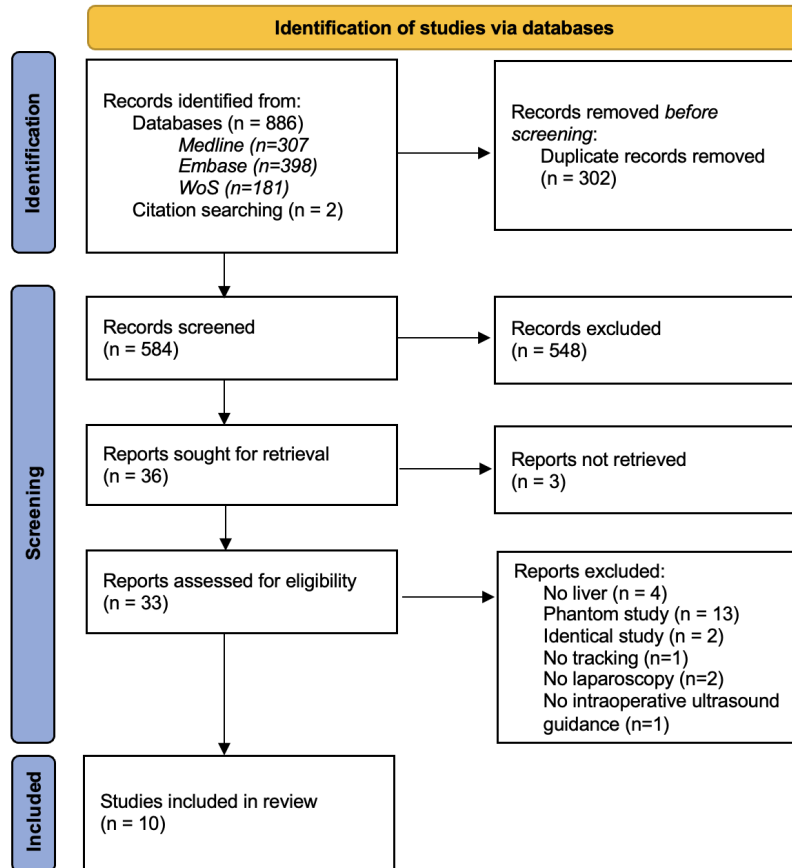


Figure 1: PRISMA flow diagram of selection study [22].

3 Results

3.1 Search results

Database searching up to the 10th of February 2023 resulted in 888 articles, two of which were retrieved through citation searching. After the removal of 302 duplicates, the remaining 584 articles were screened based on their titles and abstracts. After screening, 548 articles were excluded based on the exclusion criteria. Three articles were not retrieved as their full texts were not found through database searching. A total of 33 articles were assessed for eligibility based on full-text reviews. After further examination, another 23 articles were excluded as they did not provide relevant information for this systematic literature review. Finally, 10 articles were considered eligible and included for this review. Figure 1 shows the flow diagram of the selection process according to the PRISMA guidelines [22].

3.2 Study characteristics

The results have been presented both in tables and written format, providing an overview of the findings. Table 1 includes ten studies, of which six are non-clinical studies (five in-vivo animal experiments and one ex-vivo experiment on a porcine liver). The other four clinical studies (listed in Table 2) described three feasibility studies and one case report. Among the reviewed studies, two articles focused on enhancing the techniques of laparoscopic liver surgery (LLS), while seven studies described experiments related to laparoscopic liver resection (LLR). In addition, one study detailed their navigation method for laparoscopic liver ablation (LLA). The following section covers the methods used for navigation and the reported results.

3.3 Outcomes

3.3.1 Tracking method

Optical or EM tracking

Optical tracking was used in two studies [18, 23]. Although optical systems offer high accuracy and large working volumes compared with EM systems, they require an unobstructed line of sight between the tracking camera and the retro-reflective markers on the tracked tools [24]. This is necessary to enable the reflection of incoming light back to the cameras [25]. On the other hand, EM systems do not have this limitation but may experience reduced accuracy due to magnetic field distortions induced by the presence of electronic devices or ferromagnetic objects nearby [26]. Nevertheless, EM tracking systems are more common because they allow for tracking the tip of the laparoscopic instruments inside the patient's body. The EM tracking systems manufactured by Northern Digital (NDI Aurora, Ontario Canada) were primarily used, although other systems by Ascension Technology Ltd (Burlington, VT, USA) [17] and CIVCO Medical Solutions (Coralville, Iowa, USA) [13] were also used. Only Konishi et al. [18] used a hybrid magneto-optic tracking method. They described that optical trackers are ideal for tracking rigid laparoscopes that have external attachments to capture laparoscopic images. On the other hand, magnetic trackers are better suited for tracking the LUS probe inside the abdomen and therefore should be preferred. In addition, they developed a correction method to reduce the effect of electromagnetic distortion and improve tracking accuracy. They used an apparatus with a hybrid tracker to acquire calibration data and allow for a distortion measurement. This tool is equipped with an optical rigid body and an EM receiver on the tip, which enables simultaneous measurement of the receiver's position and orientation through optical and EM tracking methods. Using this correction they significantly reduced the tracking error (34.64 ± 15.27 to 2.590 ± 0.913 mm in position).

Instrument tracking and sensor location

All studies reported use of instrument tracking to navigate during laparoscopic liver surgery. Seven of the articles employed EM tracking of the LUS probe, where the EM sensor was often attached on the tip of the device. This is required because the LUS probe has a flexible tip and moves independently from its shaft. Since this tip has to be in contact with the liver, placing a tracker at the tip of the LUS probe improves navigation accuracy, as angulation of the tip could not cause measurement errors [27, 28]. In Figure 2, three studies displayed their used tracker mount containing an EM sensor located on LUS probe's tip [29, 21, 20]. In addition to using an externally attached EM sensor, which is not ideal for routine clinical use, Liu et al. [29] also employed a GPS LUS transducer, that contains an internally embedded EM sensor. They have shown that this tracking accuracy was comparable with that of a conventional LUS with an externally located sensor and provides a significant enhancement to the clinical practicality of EM-tracked LUS. Since several studies have attempted to determine the angle of the probe tip with respect to the shaft using EM tracking, Oguma et al. [23] proposed an optical tracking method for this. They attached optical markers on the handle of the LUS probe and the laparoscope to locate the US image in the laparoscopic image coordinate system. Real-time overlaying of US images onto laparoscopic images was made possible by detecting the angle of the LUS probe tip. The position and orientation of the tip were determined using green markers attached to the tip, which were visible on the laparoscopic image. The angle was calculated using computer vision techniques. This method can be easily implemented in real-time, with high robustness, and resulted in a 0.97mm overlaying error of US images. They evaluated a detection rate to be 83.1% through animal experiments and showed that it only failed when the probe tip was placed far from the laparoscope.

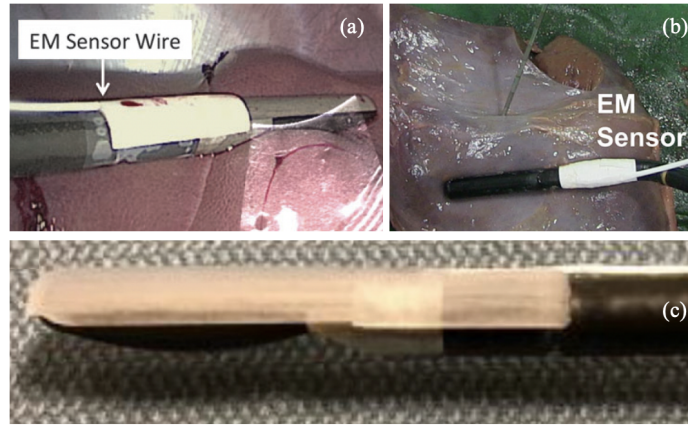


Figure 2: Tracker mounts containing EM sensor. (a) Lau et al. [21] (b) Shahin et al. [20] (c) Liu et al. [29]

Other tracking

In addition to instrument tracking, Aoki et al. [13] used a patient tracker (omniTRAX™, CIVCO) to establish a correlation between preoperative CT scans and the patient’s actual anatomy during surgery. This allows the position of the instrument to be integrated with the preoperatively acquired CT images, indicating its location relative to the displayed anatomical structures. Continuous tracking and compensation for liver deformation is needed to maintain acceptable registration accuracy. Kleemann et al. [27] achieved this through tracking of the liver surface using the LUS to scan the entire organ and obtain a detailed registration of the liver surface. This involves scanning and imaging not only the tumor, but also critical vascular structures. They repeated the liver surface registration when the patient’s position intraoperatively changed, but they did not compensate for surgical manipulations. Shahin et al. [20] proposed a fast approach to determine the tumor location and adjust for any tumor shifts during the surgery. They first reconstruct a 3D-US image and segment the tumor. During surgery, newly acquired tracked US images are used to update the tumor’s position, which is automatically detected and updated in the navigation system based on the initial tumor segmentation. Only two iterations of tumor localization were used and evaluated, while the procedure can be repeated whenever tumor position update is necessary. They successfully estimated the new tumor position in 11 out of 12 cases and reported an average time to update the tumor position of 1.15 seconds. However, it should be considered that despite using laparoscopic instruments, they only performed ex-vivo experiments not in a laparoscopic setting. The mean navigation error in a needle experiment was 1.2 ± 0.6 mm.

3.3.2 Navigation and registration

Navigation systems and methods

Self-developed navigation systems are common among the studies since no commercial navigation systems for laparoscopic liver surgery are available. Several studies performed navigation based on registration of preoperative data. Resection plans were frequently translated to the intraoperative environment and used for navigation [10, 27]. The system described by Hansen et al. [10] describes two approaches for modifying resection plans during surgery. The first approach uses an US-based navigation system, while the second approach uses the Wiimote for human-computer interaction. After registering to the preoperative data, the 2D-US plane defined by the surgeon is combined with tracking information from the navigation system. This correlates the US plane to the preoperative resection plan and allows to update the resection plan and volume calculation. The US-based approach has limitations in modifying complex shapes since this tool is planar. Therefore, the Wiimote approach was introduced as an intuitive and wireless pointing device, based on optical tracking, and wrapped in sterile plastic, for modifying (non-planar) virtual resection planes during surgery. In Figure 3 the different steps of resection planning are visualized. A combination of both approaches shows promise for defining and refining a first approximation of the desired resection plane and a time for intraopera-

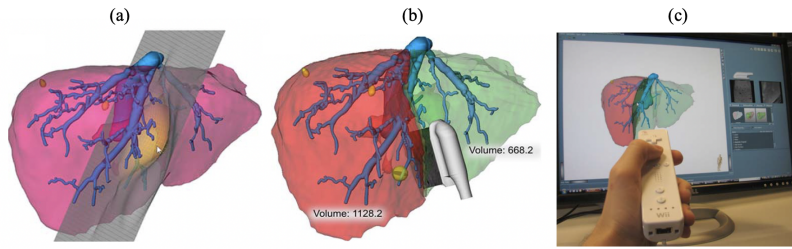


Figure 3: Hansen et al. [10] (a) Resection planning on pre-operative data (b) Merge of preoperative resection plane and intraoperatively defined resection volume (US plane), and updated volume calculation (c) Use of a Wiimote controller to modify virtual resection plane by drawing lines on a virtual 3D liver surface.

tive updating of planning data within 10 seconds was reported. The majority of the studies performed navigation based on registration of only intraoperative images. Three of these studies utilized navigation that relied on 3D images reconstructed using tracked IOUS [17, 18, 20]. The advantage of the proposed approach of Shahin et al. [20] is that it is based on routinely used LUS and enhances its functionality to estimate the tumor position in 3D. Also Harms et al. [17] used their 3D technique for precise identification of tumor location and volume, as well as a clear description of surrounding and critical anatomical structures. Aoki et al. [13] and Sakata et al. [28] performed tracking of US images to confirm the dissection plane. Lastly, three other pre-clinical studies used navigation systems based on AR, and used registration methods which superimposes images obtained from IOUS onto laparoscopic images [18, 29, 21, 23].

Registration methods

Hansen et al. [10] registers preoperative radiological data with intraoperative US-images by identifying corresponding landmarks, such as vessel branches, in both images. The registration is then computed using thin plate splines. This technique generates a smooth surface by interpolating a set of control points, where each point is considered as a position constraint. Also, Aoki et al. [13] correlates the intraoperative patient anatomy and the pre-acquired CT data by using an automatic registration method based on a patient-tacker. They reported an average fiducial registration error (FRE) of 12 mm. The navigation system (LapAssistent) described by Kleemann et al. [27] uses registration of the liver surface using the EM tracking system and alignment of planning data to the intraoperative situation by landmark. The study did not quantify registration error or navigation accuracy. Overall, the reviewed studies did not discuss any non-rigid registration methods that accounted for liver deformation. Nevertheless, Konishi et al. [18] accounted for electromagnetic distortion when performing EM tracking and significantly improved the registration accuracy of their 3D-US navigation system to an accuracy of 2 mm and within 2 min.

3D modelling and segmentation

Harms et al. [17] used a navigated 3D LUS device (Siemens Linear Array Probe LAP8-4.3D, 5 MHz) to generate 3D-US data. This device employs the same technique used for tracked 2D LUS to obtain 3D volumes, where the coordinates of each individual 2D image are used to generate 3D reconstructions, aiding in accurately identifying tumor location and margins. Among the articles reviewed, the use of 3D modeling techniques was evenly distributed between those based on pre-operative CT data and those based on real-time US images. Harms et al. [17] collected 3D-US data by moving a laparoscopic probe over a specific region of interest (ROI), which was then used to generate 3D reconstructions. The volumetric data of each lesion was compared to a 3D-CT scan but tended to underestimate the ROI volume by 3.1%. Sakata et al. [28] used a 3D simulation software (Synapse Vincent, Fujifilm) to extract anatomical structures of the liver, while other segmentation methods were also discussed. In Konishi et al. [18], tumors and vessels were extracted by controlling opacity using a histogram of the intensity of pixels in the target. Additionally, Hansen et al. [10] utilized an approach based on security margins around each tumor, the segmented liver and vessels, that were automatically determined using a mathematical model. Lastly, Shahin et al. [20] used a level set method on US images to identify intrahepatic tumors. This method is used to track the evolution of a moving boundary over

time using a mathematical function and solves partial differential equations to update its location [30].

3.3.3 Visualization of intraoperative navigation

Different software were used within the reviewed studies, such as MeVis software (MDS, Fraunhofer) [27] and Synapse Vincent (Fujifilm, Tokyo, Japan) [28]. These software display 3D models of the liver based on preoperative images. These 3D models are composed by structures like the liver, tumors, hepatic and portal vein. Furthermore, various visualization methods have been discussed to integrate IOUS images with laparoscopic images. Multiple studies superimposed 2D-US images onto the laparoscopic video. Oguma et al. [23] presented an additional semi-transparent view option (Figure 4a) and Konishi et al. [18] overlaid 3D-US volumes onto the real-time laparoscopic video (Figure 4b). The

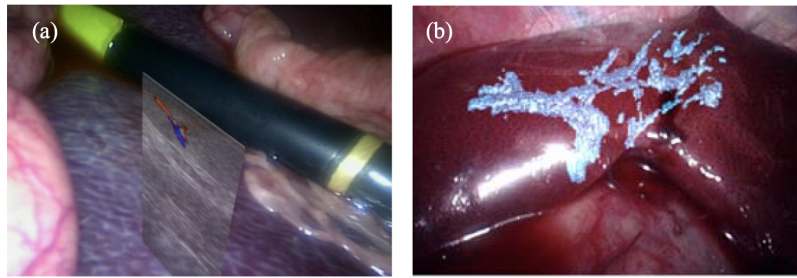


Figure 4: US images overlaid on laparoscopic video (a) Oguma et al. [23] (b) Konishi et al. [18]

standard view of navigation software is a 3D visualization that shows the position and orientation of the instruments in relation to the preoperative model. The navigation system of Sakata et al. [28] displayed images on a TV alongside corresponding CT and/or MRI. In addition, it superimposed a preoperative simulation onto the CT image and indicated the extent of resection, enabling navigation of the planned resection plane. Additionally, instrument trajectories [20, 29] and color regions [23] have been added to the intraoperative navigation screens to assist the surgeons' orientation. The software in [20] provides information on needle trajectory from the tumor centroid, allowing visualization of the trajectory in the proximity of the targeted tumor. Figure 5b shows a snapshot of the navigation screen, displaying needle alignment towards the target and a segmented tumor within surrounding tissue. It includes options to adjust transparency. Liu et al. [29] integrated the trajectory line of the needle and projecting it onto the laparoscopic video. A 2D line segment between the projected points and a circle was drawn to highlight the ROI (Figure 5a). In Figure 5c, it can be seen how Oguma et al. [23] overlays US images onto laparoscopic images, with color-coded regions on the US overlays indicating blood flow within an organ, using Doppler mode. Three other studies provided multi-modal visualizations simultaneously during navigation. Kleemann et al.'s [27] LapAssistant included virtual reality navigation with registered IOUS onto preoperative 3D-MRI-planning data, real-time laparoscopic video, and real-time US images with overlapping tumor. An overview of the screen can be seen in Figure 6a. The VRCT system of Aoki et al. [13] synchronously displays preoperative acquired CT images with real-time US-images and displays instrument tip position on multi planar reconstruction (MPR) images of CT and real-time 2D-US images. This technology improves visualization, provides needle movement tracking and displays a 3D reconstruction map of relevant liver anatomy (Figure 7).

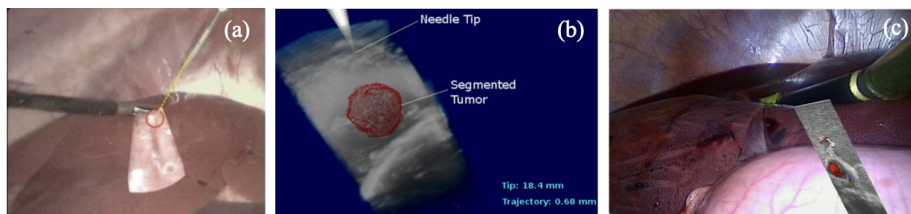


Figure 5: Instrument trajectory and color regions (a) Liu et al. [29] (b) Shahin et al. [20] (c) Oguma et al. [23]

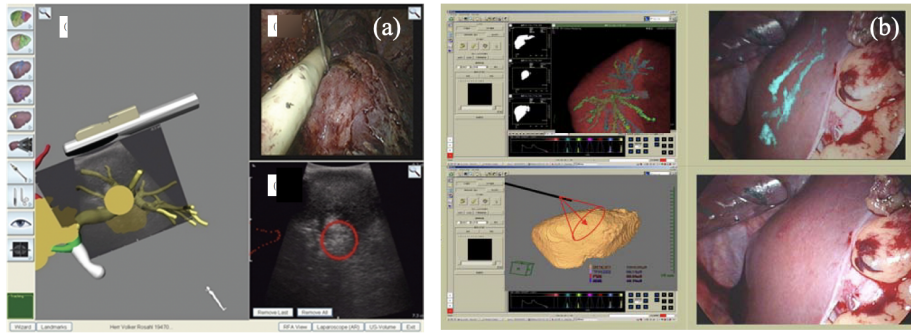


Figure 6: Multi-dimensional visual experience (a) Kleemann et al. [27] (b) Konishi et al. [18]

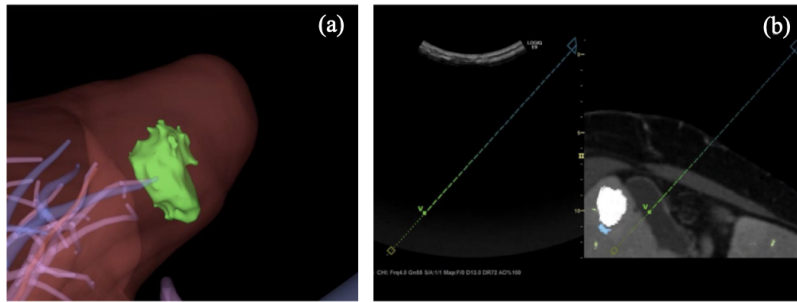


Figure 7: Screen overview Aoki et al. [13] (a) 3D reconstruction liver map (b) VRCT with instrument tracking.

Lastly, the integrated display system of Konishi et al. [18] allows simultaneous visualization of 3D-CT and augmented 3D-US images onto laparoscopic video, aiding in navigation during laparoscopic procedures (Figure 6b).

3.3.4 Experimental setting and post-operative evaluation

Proposed methods were evaluated as effective and could be used in clinical setting [18]. Shahin et al. [20] evaluated their system by navigating a needle to the center of porcine liver tumors (ex-vivo). The results showed that the tumor shift caused by needle insertion and tissue handling was up to 38 mm. Additionally, Konishi et al. [18] assessed the accuracy of needle punctures under AR guidance for liver tumors using an electromagnetic distortion correction and showed successfully puncturing of all tumors. The results showed high accuracy in needle positioning, indicating the potential of AR guidance for improving the precision of liver tumor interventions. Liu et al. [29] and Lau et al. [21] also described beneficial results of using AR guidance in laparoscopic liver surgery. However, the study of Liu et al. [29] did not compare the AR approach with a method that solely combines LUS image with the needle trajectory, and there were challenges in addressing certain factors in a pre-clinical setting that would be relevant in an actual procedure. According to Lau et al. [21], based on their initial in-vivo experience, the additional four minutes needed to complete the resection could be attributed to the larger size of the lesion and the surgeons' lack of familiarity with the system. However, AR guidance achieved negative resection margins. Overall, the majority of the presented systems showed that navigation-related activities can be performed within one minute. It is important to note that while these pre-clinical studies focused on technical aspects, not all these experiments evaluated the navigation system's performance within a clinical workflow in the operating room. As a result, the evaluations reported in these studies cannot be considered as hard evidence. The results of the four clinical studies showed findings of feasibility studies conducted on small sample sizes. Only Harms et al. [17] and Aoki et al. [13] performed their navigation method in 17 and 27 patients, respectively. However, these clinical studies showed the added value of their laparoscopic navigation systems based on IOUS. Sakata et al. [28] showed experiences of four tumors that were all succeeded to be detected by their navigation system. Aoki et al.'s [13] reported 96.3% successful resections and primarily focused

on small lesions, with an average size of 11 mm. Although three of these lesions were detected on preoperative CT, they were not visible during pre- or intraoperative US scans due to their small size (max diameter 8 mm). However, with their navigation system, all three lesions were successfully removed (with negative resection margins), despite the system’s limitations in compensating for liver deformation during the procedure. Only Aoki et al. [13] used a questionnaire to evaluate usefulness of the navigation system. It revealed high ratings for tumor and landmark detection and operability, with an acceptable score for resection plane evaluation. Accuracy was identified as the area that needs the most development.

3.4 Recommendations based on literature

- An advantage of employing an EM tracking system instead of an optical tracking system is that it does not necessitate a direct line-of-sight between the transmitter and the receiver, allowing for the tracking of the tip of laparoscopic instruments inside the patient’s abdomen [20].
- The navigation information from a tracker placed at the tip of the instrument reduces the effects of calibration error [27, 28].
- Reported calibration accuracy is ranging from 0.6-4.0mm (EM tracking) and 0.3-2.7mm (optical tracking).
- Active tracking of tumors and the liver was not performed continuously during laparoscopic liver surgery.
- Overlaying the 2D-US image onto the laparoscopic video instead of superimposing preoperative 3D-CT data onto the surgical site is independent from any registration errors while still providing guidance [27].
- The process of resection planning will be made easier through the use of a color-coded visualization and instrument trajectories that shows the spatial distances between the current resection plane and risk structures, such as vessels, and tumor margins [23, 20, 29].
- Navigation systems that provide multi-modal visualizations simultaneously during navigation can significantly improve the precision and accuracy of laparoscopic surgeries, leading to better outcomes for patients [27, 18].

4 Discussion

Several applications of US-based navigation for laparoscopic guidance were described. Studies have demonstrated that intraoperative registration can be performed without the need for preoperative data [20] and IOUS being utilized to guide the preoperative resection plan [28, 13, 10]. Despite the challenging nature of interpreting information from IOUS images, such as their 2D nature and limited field of view, it has been shown that the use of navigated 3D-LUS improves tumor localization and margin detection [18, 17]. Furthermore, studies have demonstrated that 3D reconstruction of the liver based on preoperative CT or MRI data, that includes tumors and vascular structures, enables interactive exploration and calculation of resected and remaining organ volumes, and can be registered to the intraoperative environment [10]. Different visualization methods were described and it was demonstrated that combining visualizations during navigation including 3D models, laparoscopic images and IOUS, allows the surgeon to visualize multiple interactions and dimensions in a single view [27, 18]. Additional aid was provided to assist surgeons in laparoscopic navigation through augmented features, including instrument trajectories and color coding. Overall, the reviewed studies highlight different aspects that could contribute to an all-encompassing and interesting method to improve laparoscopic liver surgery with US-based navigation.

It should be considered that the clinical studies that have been reviewed are relatively few and small. This limits the generalizability of the findings and makes it difficult to draw conclusions based on these studies. Therefore, it is important to assess these early experiences in a broader patient population [27]. Additionally, none of the studies had control groups, which means that the effectiveness of US-based navigation in comparison to other methods of navigation cannot be directly assessed. Furthermore,

the accuracy of navigation depends on the successful completion of intraoperative registration. Many studies did not consider the deformation of the liver during surgery, which impacts the accuracy of the navigation systems. This is an important factor to consider since the liver is a highly deformable organ, and its shape can change significantly during surgery. The absence of non-rigid registration methods and continuous tracking result in a lower accuracy [27, 13]. At last, there were no clear opinions given on the visualization methods of intraoperative navigation in the reviewed studies. This makes it difficult to draw conclusion on what the most effective visualization method for US-based navigation is, and further research is needed in this area to determine the optimal approach for visualization during laparoscopic procedures. Overall, the absence of a consistent and uniform approach of US-based navigation within the reviewed studies, makes it challenging to compare findings between various studies and to form definitive conclusions regarding the efficacy of these methods.

Different from the reviewed studies, a phantom study of Singla et al. [31] evaluated their navigation method in a control group and provided qualitative feedback from surgeons. They demonstrated their AR guidance system not for liver surgery, but for robotic-assisted nephrectomies. Different augmentations on the navigation screen were proposed to provide real-time guidance to the surgeon during surgery. The system was tested in simulated partial nephrectomies and compared with LUS only. The system evaluated a total system error of 2.5 ± 0.5 mm and they found that the AR guidance system was effective in providing real-time guidance to the surgeon and improved the quality of the surgery. In terms of the AR overlays, the surgeon preferred the projected path the most, followed by the traffic lights, the compass, and finally the virtual viewpoint. A different study used a method that involved registration without preoperative data, although they did not perform experiments in a laparoscopic setting. Paolucci et al. [32] presented a new technique for creating an intraoperative resection plan using navigated US based on optical tracking. The approach involves scanning the surface with navigated US, segmenting the tumor on a midsection US image, calculating an optimal resection strategy, and displaying it with tracked surgical instruments. The process of resection planning involves selecting a shape that fits around the tumor and calculating its center and diameter. Then, a desired margin and shape for resection are chosen, and the shape is fitted into the model while taking constraints into account. The start of the resection line is determined by the intersection of the resection shape and the liver surface. The surgical plan is displayed on a screen with tracked instruments, and the 3D model is projected onto the US image plane as a semitransparent overlay, allowing the surgeon to enable or disable visualization of the tumor, safety margin, cutting plane, and cutting line. The results of experiments on ex-vivo porcine models showed a 95.7% R0 resection rate, with a median resection margin of 5.9 mm. But again, optical tracking is not suitable for tracking laparoscopic instruments inside the patient's abdomen.

5 Conclusions

The reviewed studies suggests that US-based navigation can be a valuable technique for guiding laparoscopic liver surgery. However, the studies included in this review had small sample sizes and variations in the techniques used for IOUS guidance that make it difficult to draw generalized conclusions. Nevertheless, the findings have important clinical implications, as navigation techniques based on LUS may lead to improved surgical outcomes in patients undergoing laparoscopic liver surgery. Future research should focus on larger studies with standardized techniques for US-based navigation to further validate the use of this technique in clinical practice.

Table 1. Pre-clinical studies

Author & Publication Year	Study design & Type of surgery	Aim study	No. of subjects / lesions	Imaging modality	Navigation system	Tracking method & tracked tools	Registration principle	Visualization of navigation	Important findings	Important limitations
Konishi et al. (2007) [12]	In vivo Animal LLS	Demonstrate accuracy and feasibility of a 3D-US system using a miniature magnetic tracker combined with an optical tracker.	12/12	2D LUS	Self-developed, AR based navigation	Optical (Polaris, NDI) EM (microBIRD, ATI)	US - video	3D-US volumes onto laparoscopic video	- Data acquisition time was 67.8 ± 25.1 sec. - The accuracy of 3D US navigation was improved from 17.2 ± 5.27 to 1.96 ± 0.87 mm RMS ($p < 0.05$) using magnetic distortion correction	- Lacks comparison optical and EM tracking
Hansen et al. (2008) [10]	In vivo Animal LLR	Introduce a new application (IPA) which includes two novel approaches for intraoperative modification of resection plans	1/2	2D LUS	Self-developed IPA application	EM LUS probe, laparoscopic instruments	US - CT	Multi-modal visualization, intraoperative updated resection plan	- Intraoperative update of planning data within 10sec. - The combined RMS error of calibration and tracking results in a landmark localization error of ~ 4 mm	- Resection can be specified precisely, but is limited to axial slices (not appropriate for complex resections)
Oguma et al. (2014) [23]	In vivo Animal LLR	Develop a system for overlaying an ultrasound image on the laparoscopic image in real-time using probe angle detection.	1/NA	2D LUS	AR based navigation	Optical (MiconTracker, Claron Technology) LUS probe handle, laparoscopic handle	US - video	2D-US images overlaid on laparoscopic video, with color regions to represent blood flow inside organ	- Probe tip detection failed only when it is placed far from the laparoscope due to low illumination - Semi-transparency of overlay and color Doppler mode for vessel depth enhanced intuition - Phantom evaluation showed mean translation error of 0.97 ± 1 mm	- Delay of 2sec. in overlaying the US image - No method for multi-directional probe angle detection (only rotational degree of freedom of one axis)
Shahin et al. (2014) [20]	Ex vivo Animal LLR	Accurately determine the tumor position relative to the surgical tool, and update this position during laparoscopic procedure to reflect the actual changes.	1/13	2D LUS	Self-developed	EM (Aurora, NDI) Needle handle, LUS probe tip	3D reconstructed volumes by tracked 2D US registered with needle tip position	Rendered US volume and a segmented tumor, distance from needle tip to tumor and from needle trajectory to tumor	- Time required to reconstruct 3D volumes was 18s - Mean TRE in needle experiment was 1.2 ± 0.6 mm - The algorithm compensated for tumor shifts up to 38mm in an average time of 1 sec.	- Visualization of only US images on the navigation screen might be insufficient for the whole navigation procedure - Rigid registration was used

*LLR = laparoscopy liver resection, LLS = laparoscopy liver surgery, US = ultrasound, 3D = three-dimensional, 2D = two-dimensional, LUS = laparoscopic ultrasound, AR = augmented reality, EM = electromagnetic, NA = not applicable, IPA = intraoperative planning assistant, TRE = target registration error, RMS = root mean square

Table 1 (continued)

Author & Publication Year	Study design & Type of surgery	Aim study	No. of subjects / lesions	Imaging modality	Navigation system	Tracking method & tracked tools	Registration principle	Visualization of navigation	Important findings	Important limitations
Lau et al. (2019) [21]	In vivo Animal LLR	Description of the experience using a AR system for laparoscopic hepatic wedge resection and show the system's ease of use and its ability to guide a surgeon and achieve a negative margin resection.	1/2	2D LUS	Self-developed, AR based navigation	EM (Aurora, NDI) Self-designed tracking mounts at laparoscope handle and LUS probe tip	US - video	2D-US images overlaid onto laparoscopic video	- No use of preoperative imaging - Laparoscope calibration time was 3min. - Time of resection increased with 4min. by using AR - Resection under AR guidance achieved a negative margin	- Only fist in vivo experience - Additional time to complete resection using AR guidance
Liu et al. (2020) [27]	In vivo Animal LLA	Evaluate incorporated needle navigation mode to a previously developed AR system based on EM tracking in phantom setting and animal model	1/2	2D LUS	Self-developed, AR based navigation	EM (Aurora, NDI) Self-designed tracking mounts at laparoscope handle and LUS probe tip	US - video	2D-US image onto laparoscopic video with needle trajectory and circle highlighting ROI	- The centers of the target coils were about 10mm and 5mm away from the centers of the ablation zones (clinically acceptable) - Faster needle placement time with AR	- Artificial tumors were created - Limitations due to experiment design (tumor size, not compensated for needle bending) - The study did not examine the benefits of the AR approach compared to the method that solely combines the needle trajectory with the LUS image.

*LLA = laparoscopic liver ablation, LLR = laparoscopic liver resection, LUS = laparoscopic ultrasound scope, AR = augmented reality, EM = electromagnetic, 2D = two-dimensional, US = ultrasound, ROI = region of interest

Table 2. Clinical studies

Author & publication year	Study design & type of surgery	Aim study	No. of patient/ lesions	Imaging modality	Navigation system	Tracking method & tracked tools	Registration principle	Visualization of navigation	Important findings	Important limitations
Harms et al. (2001) [18]	Feasibility LLS	Compare navigated 3D LUS with 3D-navigated transcatheter US and 3D CT scan (golden standard) for clinical applicability, imaging quality, diagnostic potential, and accuracy in volumetric assessment of hepatic lesions	17/19	3D LUS	NA	EM (Flock of Birds, ATC) Sensor on tip of LUS probe	Intraoperative 3D US images with navigated LUS probe	Visualization of the 3D-US configuration of the ROI, including the volume account	- 3D LUS underestimates ROI volume by 3.1%, but is more accurate than transcatheter 3D US for volume assessment (nonsignificant difference of 2.5%)	- Technical limitations (time-consuming segmentation process, potential for incorrect positioning of the magnetic transmitter)
Kleemann et al. (2012) [25]	Case report LLS	Describe a novel tool for navigated LLS (LapAssistant system) and exemplarily report the navigated LLS in a patient	1/1	2D LUS	Self-developed	EM (3D Guidance, NDI) Laparoscopic camera, dissector, LUS Sensor on tip of LUS probe	US – MRI	Multi-modal visualization: virtual model registered with 2D-US image, real-time laparoscopic video and 2D US image with overlapping tumor	- System setup and calibration process was 18min. - The assessment of the resected tissue confirmed tumor-free resection margin - Tracker placed at tip of instrument reduces error	- No automatic non-rigid registration - Clinical use of only one patient - Poor combining of 2D-US slices, which limits the availability of a high-quality 3D-US volume
Sakata et al. (2020) [26]	Feasibility LLS	Confirm the accuracy and safety of a laparoscopic navigation system in vitro, as well as the feasibility and safety of the procedure by measuring the error between the simulation domain and the actual excision domain using gravity center of the latter as reference point in vivo	4/4	2D US	Self-developed	EM Electrocautery	US - CT	- Intraoperative images alongside corresponding CT and/or MRI image - Preoperative simulation overlaying onto CT image and highlighted extent of resection	- In vitro experiment showed tracking errors of 7.8±3.5mm at 33cm and 3.3±1.0mm at 13cm distance position of sensor on instrument - Registration time ranged from 126-186sec. - All four tumors were detected by the navigation system - Mean TRE of dissection planes were within 10mm	- Some misalignment occurred
Aoki et al. (2021) [14]	Feasibility LLS	Demonstrate experience with real-time intraoperative surgical navigation for LLS using VRCT volume navigation to provide EMT/IF-US with special position information	27/27	2D LUS	Self-developed	EM (VirtuTRAX, omniTRAX, CIVICO medical solutions) Patient tracker and sensor instrument on handle	US – CT – patient	Multi-model visualization: position of instrument tip on MPR images of CT, displayed side by side with real-time grayscale US with color coding, 3D reconstruction of relevant liver anatomy	- 26/27 lesions (96.3% mean diameter of 11 mm) were successfully performed under VRCT guidance. - Mean registration time was < 2 min, mean setup time was ±7 min./procedure - Mean FRE was 12 mm. - Surgical margins were all negative (mean of 9mm)	- No compensation for liver deformation

*EM = electromagnetic, US = ultrasound, CT = computed tomography, 3D = three-dimensional, LLS = laparoscopy liver resection, LLS = laparoscopy liver surgery, MHV = middle hepatic veins, VRCT = virtual real-time CT, EMT/IF-US = electromagnetic tracking image fusion ultrasonography, MPR = multi planar reconstruction, FRE = fiducial registration error, NA=not applicable

References

- [1] Stefan Heinrich and Hauke Lang. Hepatic resection for primary and secondary liver malignancies. *Innovative surgical sciences*, 2(1):1–8, 2017.
- [2] Sonia T Orcutt and Daniel A Anaya. Liver resection and surgical strategies for management of primary liver cancer. *Cancer Control*, 25(1):1073274817744621, 2018.
- [3] Åsmund Avdem Fretland, Vegar Johansen Dagenborg, Gudrun Maria Waaler Bjørnelv, Airazat M Kazaryan, Ronny Kristiansen, Morten Wang Fagerland, John Hausken, Tor Inge Tønnessen, Andreas Abildgaard, Leonid Barkhatov, et al. Laparoscopic versus open resection for colorectal liver metastases. *Annals of surgery*, 267(2):199–207, 2018.
- [4] Matteo Fusaglia, Hanspeter Hess, Marius Schwalbe, Matthias Peterhans, Pascale Tinguely, Stefan Weber, and Huanxiang Lu. A clinically applicable laser-based image-guided system for laparoscopic liver procedures. *International journal of computer assisted radiology and surgery*, 11:1499–1513, 2016.
- [5] Sinara Vijayan, Ingerid Reinertsen, Erlend Fagertun Hofstad, Anna Rethy, Toril A Nagelhus Hernes, and Thomas Langø. Liver deformation in an animal model due to pneumoperitoneum assessed by a vessel-based deformable registration. *Minimally Invasive Therapy & Allied Technologies*, 23(5):279–286, 2014.
- [6] C Schneider, M Allam, D Stoyanov, DJ Hawkes, K Gurusamy, and BR Davidson. Performance of image guided navigation in laparoscopic liver surgery—a systematic review. *Surgical Oncology*, 38:101637, 2021.
- [7] Douglas P Slakey, Eric Simms, Barbara Drew, Farshid Yazdi, and Brett Roberts. Complications of liver resection: laparoscopic versus open procedures. *JSLs: Journal of the Society of Laparoendoscopic Surgeons*, 17(1):46, 2013.
- [8] Sae Byeol Choi and Sang Yong Choi. Current status and future perspective of laparoscopic surgery in hepatobiliary disease. *The Kaohsiung Journal of Medical Sciences*, 32(6):281–291, 2016.
- [9] Thomas Langø, Sinara Vijayan, Anna Rethy, Cecilie Våpenstad, Ole Vegard Solberg, Ronald Mårvik, Gjermund Johnsen, and Toril N Hernes. Navigated laparoscopic ultrasound in abdominal soft tissue surgery: technological overview and perspectives. *International journal of computer assisted radiology and surgery*, 7:585–599, 2012.
- [10] Christian Hansen, Alexander Köhn, Stefan Schlichting, Florian Weiler, Stephan Zidowitz, Markus Kleemann, and Heinz-Otto Peitgen. Intraoperative modification of resection plans for liver surgery. *International Journal of Computer Assisted Radiology and Surgery*, 3:291–297, 2008.
- [11] Mattia Garancini, Luca Gianotti, Alberto Delitala, Fabrizio Romano, Luca Degrate, and Vittorio Giardini. Intraoperative ultrasound: a review on its role in liver surgery for primitive and metastatic tumors. *Minerva Chirurgica*, 71(3):201–213, 2015.
- [12] Le Roy Bertrand, Mourad Abdallah, Yamid Espinel, Lilian Calvet, Bruno Pereira, Erol Ozgur, Denis Pezet, Emmanuel Buc, and Adrien Bartoli. A case series study of augmented reality in laparoscopic liver resection with a deformable preoperative model. *Surgical Endoscopy*, 34:5642–5648, 2020.
- [13] Takeshi Aoki, Doaa A Mansour, Tomotake Koizumi, Yusuke Wada, Yuta Enami, Akira Fujimori, Tomokazu Kusano, Kazuhiro Matsuda, Koji Nogaki, Yoshihiko Tashiro, et al. Laparoscopic liver surgery guided by virtual real-time ct-guided volume navigation. *Journal of Gastrointestinal Surgery*, 25:1779–1786, 2021.
- [14] Hannes G Kenngott, Martin Wagner, Matthias Gondan, Felix Nickel, Marco Nolden, Andreas Fetzer, Jürgen Weitz, Lars Fischer, Stefanie Speidel, Hans-Peter Meinzer, et al. Real-time image guidance in laparoscopic liver surgery: first clinical experience with a guidance system based on intraoperative ct imaging. *Surgical endoscopy*, 28:933–940, 2014.

- [15] Jasper N Smit, Koert FD Kuhlmann, Oleksandra V Ivashchenko, Bart R Thomson, Thomas Langø, Niels FM Kok, Matteo Fusaglia, and Theo JM Ruers. Ultrasound-based navigation for open liver surgery using active liver tracking. *International journal of computer assisted radiology and surgery*, 17(10):1765–1773, 2022.
- [16] Matthias Peterhans, Anne vom Berg, Benoît Dagon, Daniel Inderbitzin, Charles Baur, Daniel Candinas, and Stefan Weber. A navigation system for open liver surgery: design, workflow and first clinical applications. *The international journal of medical robotics and computer assisted surgery*, 7(1):7–16, 2011.
- [17] Jens Harms, H Feussner, M Baumgartner, Armin Schneider, M Donhauser, and G Wessels. Three-dimensional navigated laparoscopic ultrasonography. *Surgical endoscopy*, 15(12):1459, 2001.
- [18] Kozo Konishi, Masahiko Nakamoto, Yoshihiro Kakeji, Kazuo Tanoue, Hirofumi Kawanaka, Shohei Yamaguchi, Satoshi Ieiri, Yoshinobu Sato, Yoshihiko Maehara, Shinichi Tamura, et al. A real-time navigation system for laparoscopic surgery based on three-dimensional ultrasound using magneto-optic hybrid tracking configuration. *International Journal of Computer Assisted Radiology and Surgery*, 2:1–10, 2007.
- [19] Andrea Teatini, Egidijus Pelanis, Davit L Aghayan, Rahul Prasanna Kumar, Rafael Palomar, Åsmund Avdem Fretland, Bjørn Edwin, and Ole Jakob Elle. The effect of intraoperative imaging on surgical navigation for laparoscopic liver resection surgery. *Scientific Reports*, 9(1):18687, 2019.
- [20] Osama Shahin, Armin Beširević, Markus Kleemann, and Alexander Schlaefer. Ultrasound-based tumor movement compensation during navigated laparoscopic liver interventions. *Surgical endoscopy*, 28:1734–1741, 2014.
- [21] Lung W Lau, Xinyang Liu, William Plishker, Karun Sharma, Raj Shekhar, and Timothy D Kane. Laparoscopic liver resection with augmented reality: a preclinical experience. *Journal of Laparoendoscopic & Advanced Surgical Techniques*, 29(1):88–93, 2019.
- [22] Page MJ, McKenzie JE, Bossuyt PM, Boutron I, Hoffmann TC, and Mulrow CD et al. The prisma 2020 statement: an updated guideline for reporting systematic reviews. *BMJ*, 372(71), 2021.
- [23] Ryo Oguma, Toshiya Nakaguchi, Ryoichi Nakamura, Tadashi Yamaguchi, Hiroshi Kawahira, and Hideaki Haneishi. Ultrasound image overlay onto endoscopic image by fusing 2d-3d tracking of laparoscopic ultrasound probe. In *Augmented Environments for Computer-Assisted Interventions: 9th International Workshop, AE-CAI 2014, Held in Conjunction with MICCAI 2014, Boston, MA, USA, September 14, 2014. Proceedings 9*, pages 14–22. Springer, 2014.
- [24] Neil D Glossop. Advantages of optical compared with electromagnetic tracking. *JBJS*, 91(Supplement.1):23–28, 2009.
- [25] François Poulin and L-P Amiot. Interference during the use of an electromagnetic tracking system under or conditions. *Journal of biomechanics*, 35(6):733–737, 2002.
- [26] Guofang Xiao, Ester Bonmati, Stephen Thompson, Joe Evans, John Hipwell, Daniil Nikitichev, Kurinchi Gurusamy, Sébastien Ourselin, David J Hawkes, Brian Davidson, et al. Electromagnetic tracking in image-guided laparoscopic surgery: Comparison with optical tracking and feasibility study of a combined laparoscope and laparoscopic ultrasound system. *Medical physics*, 45(11):5094–5104, 2018.
- [27] Markus Kleemann, Steffen Deichmann, Hamed Esnaashari, Armin Besirevic, Osama Shahin, Hans-Peter Bruch, and Tilman Laubert. Laparoscopic navigated liver resection: technical aspects and clinical practice in benign liver tumors. *Case reports in surgery*, 2012, 2012.
- [28] Koichiro Sakata, Taiki Kijima, and Osamu Arai. Initial report: A novel intraoperative navigation system for laparoscopic liver resection using real-time virtual sonography. *Scientific Reports*, 10(1):6174, 2020.

- [29] Xinyang Liu, William Plishker, Timothy D Kane, David A Geller, Lung W Lau, Jun Tashiro, Karun Sharma, and Raj Shekhar. Preclinical evaluation of ultrasound-augmented needle navigation for laparoscopic liver ablation. *International journal of computer assisted radiology and surgery*, 15:803–810, 2020.
- [30] Per-Olof Persson. The level set method lecture notes, mit 16.920 j/2.097 j/6.339 j numerical methods for partial differential equations. 2005.
- [31] Rohit Singla, Philip Edgcumbe, Philip Pratt, Christopher Ngan, and Robert Rohling. Intra-operative ultrasound-based augmented reality guidance for laparoscopic surgery. *Healthcare technology letters*, 4(5):204–209, 2017.
- [32] Iwan Paolucci, Raluca-Maria Sandu, Luca Sahli, Gian Andrea Prevost, Federico Storni, Daniel Candinas, Stefan Weber, and Anja Lachenmayer. Ultrasound based planning and navigation for non-anatomical liver resections—an ex-vivo study. *IEEE open journal of engineering in medicine and biology*, 1:3–8, 2019.

Appendices

A Search String

Medline:

((Hepatectomy/ or exp Liver Neoplasms/ or exp Liver/su or (hepatectom* or ((liver or hepat*) adj3 (resect* or surger* or tumor* or tumour* or cancer* or neoplas* or metasta* or carcino* or surger*))).ab,ti,kw.) and (exp Laparoscopy/ or Minimally Invasive Surgical Procedures/ or (laparoscop* or (minimal* adj3 invasi* adj3 surger*)).ab,ti,kw.) and (Ultrasonics/ or exp Ultrasonography/ or (ultraso* or echogra* or us-guid*).ab,ti,kw.) and (Surgical Navigation Systems/ or Surgery, Computer-Assisted/ or Imaging, Three-Dimensional/ or Augmented Reality/ or (image-guid* or us-guid* or surgical-navigat* or computer-assist* or (Navigation* adj3 System) or ((intraoperat* or intra-operat* or per-operat* or peroperat* or intrasurg* or intra-surg* or per-surg* or persurg*) adj3 (resection-plan* or liver-map*)) or three-dimension* or 3-dimension* or 3d or 3-d or (navigat* adj3 ultraso*) or (augment* adj3 reality)).ab,ti,kw. or (navigat* or guidance*).ti.) and english.la.) or (((exp *Laparoscopy/ or *Minimally Invasive Surgical Procedures/ or (laparoscop* or (minimal* adj3 invasi* adj3 surger*)).ti.) and (*Ultrasonics/ or exp *Ultrasonography/ or (ultraso* or echogra* or us-guid*).ti.) and (*Surgical Navigation Systems/ or *Surgery, Computer-Assisted/ or *Imaging, Three-Dimensional/ or *Augmented Reality/ or (image-guid* or us-guid* or surgical-navigat* or computer-assist* or (Navigation* adj3 System) or ((intraoperat* or intra-operat* or per-operat* or peroperat* or intrasurg* or intra-surg* or per-surg* or persurg*) adj3 (resection-plan* or liver-map*)) or three-dimension* or 3-dimension* or 3d or 3-d or (navigat* adj3 ultraso*) or (augment* adj3 reality)).ti. or (navigat* or guidance*).ti.) and english.la.) not (*Ablation Techniques/ or ablation*.ti.))

Embase:

('hepatectomy'/exp OR 'liver tumor'/exp OR 'liver surgery'/de OR hepatectom*:ab,ti,kw OR (((liver OR hepat*) NEAR/3 (resect* OR surger* OR tumor* OR tumour* OR cancer* OR neoplas* OR metasta* OR carcino* OR surger*)):ab,ti,kw)) AND ('laparoscopy'/exp OR 'minimally invasive surgery'/de OR laparoscop*:ab,ti,kw OR ((minimal* NEAR/3 invasi* NEAR/3 surger*):ab,ti,kw)) AND ('ultrasound'/de OR 'echography'/de OR 'peroperative echography'/de OR 'real time echography'/de OR ultraso*:ab,ti,kw OR echogra*:ab,ti,kw OR 'us guid*':ab,ti,kw) AND ('image guided surgery'/de OR 'surgical navigation system'/de OR 'computer assisted surgery'/de OR 'computer assisted surgery system'/de OR 'computer assisted navigation'/de OR 'computer assisted navigation system'/de OR 'tracking system'/de OR 'three-dimensional imaging'/de OR 'augmented reality'/de OR 'image guid*':ab,ti,kw OR 'us guid*':ab,ti,kw OR 'surgical navigat*':ab,ti,kw OR 'computer assist*':ab,ti,kw OR ((navigation* NEAR/3 system):ab,ti,kw) OR (((intraoperat* OR 'intra operat*' OR 'per operat*' OR peroperat* OR intrasurg* OR 'intra surg*' OR 'per surg*' OR persurg*) NEAR/3 ('resection plan*' OR 'liver map*')):ab,ti,kw) OR 'three dimension*':ab,ti,kw OR '3 dimension*':ab,ti,kw OR 3d:ab,ti,kw OR '3 d':ab,ti,kw OR ((navigat* NEAR/3 ultraso*):ab,ti,kw) OR ((augment* NEAR/3 reality):ab,ti,kw) OR navigat*:ti OR guidance*:ti) AND [english]/lim OR (('laparoscopy'/mj/exp OR 'minimally invasive surgery'/mj OR laparoscop*:ti OR ((minimal* NEAR/3 invasi* NEAR/3 surger*):ti)) AND ('ultrasound'/mj OR 'echography'/mj OR 'peroperative echography'/mj OR 'real time echography'/mj OR ultraso*:ti OR echogra*:ti OR 'us guid*':ti) AND ('image guided surgery'/mj OR 'surgical navigation system'/mj OR 'computer assisted surgery'/mj OR 'computer assisted surgery system'/mj OR 'computer assisted navigation'/mj OR 'computer assisted navigation system'/mj OR 'tracking system'/mj OR 'three-dimensional imaging'/mj OR 'augmented reality'/mj OR 'image guid*':ti OR 'us guid*':ti OR 'surgical navigat*':ti OR 'computer assist*':ti OR ((navigation* NEAR/3 system):ti) OR (((intraoperat* OR 'intra operat*' OR 'per operat*' OR peroperat* OR intrasurg* OR 'intra surg*' OR 'per surg*' OR persurg*) NEAR/3 ('resection plan*' OR 'liver map*')):ti) OR 'three dimension*':ti OR '3 dimension*':ti OR 3d:ti OR '3 d':ti OR ((navigat* NEAR/3 ultraso*):ti) OR ((augment* NEAR/3 reality):ti) OR navigat*:ti OR guidance*:ti) AND [english]/lim NOT ('ablation therapy'/exp/mj OR ablation*:ti))

Web of Science:

(TS=((hepatectom* OR ((liver OR hepat*) NEAR/2 (resect* OR surger* OR tumor* OR tumour* OR cancer* OR neoplas* OR metasta* OR carcino* OR surger*)))) AND ((laparoscop* OR (minimal* NEAR/2 invasi* NEAR/2 surger*))) AND ((ultraso* OR echogra* OR us-guid*)) AND ((image-guid* OR us-guid* OR surgical-navigat* OR computer-assist* OR (Navigation* NEAR/2 System) OR ((intraoperat* OR intra-operat* OR per-operat* OR peroperat* OR intrasurg* OR intra-surg* OR per-surg* OR persurg*) NEAR/2 (resection-plan* OR liver-map*)) OR three-dimension* OR 3-dimension* OR 3d OR 3-d OR (navigat* NEAR/2 ultraso*) OR (augment* NEAR/2 reality)))) NOT DT=(Meeting Abstract OR Meeting Summary) AND LA=(English) OR (TI((((laparoscop* OR (minimal* NEAR/2 invasi* NEAR/2 surger*))) AND ((ultraso* OR echogra* OR us-guid*)) AND ((image-guid* OR us-guid* OR surgical-navigat* OR computer-assist* OR (Navigation* NEAR/2 System) OR ((intraoperat* OR intra-operat* OR per-operat* OR peroperat* OR intrasurg* OR intra-surg* OR per-surg* OR persurg*) NEAR/2 (resection-plan* OR liver-map*)) OR three-dimension* OR 3-dimension* OR 3d OR 3-d OR (navigat* NEAR/2 ultraso*) OR (augment* NEAR/2 reality)))) NOT DT=(Meeting Abstract OR Meeting Summary) AND LA=(English))

Database searched	Platform	Years of coverage	Records	Records after duplicates removed
Medline ALL	Ovid	1946 - Present	307	306
Embase	Embase.com	1971 - Present	398	223
Web of Science Core Collection*	Web of Knowledge	1975 - Present	181	55
Total			886	584

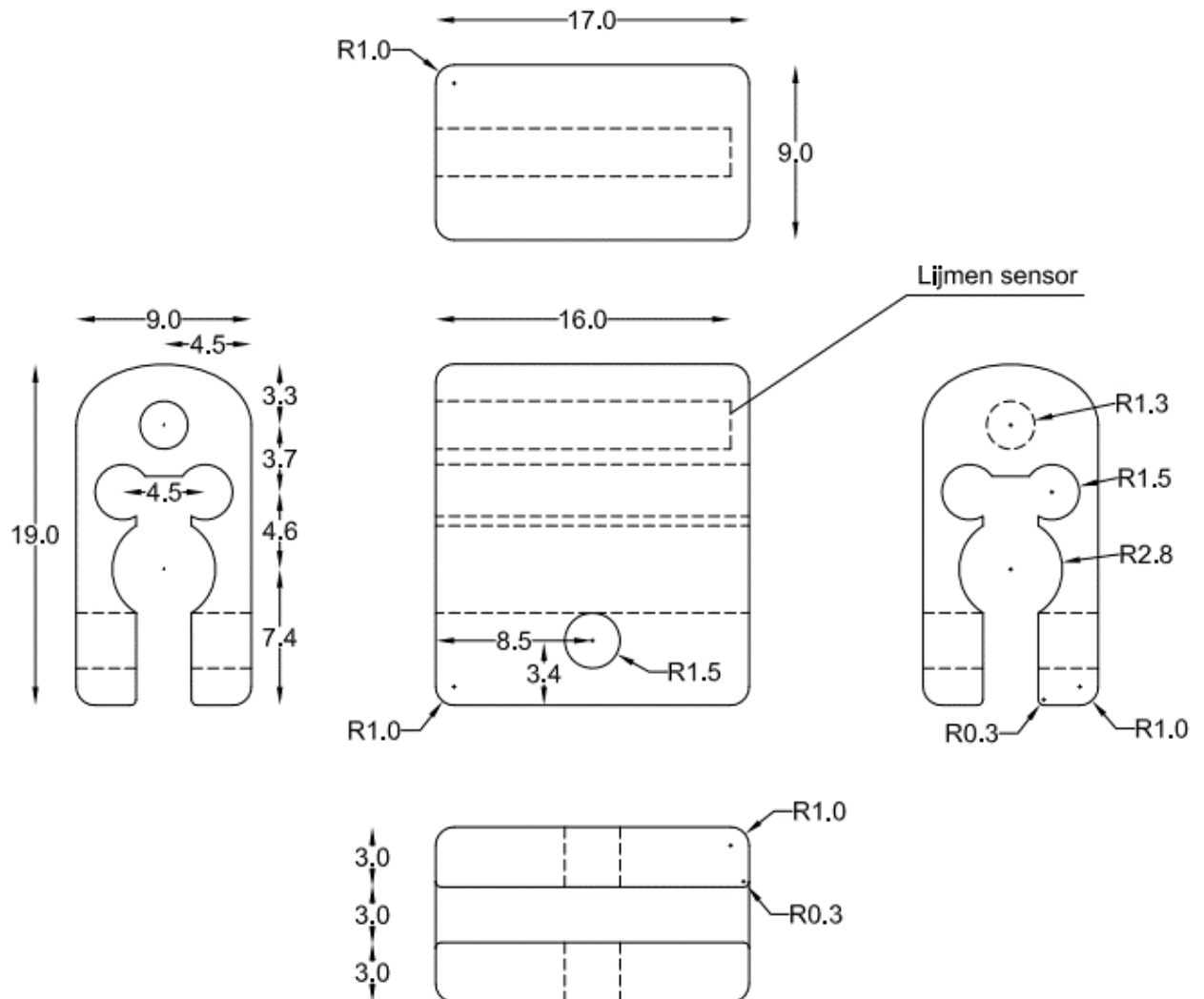
*Science Citation Index Expanded (1975-present) ; Social Sciences Citation Index (1975-present) ; Arts & Humanities Citation Index (1975-present) ; Conference Proceedings Citation Index- Science (1990-present) ; Conference Proceedings Citation Index- Social Science & Humanities (1990-present); Emerging Sources Citation Index (2005-present)

Figure 8: Results database searching

B

Technical Drawing Adapter

This appendix contains the technical drawing of the adapter for the laparoscopic resection tool (LigaSure Maryland). 'Lijmen sensor' means that here, the EM sensor is being glued in place.



Summary study protocol

This appendix contains a summary of the study protocol. 28 patients are included for laparoscopic procedures. The study duration will span 4.5 years.

Objectives:

The primary objective of this study is to develop and assess the performance of a novel ultrasound-based navigation system for use in both open and laparoscopic oncological liver surgery.

The secondary objectives include:

- Evaluating the feasibility and accuracy of an electromagnetic (EM)-tracked 3D ultrasound imaging system using a navigation system developed in-house.
- Assessing the accuracy of the registration process between intraoperative 3D ultrasound images and preoperative magnetic resonance imaging (MRI) in open and laparoscopic liver surgery.
- Evaluating the usability of the newly introduced navigation system through the use of usability questionnaires administered to the system users.

Methodology:

Prior to the surgery, a patient-specific 3D model of the patient's liver, including its shape, vascular system, and specific lesions, is created using diagnostic MR images. On the day of the surgery, the procedure starts in accordance with standard protocols. Following pneumoperitoneum, a single 6-degrees-of-freedom electromagnetic (EM) marker is affixed to the liver's surface near the intended lesion. This marker records the precise location of the liver during the operation. Subsequently, the surgeon conducts an ultrasound scan in the vicinity of the target lesion, generating a 3D ultrasound image of the liver. Manual registration aligns the liver with the diagnostic MRI and the 3D model, and the target lesion is designated within the navigation system. The accuracy of this registration is assessed using the target registration error.

Inclusion and exclusion criteria:

Patients eligible for this study must meet several criteria, including being at least 18 years old, providing written informed consent, and being scheduled for open liver resection and/or ablation, laparoscopic resection, or staging laparotomy. Additionally, they should have at least one liver lesion located centrally, with a diameter of less than 8 cm and situated within 5 cm of the liver's surface. Furthermore, they should have undergone a contrast-enhanced MRI or CT scan within the past 2 months. These criteria help ensure that the study focuses on patients with specific characteristics relevant to the research.

The study's exclusion criteria include patients with abdominal or thoracic metal implants that might interfere with EM tracking, those with isoechoic or completely treated liver lesions, pregnant individuals, patients with pacemakers, those with large cysts near the targeted liver lesion (over 5 cm in diameter), and individuals with MR scans older than 2 months at the time of surgery. These criteria are in place to ensure research integrity and accurate EM tracking.

Risk evaluation:

Participating in this study does not impose any extra burden or risk and does not disrupt the standard clinical workflow. The only modification involves temporarily attaching one electromagnetic sensor to the liver. This may extend surgery time by a maximum of 15 minutes, which is needed for sensor placement, extra ultrasound scans, and accuracy checks. No extra radiation exposure or intravenous contrast agents are used.

Navigation workflow and responsibilities:

Workflow laparoscopic navigated liver surgery

A custom-made clip-on tool with a 6DOF wired electromagnetic sensor is attached to the laparoscopic ultrasound transducer and laparoscope (**researcher's responsibility**). Both instruments are covered with a sterile cover by the surgical assistant.

The surgical procedure follows the standard protocol.

During surgery, a sterile 6DOF electromagnetic marker is affixed to the liver surface near the targeted lesion using medical adhesive (Glubran® 2 Synthetic Surgical Glue, GEM). This marker enables tracking the liver's exact location during intraoperative movements (**surgeon's responsibility**).

The electromagnetic field generator (Aurora, NDI) tracks the position of the liver marker and the electromagnetically tracked ultrasound transducer and laparoscope. Real-time tracking is possible when they are within the field of view of the EM field generator. The EM pointer and LigaSure Maryland can also be connected for tracking (**researcher's responsibility**).

The surgeon performs an electromagnetically tracked ultrasound sweep of the patient's liver, focusing on the targeted lesion area (**surgeon + researcher's responsibility**).

Anatomical landmarks visible on the ultrasound are registered to corresponding points on the 3D model (**surgeon + researcher's responsibility**).

The registration data is loaded into the augmented reality software, projecting a semi-transparent overlay of the 3D model onto the laparoscopic image (**researcher's responsibility**).

The accuracy of the navigation is visually assessed based on superficial landmarks on the liver, such as the liver contour, ligaments, and superficial lesions (**surgeon + researcher's responsibility**).

The target registration error is postoperatively calculated by measuring the distance (in mm) between the center of the lesion in the ultrasound volume and the center of the lesion in the registered MR images.

Figure C.1: Clinical workflow steps for navigated laparoscopic liver resection